

https://dspace.org/

Two new basal anomodont specimens from the Lower Abrahamskraal Formation (Beaufort Group: Karoo Supergroup) - implications for anomodont phylogeny and palaeoecology

Matlhaga, Fonda Ricardo

2025-03

University of the Witwatersrand, Johannesburg

https://hdl.handle.net/10539/47704

Matlhaga, Fonda Ricardo. (2025). Two new basal anomodont specimens from the Lower Abrahamskraal Formation (Beaufort Group: Karoo Supergroup) - implications for anomodont phylogeny and palaeoecology. [Master's dissertation, University of the Witwatersrand, Johannesburg]. WIReDSpace. https://hdl.handle.net/10539/47704

Downloaded from a DSpace repository. https://dspace.org/

UNIVERSITY OF THE WITWATERSRAND, JOHANNESBURG

Two new basal anomodont specimens from the Lower Abrahamskraal Formation (Beaufort Group: Karoo Supergroup) - implications for anomodont phylogeny and palaeoecology.

By

Fonda Ricardo Matlhaga

(1726932)

ORCID: 0000-0003-1496-9093

A dissertation submitted to the Faculty of Science, University of the Witwatersrand, Johannesburg, in fulfilment of the requirements of Master of Science.

Supervisor: Prof. Julien Benoit

Co-supervisor: Prof. Bruce Rubidge

DECLARATION

I, Fonda Ricardo Matlhaga, declare that this dissertation titled “Two new basal anomodont specimens from the Lower Abrahamskraal Formation (Beaufort Group: Karoo Supergroup) - implications for anomodont phylogeny and palaeoecology” and the work presented in it are my own. I hereby confirm that:

1. This work was done while registered as a student for the degree of Master of Science in Palaeontology in the academic year 2023-2024.
2. The work submitted is my own unaided work, except as acknowledged in the text.
3. Neither part of this work has been submitted in the past or submitted for a degree at another university.
4. I have adhered to the guidelines in referencing the ideas and thoughts of others.

Signature: 

Date: 13/03/2025

ACKNOWLEDGEMENTS

I would like to express my sincere gratitude to the esteemed faculty members, Assoc. Prof. Julien Benoit and Prof. Bruce Rubidge, who provided me with support and guidance throughout my MSc project. I would also like to thank Dr Christian Kammerer for his expertise in anomodont taxonomy. Additionally, I would like to thank Christopher Pestana and Dr Kimberley Chapelle for assisting me with the coding to achieve the body size results.

I extend my sincere appreciation to Dr Aliénor Duhamel for her assistance in the anatomical identification of bones and also for sharing with me relevant information about anomodonts and their phylogeny. I am deeply grateful to the staff and students at the Evolutionary Studies Institute for their efforts in collecting, preparing, and curating the specimens.

Furthermore, I am grateful to Ms. Zaithuna Skhosan from Iziko South African Museum of Natural History, Dr Sifelani Jirah from the Evolutionary Studies Institute, and Ms. Sekhomotso Gubuza from the National Museum for their benignancy in giving me access to the holotypes and specimens used for anatomical comparisons in this study. Finally, I'd like to thank GENUS, Centre of Excellence in Palaeosciences, the DSI-NRF National Research Foundation of South Africa, and PAST for funding, which made this research possible.

I am also incredibly thankful to my parents, who offered me consistent support and love throughout my life and even during my MSc.

ABSTRACT 12

CHAPTER 1: INTRODUCTION 14

1.1 General background 14

1.2 Non-dicynodont anomodonts (basal anomodonts) 15

1.3 Basal dicynodont anomodonts 16

1.4 Non-dicynodont anomodonts and dicynodont anomodonts 17

1.5 This study 18

1.6 Significance of this study 19

1.7 Scientific questions to be addressed 20

1.8 Aims and objectives 20

CHAPTER 2: METHODS AND MATERIALS 21

2.1 Material 21

2.1.1 Specimens used in this study 21

2.2 Methods 23

2.2.1 Specimen preparation 23

2.2.2 Scanning and 3D reconstructions 23

2.2.3 Matrix construction for phylogenetic analysis 25

2.2.4 Phylogenetic analysis 26

2.2.5 Body size estimation 26

CHAPTER 3: GEOLOGY 29

3.1 Geological background 29

3.2 Combrinkskraal Member.....31

3.3 Boundaries of the *Eodicynodon* Assemblage Zone.....32

3.4 Correlations of the *Eodicynodon* Assemblage Zone.....33

3.5 Palaeoenvironment of the *Eodicynodon* Assemblage Zone.....33

CHAPTER 4: RESULTS.....34

4.1 Cranial descriptions.....34

4 1.1 Description of specimen BP/1/8740 (*Patranomodon*).....34

4.1.2 Description of specimen BP/1/8500 (basal dicynodont).....60

4.2 Phylogenetic analysis.....72

4.2.1 Description of phylogenetic results.....73

4.3 Body size estimates.....76

4.3.1 Description of body size estimation.....79

CHAPTER 5: DISCUSSION.....81

5.1 Identification and comparison.....81

5.1.1 Identification of BP/1/8740 as *Patranomodon*.....81

5.1.3 Identification of BP/1/8500 and comparison.....84

5.2 Implication for body size evolution.....89

CHAPTER 6: CONCLUSION.....91

REFERENCES.....94

APPENDICES..... 115

Appendix 1..... 115

Appendix 2 116

Appendix 3 117

Appendix 4 132

Appendix 5 133

Appendix 6 139

List of Figures

Figure 1: Locality and stratigraphic information for specimen BP/1/8740 and BP/1/8500. **A.** map showing the Karoo Supergroup, **B.** google earth image of the study area showing the locality of BP/1/8740 with a red arrow and BP/1/8500 with a green arrow, **C.** part of the stratigraphic section and thickness of the Abrahamskraal Formation in the Combrinkskraal area (from Day & Rubidge, 2014). The red arrow indicates the location of BP/1/8740, and the green arrow indicates the location of BP/1/8500. *Abbreviations*: CK, Combrinkskraal Member; GF, Grootfontein Member; Ab, Abrahamskraal Formation.

Figure 2: Right lateral view of BP/1/8740. **A**. Photograph; **B**. line illustration with bone labels *Abbreviations:* Pin, pineal foramen; Pob, postorbital bar; Fr, frontal; Pfr, postfrontal; Prp, preparietal; Par, parietal; Na; nasal; Prf, prefrontal; La, Lacrimal; Pmx, premaxilla; Dt, dentary; Mx, maxilla; Mf, mandibular fenestra; Ju, jugal; Ang, angular; Rl, reflected lamina; Sa, surangular; Q, quadrate; Sq, squamosal. Scale bar is 3cm.

Figure 3: Dorsal view of BP/1/8740. **A**. Photograph; **B**. line illustration with bone labels. *Abbreviations*: Na, nasal; Prf, prefrontal; La, lacrimal; Fr, frontal; Mx, maxilla; Ju, jugal; Pin, pineal foramen; Prp, preparietal; Pfr, postfrontal; Pob, postorbital bar; Par, parietal; Pop, postparietal; Sq, squamosal; Ta, tabular; Spr, supraoccipital; Exo, exoccipital; Fm, foramen magnum. Scale bar is 3 cm.

Figure 4: Occipital view of BP/1/8740. **A**. Photograph; **B**. line illustration with bone labels. *Abbreviations*: Pin, pineal foramen; Pob, postorbital bar; Pa, parietal; Pop, postparietal; Sq, squamosal; Ta, tabular; Spr, supraoccipital; Exo, exoccipital; Fm, foramen magnum; Tf, temporal fenestra. Scale bar is 3 cm.

Figure 5: Ventral view of BP/1/8740. **A**. Photograph; **B**. line illustration with bone labels. *Abbreviations*: Mx, maxilla; Ju, jugal; Dt, dentary; Vo, vomer; Ch, choana; Pal, palatine, Pt, pterygoid; Ect, ectoperygoid; Tpt, transverse process of pterygoid; Sa, surangular; Qpt, quadrate process of pterygoid; Sq, squamosal; An, angular; Ar, articular; Pa, prearticular; Pbs, parabasisphenoid. Scale bar is 3cm.

Figure 6: Skull and postcranial elements of BP/1/8740 in dorsal view. **A**. Photograph; **B**. line illustration with bone labels *Abbreviations*: Ac, atlas; Ax, axis; Pz, prezygapophysis; Poz, postzygapophysis; Tp, transverse process; C3, third cervical; C4, fourth cervical; C5, fifth cervical; T1, first thoracic; Proc, procoracoid; Co, coracoid; Gle, glenoid; Tc, tuber coracoidens; Pe, proximal epiphysis; Di, diaphysis; De, distal epiphysis; Mc, medullary cavity; Ms, medial supracondylar; Le, lateral epicondyle. Scale bar is 3cm.

Figure 7: Vertebrae of BP/1/8740 in dorsal view. **A**, photograph; **B**, illustration. *Abbreviations*: Ac, atlas; Ax, axis; Pz, prezygapophysis; Poz, postzygapophysis; Tp, transverse process; C3, third cervical; C4, fourth cervical; C5, fifth cervical; T1, first thoracic. Scale bar is 3cm.

Figure 8: Humerus of BP/1/8740 in oblique view. **A**. Photograph; **B**. line illustration with bone labels *Abbreviations*: Pe, proximal epiphysis; Di, diaphysis; De, distal epiphysis; Mc, medullary cavity; Ms, medial supracondylar; Le, lateral epicondyle. Scale bar is 3cm.

Figure 9: Scapula of BP/1/8740 in dorsal view. **A**. Photograph; **B**. line illustration with bone labels. *Abbreviations*: Proc, procoracoid; Co, coracoid; Gle, glenoid; Tc, Tuber coracoidens. Scale bar is 3cm.

Figure 10: Left lateral view of BP/1/8500. **A**. Photograph; **B**. line illustration with bone labels. *Abbreviations*: Pmx, premaxilla; Na, nasal; Mx, maxilla; La, lacrimal; Ju, jugal; Fr, frontal; Prf, prefrontal; Tu, tusk; Pcn, postcanine; Pal, palatine; Inp, interparietal; Pob, postorbital; Sq, squamosal. Scale bar is 3cm.

Figure 11: Right lateral view of BP/1/8500 with the occiput folded. **A**. Photograph; **B**. line illustration with bone labels. *Abbreviations*: Ju, jugal; Pa, parietal; Ptf, post temporal fenestra; Sq, squamosal; Q, quadrate; Inp, interparietal; Pt, pterygoid; Orb, orbit; Mx, maxilla; Rtu, right tusk; Prf, prefrontal; Tf, temporal fenestra. Oblique lines indicate unidentifiable bones. Scale bar is 3cm.

Figure 12: Occipital view of BP/1/8500. **A**. Photograph; **B**. line illustration with bone labels. *Abbreviations*: Pa, parietal; Inp, interparietal; Fm, foramen magnum; Ptf, post temporal fenetra; Sq, squamosal; Q, quadrate; Tf, temporal fenestra; Pob, post orbital bar. Oblique lines indicate unidentifiable bones. Scale bar is 3cm.

Figure 13: Ventral view of BP/1/8500; **A**. photograph of specimen BP/1/8500 in ventral view; **B**. closeup view of the anterior portion of the palate; **C**. line illustration with bone labels; **D**. CT scan of BP/1/8500 with segmentation of the tusks and alveoli. The grey material on the CT scans represents the skull. *Abbreviations*: Pmx, premaxilla; Vo, vomer; Mx, maxilla; Pcn, postcanine; Tu, tusk; Pt, pterygoid; Sq, squamosal; Ltu, left tusk; Rtu, right tusk; Alv, alveoli. Scale bar for A, C, and D is 3cm, and the scale bar for B is 4cm.

Figure 14: Strict consensus of 20 most parsimonious cladograms from the phylogenetic analysis. Numbers at the nodes are Bremer support values. Specimens described here are indicated by the black rectangles.

Figure 15: A projection of basal skull length onto the anomodont phylogenetic tree. The colour gradient shows changes in skull length over time (millions of years). The red colour indicates smaller skulls (minimum skull length being 38mm), yellow colour indicates slightly larger skulls, green colour indicates moderately large skulls, and the blue colour indicates larger skulls (maximum skull length of 920mm).

Figure 16: Log skull length (proxy for body size) of anomodont taxa from the Middle Permian to Late Triassic plotted at the stratigraphic range midpoints for each taxon with the Lowess regression line fitted. The circles in the graph represent each taxon used in the body size analysis. This figure is a graphical representation of the phylogeny in Figure 15. *Abbreviations*: Wor, Wordian; Cap, Capitanian; Wuc, Wuchiapingian; Cha, Changsingian; Ind, Induan; Ole, Olenekian; Ani, Anisian; Lad, Ladinian; Car, Carnian; Nor, Norian; Rha, Rhaetian.

Figure 17: Comparison of three basal anomodonts taxa from Gondwana. **A**) Left lateral view of BP/1/8500 from Middle Permian of South Africa, **B**) illustration of BP/1/8500, **C**) left lateral view of *Tiarajudens eccentricus* (UFRGS PV393P) from Middle Permian of Brazil, **D**) illustration of *Tiarajudens eccentricus* obtained from Cisneros et al. 2011, **E**) right lateral view of *Anomocephalus africanus* (BP/1/5582) from Middle Permian of South Africa, **F**) illustration of *Anomocephalus africanus* obtained from Cisneros et al. 2015. The scale bar for A, B, E and F is 3cm and the scale bar for C and D is 2cm.

List of Tables

Table 1: List of specimens in South African collections that were used for morphological comparison with BP/1/8740 and BP/1/8500.

ABSTRACT

Anomodontia is among the most prosperous therapsid clades in terms of abundance and diversity. Their largest subclade, the Dicynodontia, were present from the Middle Permian to the Late Triassic, reaching their maximum diversity during the Late Permian, before the end-Permian extinction event 252 million years ago. Basal anomodonts are known from South Africa, Russia, China, and Brazil. They are comparatively rare, and, as such, the earliest stages of anomodont evolutionary radiation remain obscure. Here, the cranial morphology of two new anomodont specimens from the *Eodicynodon* Assemblage Zone, lower Beaufort Group of South Africa are described: BP/1/8500 and BP/1/8740. The large size of BP/1/8500 makes it unique among early dicynodonts, and it combines features of both basal anomodonts and dicynodonts. Specimen BP/1/8500 is recovered as the second most basal dicynodont, stemwards to *Nyaphulia oelofseni*. In contrast, specimen BP/1/8740 is very small, and the large orbit and lack of canines are reminiscent of *Patranomodon*, *Galechirus*, and *Galepus*. A detailed description of this specimen indicates that it is a second specimen of *Patranomodon* and, most likely, a juvenile. This is supported by the phylogenetic analysis, which recovers it as a sister taxon to the holotype of *Patranomodon*. In addition, an analysis of body size suggests that anomodont body size has increased gradually over time while diversity decreased. Small-bodied anomodonts dominated before the end-Capitanian crisis, then large-bodied anomodonts appeared during the Lopingian and went extinct at the end of the Permian. Anomodont size increased consistently during the Triassic, but the taxonomic diversity was extremely low. This supports that, as for many other tetrapod groups, large body size was a refugium niche for anomodonts as they approached extinction.

KEYWORDS: Anomodont, dicynodont, Chainosauria, *Eodicynodon,* Venyukovioidea.

CHAPTER 1: INTRODUCTION

1.1 General background

Anomodontia is a speciose clade of non-mammalian synapsids which was dominant during the Permian Period (Angielczyk & Kammerer, 2018) and was among the first herbivorous clades of tetrapods to experience tremendous evolutionary radiation (Reisz & Sues, 2000; Reisz, 2006). Though mostly herbivorous, they were morphologically and ecologically diverse and were adapted to semi-aquatic, arboreal, and fossorial ecological niches (King & Cluver, 1991; Fröbisch & Reisz, 2008). They also evolved a wide range of body sizes, from mouse-sized to rhinoceros-sized animals (Romano & Manucci, 2021).

Anomodonts were geographically widespread, their remains having been found on every continent (Fröbisch, 2009), and the taxonomic diversity of this group reached its climax during the Late Permian, when they made up a large component of the terrestrial vertebrate fauna globally (Rubidge & Sidor, 2001). They survived the catastrophic end-Permian extinction event until the end-Triassic (Sulej et al. 2010; Ruta et al. 2013). Derived anomodont therapsids had a complex masticatory system based on the palinal sliding of the mandible, which may account for their evolutionary success (Angielczyk, 2004). Previously, the taxon Anomodontia was considered to comprise both dicynodonts and dinocephalians (Romer, 1966; King, 1988), but subsequent phylogenetic analysis has refuted this relationship, and the Anomodontia currently includes only dicynodonts and non- dicynodont anomodonts.

1.2 Non-dicynodont anomodonts (basal anomodonts)

Early non-dicynodont anomodonts are not common in the fossil record. Currently, the clade comprises 11 species which are known from the Permian rocks of South Africa, Russia, China, and Brazil (Liu et al. 2010). All basal anomodonts from South Africa: *Patranomodon nyaphulii* (Rubidge & Hopson, 1990), *Anomocephalus africanus* (Modesto et al. 1999), *Galechirus scholtzi* (Broom, 1907), *Galepus jouberti* (Broom, 1910), and *Galeops whaitsi* (Broom, 1912) are accommodated in the "Chainosauria" (Duhamel et al. 2024).

Basal anomodonts from Russia fall within the Venyukovioidea, which comprises *Otsheria netzvetajevi* (Tchudinov, 1960), *Ulemica* (*U.invisa* and *U.efremovi*) from the Middle Permian, and *Suminia getmanovi* (Rybczynski, 2000) from the Late Permian. *Suminia* is notable among non-dicynodont anomodonts as its teeth and cranial anatomy suggest a highly specialised herbivorous diet (Rybczynski, 2000; Fröbisch & Reisz, 2008).

The only non-dicynodont anomodont described from China is *Biseridens qilianicus* (Liu et al. 2010) from the upper part of the Xidagou Formation, which correlates with the *Tapinocephalus* Assemblage Zone of South Africa and is of Middle Permian age (Battail, 2000; Rubidge, 2005; Liu et al. 2010). *Biseridens* is considered the oldest anomodont and was previously described as an eotitanosuchian by Li and Cheng (1997). Later, it was re-described as an anomodont close to *Ulemica* (Battail, 2000), with the lower postcanine teeth organised in two rows, and it has small teeth displaced dorsally on the pterygoids (Battail, 2000).

The first and only basal anomodont described from South America is *Tiarajudens eccentricus* from the Middle Permian Rio do Rasto Formation of Brazil (Cisneros et

al. 2011). This genus has unusual features which include gastralia, long maxillary caniniforms, and enlarged pterygoid teeth that functionally replace the postcanine teeth (Cisneros et al. 2011). The skull is similar to that of *Anomocephalus africanus* (Modesto et al. 1999), a basal anomodont from South Africa, and they share the presence of transversely expanded palatal teeth, a short snout, large orbits, a squamosal that is not flared, and temporal fenestrae that are smaller than the orbit.

1.3 Basal dicynodont anomodonts

Dicynodonts are the most diverse anomodonts (Benoit et al. 2018) and include more than 100 species (Fröbisch, 2009). The oldest dicynodonts are from the *Eodicynodon* Assemblage Zone (Beaufort Group) of the South African Karoo Basin, where they represent over 80% of species discovered (Sidor & Smith, 2007; Smith et al. 2012). Described basal dicynodonts from the *Eodicynodon* Assemblage Zone of the Karoo Basin include *Eodicynodon* (*E. oosthuizeni*) (Barry, 1974), and *Nyaphulia oelofseni* (Rubidge, 1990a; Duhamel et al. 2024). Dicynodonts from the *Tapinocephalus* Assemblage Zone of the South African Beaufort Group include *Colobodectes cluveri* (Modesto et al. 2003), *Lanthanostegus mohoii* (Modesto et al. 2002; Rubidge et al. 2021), *Robertia broomiana* (Boonstra, 1948; King & Cluver, 1991; King & Rubidge, 1993), *Eosimops newtoni* (Broom, 1921; Angielczyk & Rubidge, 2013), *Diictodon feliceps* (Owen, 1876; Cluver & King, 1983; Angielczyk & Sullivan, 2008; Laaß et al. 2017), *Pristerodon mackayi* (Huxley, 1868; Cluver & King, 1983; Laaß, 2015), and *Brachyprosopus broomi* (Cluver, 1975; Angielczyk et al. 2016).

Previously, *Eodicynodon oosthuizeni* was considered the basal-most dicynodont because it retains several basal characters such as an enlarged lateral process of the pterygoid, a paired vomer, and paired premaxilla (Cluver & King, 1983; Rubidge,

1990), and the choanae extend anteriorly beyond the posterior margin of the canines, whereas in later dicynodonts they do not extend as far anteriorly (Barry, 1974). Duhamel et al. (2024) recently redescribed NMQR 2913 as *Nyaphulia oelofseni* (described originally as the basal dicynodont *Eodicynodon oelofseni* (Rubidge, 1990a)), the most basal dicynodont.

1.4 Non-dicynodont anomodonts and dicynodont anomodonts

All anomodonts are characterised by a short antorbital region of the skull, zygomatic arch that is bowed dorsally, reduced lateral pterygoid processes (except basal anomodonts), and the presence of a mandibular fenestra (King, 1988; Modesto et al. 1999).

The dicynodonts in turn have skulls which are modified to accommodate propalinal movement of the mandible, a character which is associated with herbivory (Botha & Angielczyk, 2010; Castanhinha et al. 2013). These cranial modifications include a bony secondary palate formed by the ventral expansion of the premaxillae, loss of premaxillary teeth and reduced postcanine teeth, enlarged temporal openings, the squamosal that is flared, and vomers forming the anterior border of the interpterygoid vacuity (King, 1993; Angielczyk, 2004, Benoit et al. 2018).

On the other hand, non-dicynodont anomodonts still retain teeth on the premaxilla (except *Galeops*), maxilla and dentary, orbits larger than the temporal fenestra, thin postorbital, broad parietal region, no secondary palate, expanded lateral flange of the pterygoid and squamosal that is not flared to provide surface for the origin of the external adductor muscle, with the exception of *Suminia.*

Anomodonts evolved and diversified early in therapsid evolutionary history, making the Middle Permian a critical period to understand anomodont origins and the

subsequent evolutionary radiation of dicynodonts. Accordingly, much scientific attention has recently been directed towards anomodonts which lived during this period (Day & Rubidge, 2014).

1.5 This study

In 2021, as a result of fieldwork in the lower Beaufort on the farm Combrinkskraal in the Prince Albert district, two basal anomodont skulls were discovered. Both specimens were discovered from the same stratigraphic level in the upper part of the *Eodicynodon* Assemblage Zone (Rubidge, Pers. Comm.).

Specimen BP/1/8500 is an almost complete skull that is slightly laterally distorted. Most of the bone has been eroded, leaving the impressions of their former shape. This specimen is a medium-sized dicynodont with a skull length of 19cm and a pair of large tusks. It has a seemingly broad intertemporal region, as is the condition with all dicynodonts from the Abrahamskraal Formation. It superficially differs from *Lanthanostegus* (the only other medium to large-sized dicynodont from the Middle Permian of South Africa) by its laterally (rather than anteriorly) oriented orbits (Modesto et al. 2002).

Specimen BP/1/8740 conversely comprises a very small anomodont skull and partial skeleton with a skull length of 3.5cm. The skull has relatively large orbits, small temporal fenestrae, a small pineal foramen, and no beak nor tusks. The lower jaw of this specimen is preserved in occlusion, and the partial skeleton includes the cervical vertebrae, some shoulder elements, and a humerus. This specimen has relatively few small teeth, which differs from the condition in *Patranomodon*, *Galechirus*, and *Galepus* (Rubidge & Hopson, 1996). As basal anomodonts from South Africa are rare, with most described genera comprising only a single specimen, any newly

discovered specimens have the potential to add to the understanding of basal anomodont anatomy.

As specimen BP/1/8500 is the largest dicynodont from the *Eodicynodon* Assemblage Zone and is much larger than any anomodont from the same biozone, and specimen BP/1/8740 is the smallest anomodont from this stratigraphic horizon, this study also includes an analysis of body size in early anomodonts. These two specimens thus have the potential to broaden understanding of the disparity in body size of Middle Permian anomodonts, which may alter the current understanding of the early evolutionary radiation of anomodonts (Brocklenhurst, 2019).

Body size is strongly correlated to the physiological and ecological properties of an organism. Accordingly, understanding the evolution of body size in the fossil record enables the reconstruction of palaeobiological changes across phylogenies and macroevolutionary patterns and processes of vertebrates (Hutchinson et al. 2011; Campione et al. 2014). The reconstruction of body size is extremely significant when analysing the change in body size in a specific clade (Romano & Manucci, 2021).

Therefore, the reconstruction of body size in early anomodonts could shed new light on the ecological diversity of this clade in the Middle Permian and add to understanding anomodont radiation and changes in body size in early therapsids.

1.6 Significance of this study

The description of these two newly discovered specimens is important as fossils from the *Eodicynodon* Assemblage Zone are rare, and they are amongst the oldest anomodonts yet discovered. They are thus crucial to understanding the early evolutionary radiation of anomodonts during the Middle Permian. Their inclusion in the updated phylogenetic analyses of anomodonts (Angielczyk et al. 2021; Duhamel

et al. 2024) will shed new light on the diversification of mid-Permian anomodonts. Furthermore, as these two specimens are from the uppermost levels of the *Eodicynodon* Assemblage Zone, they are of great importance to help unravel the faunal transition between the *Eodicynodon* and *Tapinocephalus* Assemblage Zones.

1.7 Scientific questions to be addressed

Are the newly discovered specimens (BP/1/8500 and BP/1/8740) new Middle Permian anomodont species, or do they belong to already existing taxa? Is their vastly different size indicative of a much earlier ecological diversification of anomodonts than previously envisioned or simply the effect of different ontogenetic stages?

1.8 Aims and objectives

To answer the above scientific questions, the following objectives will be pursued:

Objective 1: Describe the gross anatomy of the specimens.

Objective 2: Address their phylogenetic position among anomodonts.

Objective 3: Use basal skull length measurements as a proxy for body size.

Objective 4: Use a phylogenetic comparative approach to study the evolution of body size across early anomodonts

CHAPTER 2: METHODS AND MATERIALS

2.1 Material

2.1.1 Specimens used in this study

The material used in this study for comparative purposes is curated in the collections of the Evolutionary Studies Institute, Iziko South African Museum of Natural History in Cape Town, and the National Museum in Bloemfontein (Table 1). Specimens described in this study are all from the *Eodicynodon* Assemblage Zone of the Abrahamskraal Formation of the Beaufort Group and they are:

Specimen BP/1/8740 – Comprises a small skull with a lower jaw in occlusion and partial skeleton, including cervical vertebrae, scapula, and right humerus in a single block.

Specimen BP/1/8500 – A laterally compressed skull without a lower jaw.

Locality and horizon – Specimen BP/1/8740 and BP/1/8500 were found on the farm Combrinkskraal, Prince Albert District, Western Cape, South Africa. They are from the same stratigraphic horizon, the upper-most Combrinkskraal Member of the *Eodicynodon* Assemblage Zone, Abrahamskraal Formation, Beaufort Group, Karoo Basin. The provenances of the two specimens are about 1km from each other (Fig. 1).

Table 1: List of specimens in South African collections that were used for morphological comparison with BP/1/8740 and BP/1/8500.

Specimen number	Species	Type	Collection
BP/1/5582	*Anomocephalus africanus*	Holotype	Evolutionary Studies Institute
BP/1/6230	*Eodicynodon oosthuizeni*	Referred specimen	Evolutionary Studies Institute
SAM-PK-001068	*Galechirus scholtzi*	Holotype	Iziko South African Museum
SAM-PK-004005	*Galeops*	-	Iziko South African Museum
SAM-PK-011896	*Galechirus*	-	Iziko South African Museum
SAM-PK-012261	*Galeops*	-	Iziko South African Museum
SAM-PK-007630	*Galeops whaitsi*	-	Iziko South African Museum
SAM-PK-011879	*Eodicynodon oosthuizeni*	-	Iziko South African Museum
NMQR 02913	*Nyaphulia oelofseni*	Holotype	National Museum
NMQR 02978	*Eodicynodon oosthuizeni*	Referred specimen	National Museum
NMQR 03159	*Eodicynodon oosthuizeni*	-	National Museum
NMQR 03134	*Eodicynodon sp.*	-	National Museum
NMQR 03392	*Eodicynodon sp.*	-	National Museum
NMQR 3000	*Patranomodon nyaphulii*	Holotype	National Museum

2.2 Methods

2.2.1 Specimen preparation

Specimens BP/1/8740 and BP/1/8500 were prepared by Mr Charlton Dube at the Evolutionary Studies Institute, University of the Witwatersrand. These specimens were prepared mechanically using air scribes fitted with tips of tungsten carbide. Freshly exposed surfaces were consolidated with a layer of very diluted paraloid glue (B-72).

2.2.2 Scanning and 3D reconstructions

The two specimens were initially scanned with the normal CT scanning at the Evolutionary Studies Institute; however, this initial scanning experiment was not successful. The second scanning attempt was with neutron scanning, and the two specimens were CT-scanned at the Dingo-Neutron Imaging facility, ANSTO (Australia). Three-dimensional reconstructions, visualisation, and 3D renderings of the CT data were generated using AVIZO 9.0 lite (FEI VSG, Hillsboro, OR, USA).

2.2.2.1 Experimental setup and data reconstruction of BP/1/8740

Specimen BP/1/8740 was scanned using a quasi-parallel collimated beam of thermal neutrons from OPAL with a maximum spectrum intensity at 1.08 Å (70 meV) and full-width-at-half-maximum (FWHM) of 0.9 Å (100 meV). For this study, a collimation ratio (L/D) of 500 (Garbe et al. 2015) was used, where L is the neutron aperture-to-sample length and D is the neutron aperture diameter. The field of view was set to 66.8 x 100 mm^2 with a voxel size of 16.0 × 16.0 × 16.0 µm. Neutrons were converted to photons with a 30 µm thick terbium-doped Gadolinium oxide scintillator screen (Gd_2O_2S:Tb, RC Tritec AG); photons were then detected by a ZWO ASI2600MM Pro cMOS camera (liquid-cooled, 16-bit, 6248 × 4176 pixels) coupled with a Makro

Planar 100 mm Carl Zeiss lens. The tomographic scan consisted of a total of 1250 equally-spaced angle shadow-radiographs obtained every 0.144° as the sample was rotated 180° about its vertical axis. Both dark (closed shutter) and beam profile (open shutter) images were obtained for calibration before initiating shadow-radiograph acquisition. To reduce anomalous noise, a total of 3 individual radiographs with an exposure length of 27s were acquired at each angle following the procedure of Mays et al. (2017). These individual radiographs were averaged in post-acquisition processing using the Grouped ZProjector function in ImageJ v.1.51h. The total scan time was 30 h. Unfortunately, the results for this specimen lacked contrast and could not be used (Appendix 1). In particular, the material is filled with large amounts of ferruginous mineral goethite crystals and glue that blocked the neutron beam.

2.2.2.2 Experimental setup and data reconstruction of BP/1/8500

For BP/1/8500, DINGO was configured in high-intensity mode with a collimation (*L*/*D*) ratio of 500, where *L* is the neutron aperture-to-sample length and *D* is the neutron aperture diameter. Neutrons were converted to photons using a 200 × 200 × 0.030 mm scintillation screen (Gd_2O_2S:Tb, RC Tritec AG) and photons detected by a ZWO ASI2600MM Pro camera (liquid cooled, 16-bit, 6248 × 4176 pixels) coupled with a 50 mm fixed focal length Carl Zeiss lens to achieve a pixel size of 0.040 mm and field-of-view of 200 × 167 mm. A total of 1000 equally spaced radiographs of 8s exposure were acquired as the specimen was rotated 180° about its vertical axis. Total scan time, including the acquisition of bright and dark field images was 200 min. The raw radiographs were spot-filtered and binned to 0.120 mm using ImageJ v1.51h, and tomographic reconstruction of the cleaned 16-bit radiographs was achieved using Octopus Reconstruction v.8.8.

Neutron radioactivation of the specimen was recorded 9 days post-scan using a Canberra Radiagem Survey Meter Dosimeter, yielding a 30s average dose rate on contact of 0.50 mSv/h. After another 3 days, the specimen's activity had decayed to background levels and was subsequently cleared by radiation physics for return.

Tomographic reconstruction of the 16-bit raw data was performed using Octopus Reconstruction v.8.8 (Inside Matters NV), yielding virtual slices perpendicular to the rotation axis. When these slices are stacked in a sequence, they form a three-dimensional volume image of the sample.

2.2.3 Matrix construction for phylogenetic analysis

The specimens described here (BP/1/8740 and BP/1/8500) were included in the pre-existing phylogenetic matrices of Angielczyk et al. (2021) and Duhamel et al. (2024). Mesquite v3.2 (Maddison & Maddison, 2015) was used to score the specimens in the phylogenetic analyses. No taxa or characters were removed from the original matrices. The Angielczyk et al. (2021) matrix is a significant starting point, and it is the matrix used throughout this study as it includes all anomodonts and has more characters while the Duhamel et al. (2024) matrix encompasses the most recent taxonomic revision of *Patranomodon nyaphulii*, *Eodicynodon oosthuizeni*, and *Nyaphulia oelofseni* (previously *Eodicynodon oelofseni*) and has few taxa and characters. The two matrices gave consistent results in terms of where BP/1/8740 and BP/1/8500 are positioned in the phylogeny (see Fig. 14 & Appendix 2).

Modifications made to the data matrix of Angielczyk et al. (2021) include updates to character state codings for *Patranomodon nyaphulii*, *Eodicynodon oosthuizeni*, and *Nyaphulia oelofseni*, and codings for BP/1/8740 and BP/1/8500 (Appendix 4). The final dataset included 116 operational taxonomic units (OTUs) and 174 characters.

These 174 characters are discrete binary or multistate characters (Appendix 3) and were weighted equally. Discrete states with unknown and inapplicable data were coded as '?' (Strong & Lipscomb, 2000).

2.2.4 Phylogenetic analysis

Cladistic analyses were run using TNT 1.1 (May 2014 version) (Goloboff et al. 2008), using two search strategies. The first search strategy used the new technology method of TNT, specifically a driven search. The initial driven search level was set to 65 and checked every five hits. The initial number of addition sequence replicates was 1000, and the search was required to find the trees with the shortest length 20 times. The analysis was run with default settings for sectorial searching, tree fusing, parsimony ratchet, and tree drifting. The second search strategy used the traditional search method of tree bisection reconnection (TBR) branch swapping with 10000 random seeds and 100 trees held per replicate. *Biarmosuchus* was used as the outgroup to root the most parsimonious tree from both analyses as in previous anomodont studies (Castanhinha et al. 2013; Angielczyk et al. 2016; Angielczyk & Kammerer, 2017; Angielczyk et al. 2021).

2.2.5 Body size estimation

Body size estimates for non-mammalian synapsids have not been addressed in detail for anomodonts (Hurlburt, 1999; Blob, 2001; Ray & Chinsamy, 2004). In this study, to estimate the body size, basal skull length (measured from the anteriormost part of the premaxilla to the posteriormost point of the occipital condyles) was used as a proxy for body size as per Angielczyk & Walsh (2008).

This method was chosen because many anomodont specimens comprise only skulls. Measurements were collected from specimens at the Evolutionary Studies

Institute, Iziko Museum, and National Museum. These measurements were taken in millimetres using callipers and measuring tape, depending on the size of the specimen. For specimens that are not curated in the above museum collections, I used the measurements available in the literature. For specimens that had both juvenile and adult specimens, I measured only the specimen with the larger skull length (i.e. the adult specimen). The skull length data was saved as a CSV in Microsoft Excel and is presented in Appendix 5.

The first and last appearance stratigraphic data of anomodont species were taken from the literature (Smith et al. 2020). These stratigraphic ranges were also saved as CSV in Microsoft Excel (Appendix 5). Once the skull length and stratigraphic ranges were collated, they were used to match the tree obtained by the phylogenetic analysis. R-software was used to examine body size changes in anomodonts. R packages used include: *ape*, which functions in manipulating, analysing, simulating phylogenetic trees and analysis of diversification; *phytools*, which performed the phylogenetic comparative analysis including visualisation of trees and fitted models; *paleotree*, which performed the posteriori time-scaling and modifying phylogenies containing extinct lineages; and *geiger*, which fitted macroevolutionary models to phylogenetic trees.

To calibrate the tree, the time-scaling method of Bapst (2014) was used. Accordingly, the cal3-dating method was used to resolve the polytomies (Stanley, 1985; Bapst, 2013; Foote, 2000b, 2001a; Friedman & Brazeau, 2011). To analyse the skull length, which is a continuous trait on the tree, contMap which projected the skull length values onto the tree using a colour gradient was used. To summarise this analysis, I constructed a line plot of log skull length and midpoints of stratigraphic ranges for each taxon with the Lowess (Locally weighted scatterplot smoothing) regression line

fitted (see code in Appendix 6). This regression line is useful as it visualises trends in a scatter plot and identifies underlying patterns without assuming fixed functional forms. It also represents relationships between variables that cannot be accurately represented by a straight line or a basic polynomial function.

CHAPTER 3: GEOLOGY

3.1 Geological background

Specimens BP/1/8740 and BP/1/8500 were found on the farm Combrinkskraal in the Prince Albert district. These specimens were discovered from the uppermost part of the *Eodicynodon* Assemblage Zone of the Beaufort Group (Aldelaide Subgroup, Karoo Supergroup) which correlates to the uppermost Combrinkskraal Member of the Beaufort Group (Fig. 1). This assemblage zone is the lowermost tetrapod biozone of the Beaufort Group (Rubidge, 1990) and forms the lower boundary of the Abrahamskraal Formation (Rubidge, 1990, 2005; Rubidge et al. 1999; Jinnah & Rubidge, 2007; Cole et al. 2016; Rubidge & Day, 2020).

Currently, the *Eodicynodon* Assemblage Zone is recognized only in the south-eastern part of the Beaufort Basin, between the towns of Rietbron in the east and Laingsburg in the west (Jinnah & Rubidge, 2007; Day & Rubidge, 2014). The biozone is thickest in the Prince Albert Road area (1 100m thick) and thins to 320m to the east and west (Jinnah & Rubidge, 2007; Rubidge & Angielczyk, 2009).

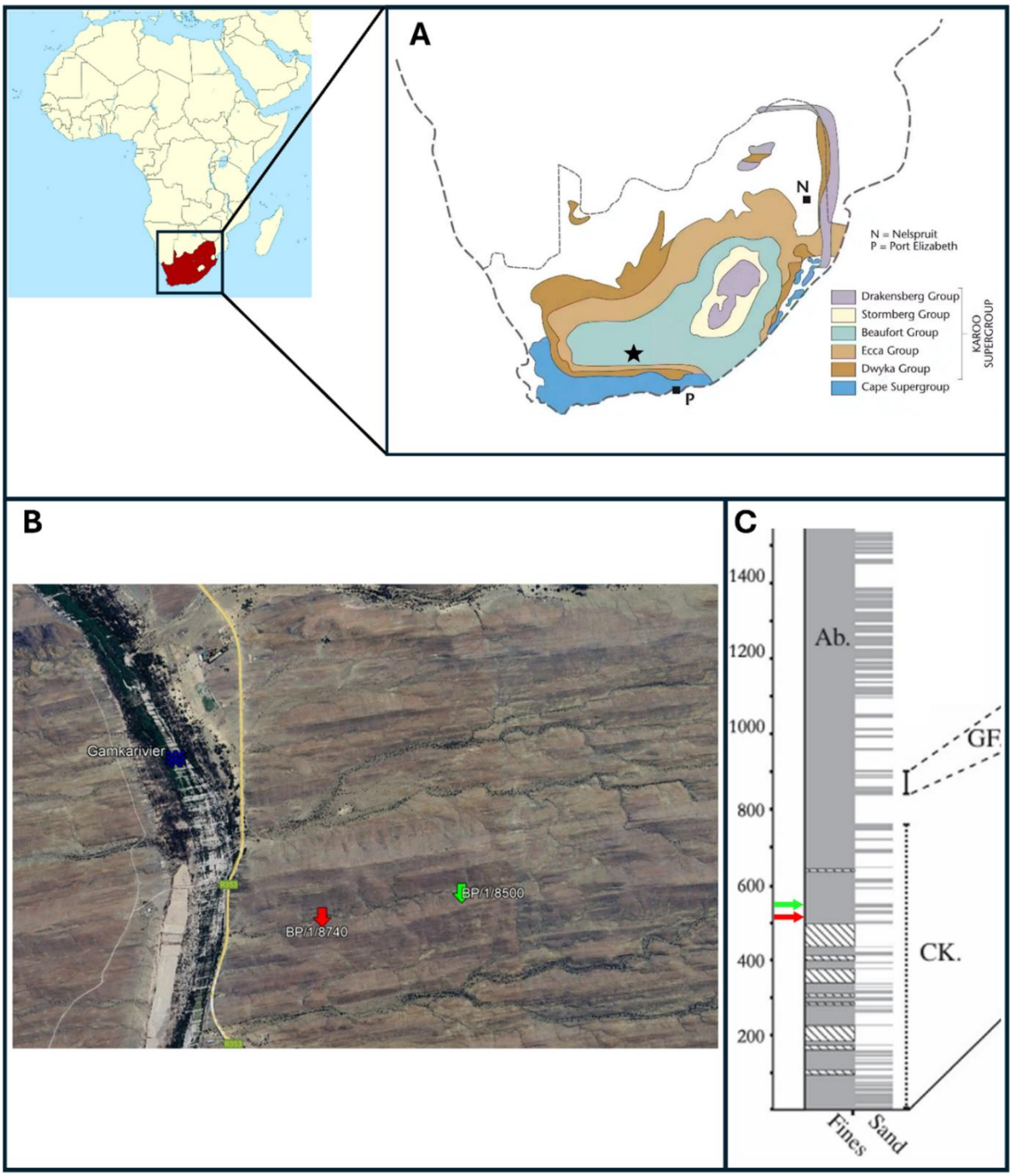


Figure 1: Locality and stratigraphic information for specimen BP/1/8740 and BP/1/8500. **A.** map showing the Karoo Supergroup, **B.** google earth image of the study area showing the locality of BP/1/8740 with a red arrow and BP/1/8500 with a green arrow, **C.** part of the stratigraphic section and thickness of the Abrahamskraal

Formation in the Combrinkskraal area (from Day & Rubidge, 2014). The black star indicates the study area. The red arrow indicates the location of BP/1/8740, and the green arrow indicates the location of BP/1/8500. *Abbreviations*: CK, Combrinkskraal Member; GF, Grootfontein Member; Ab, Abrahamskraal Formation.

3.2 Combrinkskraal Member

The Combrinkskraal Member is the name assigned to the sequence of sandstone packages in the lowermost Abrahamskraal Formation, and the type locality is on Combrinkskraal farm and extends westwards to Verlantenkloof Pass in the Northern Cape (Le Roux, 1985; Cole & Wipplinger, 2001). This member was initially recognised by Le Roux (1985) who defined it as the sandy lower section of the first third-order fining-upward cycle of the Abrahamskraal Formation but provided limited information regarding the thickness and how the unit is distributed. It was later recognised by Loock et al. (1994) to be 550m thick in the Modenaarskaroo region and separated from more younger sandstone packages by definite argillaceous layer; however, his stratigraphic section provided very low lithological resolution (Day & Rubidge, 2014).

Although the Combrinkskraal Member in the Modenaarskaroo is not clearly defined, Day and Rubidge (2014) measured a section on the farm Wilgebos in the Laingsburg district, a locality near Modenaarskaroo, which provided a higher resolution of the stratigraphy in the lower part of the basin. From this work, it is clear that the Combrinkskraal Member reaches a maximum thickness of 750m above the Ecca-Beaufort contact. The strata of the Combrinkskraal Member are intensely folded in the southern margin of the Karoo Basin with high angles of dip (Day & Rubidge, 2014), and the Member thins to the north and northwestern part of the basin. Cole and Wipplingler (2001) recorded this member to be 130m thick at Verlantenkloof to

the northwest. The Combrinkskraal Member is also present in Ouberg Pass, west of Sutherland, and here comprises stacked sandstones with a thickness of 123m and 327m above the base of the Abrahamskraal Formation. However, the correlation of this arenaceous package at Ouberg Pass with the Combrinkskraal member along the southern margin of the basin is open to question (Day & Rubidge, 2014). In the southeastern part of the basin, this member is poorly exposed.

3.3 Boundaries of the *Eodicynodon* Assemblage Zone

This biozone directly overlies the Waterford Formation of the Ecca Group (*sensu* Day & Rubidge, 2014; Rubidge & Day, 2020), which borders the base of the Abrahamskraal Formation. The contact between the Waterford Formation of the Ecca Group and the base of the Abrahamskraal Formation represents the palaeoshoreline of the Ecca sea, i.e. the transition from subaqueous delta front environment to that of the subaerial delta plain (Rubidge, 1987,1990, 2005; Rubidge et al. 1995, 2000; Hancox & Rubidge, 2001; Jinnah & Rubidge, 2007). This boundary coincides with the first appearance of *Eodicynodon oosthuizeni* (Rubidge, 1984, 1988, 1990, 1995; Rubidge et al. 2000; Angielczyk, 2001; Jinnah & Rubidge, 2007; Rubidge & Day, 2020).

The *Eodicynodon* Assemblage Zone underlies the *Eosimops-Glanosuchus* subzone of the *Tapinocephalus* Assemblage Zone, which is characterised by the first appearance of *Eosimops newtoni* (Rubidge & Day, 2020). The upper boundary of the *Eodicynodon* Assemblage Zone is not well-constrained because of the paucity of fossils in the lower Abrahamskraal Formation (Jinnah & Rubidge, 2007; Rubidge & Day, 2020).

3.4 Correlations of the *Eodicynodon* Assemblage Zone

Based on the fossil fauna present, the *Eodicynodon* Assemblage Zone is considered Wordian in age (Rubidge, 2005; Rubidge & Day 2020), and has been correlated with the Dashankou fauna of Xidagou Formation, North China (Olroyd & Sidor, 2018); the lower Isheevo Assemblage, Ocher Subassemblage of the Ocher Assemblage, Mezen Assemblage of Russia (Modesto & Rybczynski, 2000; Sennikov & Golubev, 2017); and parts of the Rio do Rasto Formation of the Parana Basin of Brazil (Langer, 2000; Dias-da-Silver, 2012).

3.5 Palaeoenvironment of the *Eodicynodon* Assemblage Zone

The lowermost biozone of the Beaufort Group (*Eodicynodon* Assemblage Zone) preserves the earliest terrestrial environments of Gondwana (Jirah & Rubidge, 2014; Rubidge & Day, 2020). This distinctive fauna was first recognised by Rubidge (1990), who proposed the name *Eodicynodon* Assemblage Zone after the most abundant vertebrate fossil which occurs in this stratigraphic interval. These tetrapod fossils occur in association with well-preserved fossil remains of *Glossopteris* and the equisetalian *Schizoneura* and are considered to have lived in a subaerial delta plain environment immediately above the stratigraphic position of the palaeoshoreline of the Karoo sea (Rubidge, 1998; Rubidge et al. 2000). The earliest tetrapods to colonise land in southern Africa thus lived between the interdistributary lakes and low sinuosity canals of a subaerial delta plain environment.

CHAPTER 4: RESULTS

4.1 Cranial descriptions

4.1.1 Description of specimen BP/1/8740 (*Patranomodon*)

SYSTEMATIC PALAEONTOLOGY

THERAPSIDA Broom (1905)

ANOMODONTIA Owen (1859)

Definition - The common ancestor of *Biseridens*, *Anomocephalus*, *Patranomodon*, *Galeops*, *Eodicynodon*, *Dicynodon*, and all its descendants (Duhamel et al. 2024).

Genus *Patranomodon* Rubidge & Hopson (1990)

Diagnosis – Following Sidor (2001), the antorbital region is reduced to less than half of the total skull length, zygomatic arch positioned above the upper tooth row margin, completely revealing the quadrate and quadratojugal in lateral view, the squamosal having an extended ventral ramus that supports the quadrate, presence of the mandibular fenestra, upper tooth row diminish in size posteriorly with the upper canine showing little to no differentiation, and the presence of the preparietal.

Species *Patranomodon nyaphulii* Rubidge & Hopson (1990)

Diagnosis – As for the genus.

Material – This description is based on the only two known specimens of *Patranomodon nyaphulii,* which were both found on the farm Combrinkskraal in the Prince Albert district.

The holotype (NMQR 3000) is curated at the National Museum in Bloemfontein, South Africa.

A second specimen of *Patranomodon* (BP/1/ 8740) found in 2021, which is smaller than the holotype, is curated in the collection of the ESI at the University of the Witwatersrand, Johannesburg, South Africa.

Type locality – Combrinkskraal farm, Combrinkskraal Member of the Abrahamskraal Formation. *Eodicynodon* Assemblage Zone, Beaufort Group, Karoo Supergroup, South Africa.

Assessment of ontogenetic status – Specimen BP/1/8740 is interpreted as a juvenile based on several morphological indicators. Some cranial sutures remain open particularly the frontal-nasal suture and prefrontal-nasal suture, suggesting incomplete fusion. The bone surface of the frontal exhibits a finely textured, striated appearance, lacking the smooth and remodeled characteristics present in the holotype of *Patranomodon* (NMQR 3000). Additionally, this specimen possesses a small skull, large orbits, few teeth, and small pineal foramen. The overall skeletal robustness is reduced, with gracile limb elements.

Description – The following description focuses on the skull and partial skeleton of BP/1/8740, which was prepared for this study. The skull is well preserved in that it is not distorted; however, it has suffered a great deal of surface weathering. The lower jaw is still in occlusion with the skull. The following description of BP/1/8740 is based on direct observations, and as this is only the second specimen known of *Patranomodon*, a full description of BP/1/8740 is provided to ensure detailed recording of the cranial anatomy of the specimen. This description includes comparison with the holotype (NMQR 3000) when appropriate. The skull is relatively undistorted, lacks ornamentation and pachyostosis, and has a smooth bone surface. It is 3.8cm long from the tip of the snout to the occiput. It has a short snout and anterolaterally oriented orbits which are larger than the temporal fenestra (Fig. 2).

The *premaxilla* forms the anterior-most part of the snout and part of the external nares. The anterior-most part of the premaxilla is weathered on both sides of the specimen. Laterally, the premaxilla is in contact with the maxilla (Fig. 2), but their suture is not clearly visible. At least two premaxillary teeth are visible on either side of the premaxilla, and even though they are weathered, it appears that the teeth decrease in diameter mesially, unlike in *Anomocephalus* and *Suminia*, in which the premaxillary teeth increase in diameter mesially (Modesto et al. 1999).

The premaxillary teeth are peg-like and slightly project forward , as in *Anomocephalus*, *Galechirus*, and *Suminia* (Brinkman, 1981; Rybczynski, 2000) but differ from the condition in *Galepus* in which the premaxillary teeth are vertical, and *Galeops* which has an edentulous premaxilla (Brinkman, 1981). In ventral view, the palatal process of the premaxilla is not visible, and the premaxilla contacts the vomers posteromedially. This contact is similar to the interdigitating contact present in the holotype of *Patranomodon* (Rubidge & Hopson, 1996). This specimen does not have a secondary palate, similar to the condition in the holotype of *Patranomodon*, and also *Ulemica*, *Otsheria*, and *Biseridens*, but differs from the condition in *Eodicynodon* and more derived dicynodonts (Rubidge & Hopson, 1996). In *Anomocephalus* (Modesto et al. 1999) and *Tiarajudens* (Cisneros et al. 2011), a secondary palate is also not present . The ascending process of the premaxilla is not exposed in BP/1/8740.

The *maxilla* is a large element forming the lateral side of the snout and the anterior part of the zygomatic arch. The bone surface of the maxilla on the left is weathered, and on the right side, the posterior part of the maxilla is well preserved. Anteriorly, the maxilla contacts the premaxilla, but their sutural contact is not clearly visible. Because of weathering of the bone surface, it is difficult to determine whether the

maxilla contributes to the external nares. Posterodorsally, the maxilla does not contact the prefrontal. Posteriorly, it is in contact with the lacrimal, and this suture is at the same level as the last postcanine (Fig.

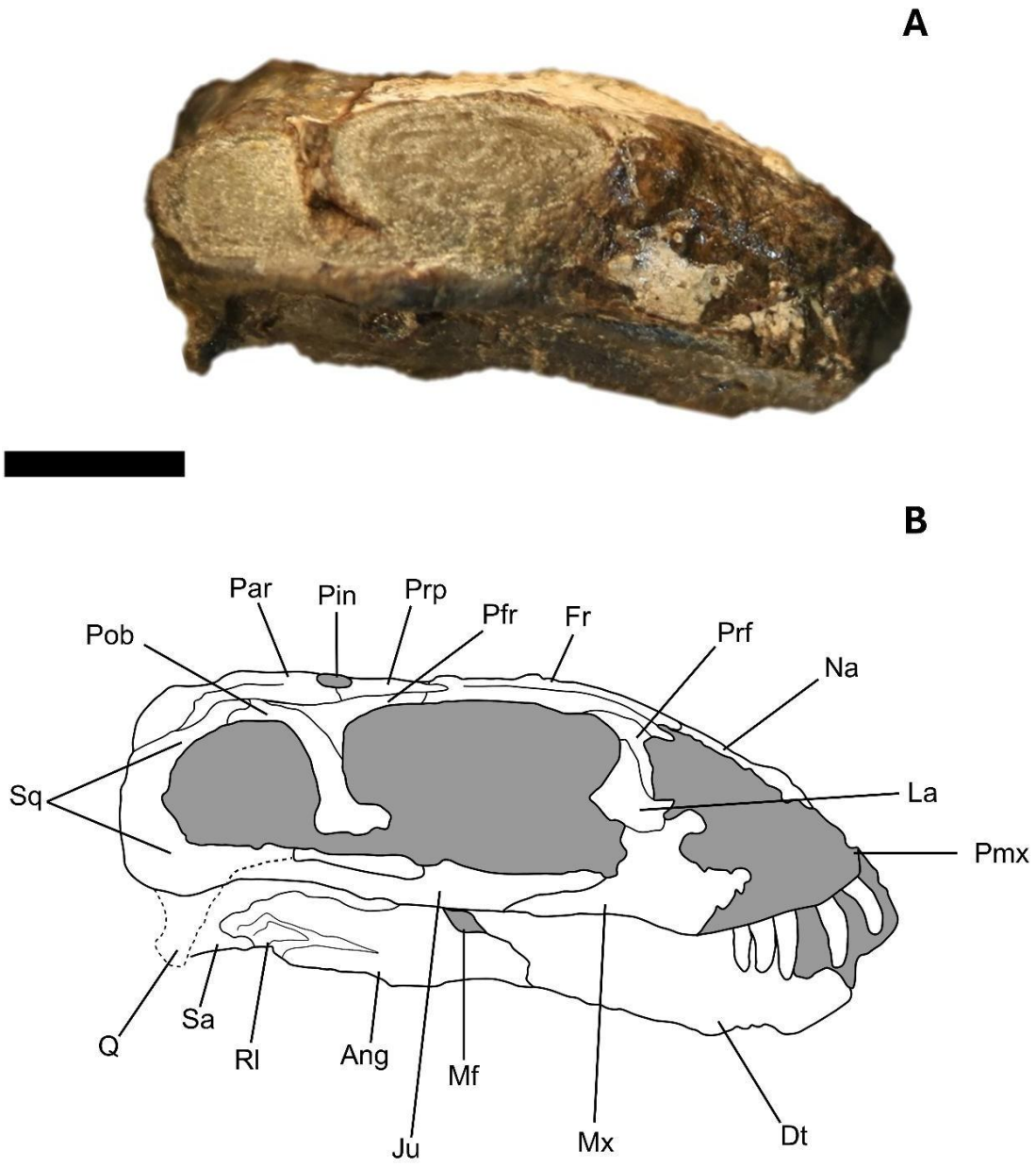


Figure 2: Right lateral view of BP/1/8740. **A**. Photograph; **B**. line illustration with bone labels *Abbreviations:* Pin, pineal foramen; Pob, postorbital bar; Fr, frontal; Pfr, postfrontal; Prp, preparietal; Par, parietal; Na; nasal; Prf, prefrontal; La, Lacrimal; Pmx, premaxilla; Dt, dentary; Mx, maxilla; Mf, mandibular fenestra; Ju, jugal; Ang, angular; Rl, reflected lamina; Sa, surangular; Q, quadrate; Sq, squamosal. Scale bar is 3cm.

The zygomatic process of the maxilla extends posteriorly to form the anteroventral border of the suborbital bar. This zygomatic process of the maxilla extends posteriorly along the ventral margin of the jugal and tapers at about the middle of the orbit (Fig. 2). In ventral view, it is difficult to identify the maxillary processes as the jaws are occluded, but the maxilla is not involved in a secondary palate. On the right side, three maxillary teeth are preserved, and two on the left.

The *nasal* forms the anterodorsal part of the snout even though most of it is weathered on the right side (Fig. 3). This element appears to form the lateral margins of the dorsal process of the premaxilla, although its contact with the premaxilla is unclear and appears to meet the premaxilla anteromedially. The nasal on the left side is almost complete and extends posteriorly to meet the frontal at the level of the anterior border of the orbit, similar to that seen in the holotype of *Patranomodon* and *Suminia* (Rubidge & Hopson, 1996; Rybczynski, 2000). The nasal and frontal share a V-shaped suture (Fig. 3), similar to the condition in the holotype of *Patranomodon* (Rubidge & Hopson, 1996; Duhamel et al. 2024). Laterally, the nasal is in contact with the maxilla, but the suture is not visible. Posteroventrally, it contacts the prefrontal as in the holotype of *Patranomodon* (Rubidge & Hopson, 1996).

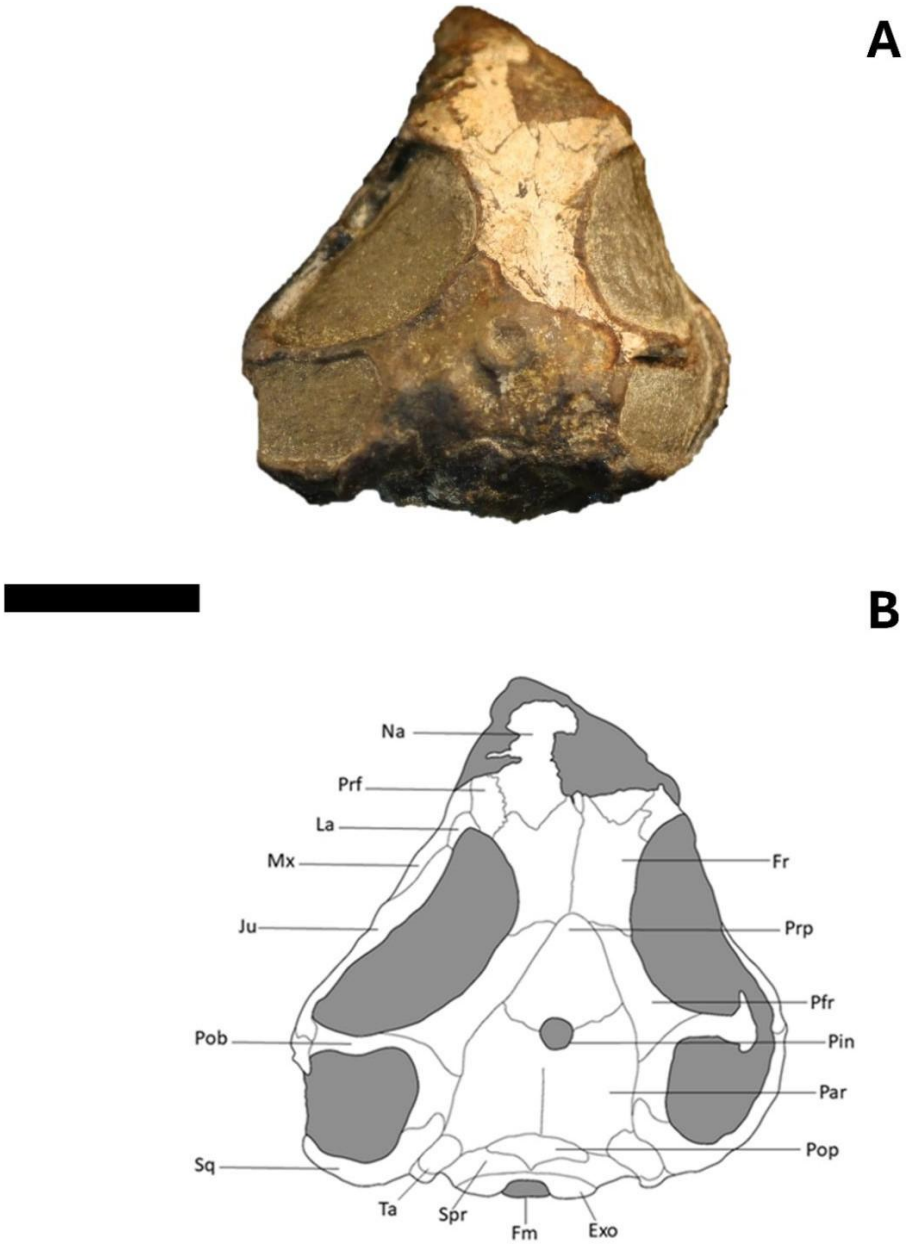


Figure 3: Dorsal view of BP/1/8740. **A**. Photograph; **B**. line illustration with bone labels. *Abbreviations*: Na, nasal; Prf, prefrontal; La, lacrimal; Fr, frontal; Mx, maxilla; Ju, jugal; Pin, pineal foramen; Prp, preparietal; Pfr, postfrontal; Pob, postorbital bar; Par, parietal; Pop, postparietal; Sq, squamosal; Ta, tabular; Spr, supraoccipital; Exo, exoccipital; Fm, foramen magnum. Scale bar is 3 cm.

The *lacrimal* is a roughly triangular element forming the anterior border and a short portion of the anteroventral rim of the orbit (Fig. 2). It is better preserved on the left side than on the right. Dorsally, the lacrimal contacts the prefrontal along a straight short suture. Anteriorly and ventrally, it contacts the maxilla. Posteroventrally, it meets the jugal, and their sutural contact runs for 0.7cm obliquely below the orbit. In lateral view, the lacrimal is slightly concave, forming a fossa anterior to the orbit, similar to the condition in *Biseridens* (Liu et al. 2010); however, this feature is not present in other early anomodonts (Sidor & Welman, 2003; Rubidge et al. 2006) and its function is unknown (Liu et al. 2010). The lacrimal foramen is not preserved on either side of this specimen and is also absent in the holotype of *Patranomodon* (Duhamel et al. 2024).

The *jugal* is the largest bone of the suborbital bar. It forms the ventral and posteroventral margins of the orbit and the anteroventral border of the temporal fenestra (Fig. 2). The right jugal is better preserved than the left. Anteriorly, the jugal meets the lacrimal along the anteroventral margin of the orbit and excludes the maxilla from contacting the orbital margin. Posteriorly, the jugal rises to form the postorbital process of the jugal, which contacts the postorbital bar at the posteroventral point of the orbital margin. In dorsal view, the jugal curves anteriorly on the ventral side of the orbit and tapers posteriorly. The jugal meets the squamosal posteriorly but this contact is not clear.

The *postorbital* is a slender curved bone making up the entire postorbital bar and part of the skull roof. The left postorbital is complete and well-preserved, but the right one has been damaged by weathering (Fig. 3). The postorbital forms the anterior and anterodorsal borders of the temporal fenestra and separates the temporal fenestra from the orbit. Ventrally, this element reaches the jugal and the zygomatic

arch along an oblique suture. Dorsally, the postorbital extends onto the skull roof and forms the anterior half of the dorsal border of the temporal fenestra (Fig. 3). Anterodorsally, at the posterodorsal end of the orbit, the postorbital has a short sutural contact with the postfrontal. Medially, the postorbital has a long sutural contact with the parietal on the skull roof and posteriorly meets the squamosal with a short interdigitating suture.

The *squamosal* is a triradiate element forming the posteroventral, posterodorsal, and posterior margin of the temporal fenestra. The left squamosal is missing the zygomatic process as this was broken as a result of weathering (Fig. 3). In occipital view, the dorsal process of the squamosal is covered by the tabular and supraoccipital. The squamosal is not flared, similar to the condition in the holotype of *Patranomodon* (Rubidge & Hopson, 1996), providing no attachment area for the lateral external adductor muscle on the dorsal and posterior surface of the squamosal. Dorsally, the squamosal is gently curved instead of being folded, and it forms the posterodorsal border of the temporal fenestra. Anterodorsally, it contacts the postorbital as is the case in dicynodonts, the holotype of *Patranomodon* (Rubidge & Hopson, 1996), and *Suminia* (Rybczynski, 2000). Anteroventrally, the squamosal contacts the jugal, but their sutural contact is not clear.

The *prefrontal* is a roughly triangular bone forming the anterodorsal margin of the orbit. It is not pachyostotic, and it differs from *Suminia*, *Ulemica*, and *Otsheria* as they have pachyostotic prefrontals (Tchudinov, 1983; King, 1988; Rybczynski, 2000). The left prefrontal is almost complete and well preserved whereas the right one is completely weathered (Fig. 3). As the contact between the prefrontal and maxilla is not visible, it is unclear as to how far the prefrontal extends anteriorly but possibly extends halfway to the external nares as in *Suminia* and the holotype of

Patranomodon (Rubidge & Hopson, 1996; Rybczynski, 2000). This is the condition present in all primitive therapsids, sphenacodontids (Hopson & Barghusen, 1986), and other Russian basal anomodonts (Tchudinov, 1983). Posteromedially, the prefrontal meets the frontal along a short interdigitating suture that is well exposed on the left side of the specimen (Fig. 3). Anterodorsally, the prefrontal meets the nasal along an oblique suture. Ventrally, the prefrontal meets the lacrimal along a straight suture.

The *frontal* contributes to most of the dorsal border of the orbit and forms a significant portion of the skull roof between the orbits. It contacts the nasals anteromedially with a V-shaped suture (Fig. 3). Anterolaterally, the frontal contacts the prefrontal along a short interdigitating suture, which is an extension of the V-shaped suture connecting the frontal with the nasal. The frontals share a midline suture, but it is unclear whether it runs along the entire length of the bones, while in the holotype of *Patranomodon* the midline suture is straight and runs along the entire length of the frontal (Duhamel et al. 2024). Posteriorly, it is unclear where the frontal contacts the postorbital as it appears to form a continuous co-ossified structure with the postorbital bar. The frontal contacts the preparietal posteriorly but this suture is not clear. Posterolaterally, the frontal is in contact with the postfrontal along a curved suture.

The *postfrontal* is an elongated and roughly triangular bone forming the dorsal margin of the orbit. Anteriorly, it contacts the frontal along a short horizontal suture, and anteromedially, it has a straight sutural contact with the preparietal. Posteromedially, the postfrontal contacts the parietal along a slightly curved suture, and posteriorly, it contacts the postorbital bar but this suture is unclear.

The *preparietal* is a prominent element forming the anterior border of the pineal foramen (Fig. 3). It has a less pronounced triangular process extending anteriorly between the frontals (Fig. 3). This bone is rare among basal anomodonts (Broom, 1914; Rubidge & Hopson, 1996) and is more common in dicynodonts. It is present in the holotype of *Patranomodon* (Rubidge & Hopson, 1996) and possibly *Galeops* (Brinkman, 1981), but absent in *Otsheria*, *Venyukovia* (Tchudinov, 1960, 1980), *Suminia* (Rybczynski, 2000), and it cannot be confirmed in *Galepus* (Brinkman, 1981) due to the obliteration of sutures. This element is not preserved in *Anomocephalus* (Modesto et al. 1999). In BP/1/8740, the preparietal forms a rather low blunt boss, a feature which is not present in the holotype of *Patranomodon* (Rubidge & Hopson, 1996) and *Galeops* (Brinkman, 1981). The preparietal contacts the parietal posterolaterally along an interdigitating suture.

The *parietal* occupies a significant portion of the intertemporal region of the skull, including the posterior and lateral borders of the pineal foramen (Fig. 3), and forms the transition between the occiput and the skull roof. A straight midline suture extends from the posterior margin of the pineal foramen to the anterodorsal border of the postparietal. A similar suture is also present in the holotype of *Patranomodon* and *Suminia* and divides the left and right parietals posterior to the pineal foramen. On either side of this suture, the parietal bears a shallow longitudinal depression, a condition similar to the holotype of *Patranomodon* (Rubidge & Hopson, 1996), *Galepus*, and *Galeops* (Brinkman, 1981). The parietal contacts the preparietal anteriorly, the postorbital bar anterolaterally, and the squamosal posterolaterally, but their sutural contacts are unclear. Posteriorly, it meets the postparietal and tabular along a short, curved suture on the occipital surface. The anterior surface of the pineal is formed by the frontal, and the parietals constitute its lateral and posterior

margins. In dorsal view, the parietal has shallow depressions on both sides of the specimen around the pineal foramen.

The *postparietal* is a small unpaired bone located immediately posterior to the parietal (Figs. 3 & 4). This element lies transversely across the skull. In posterior view, the dorsal aspect of this element overlaps with the parietal. Ventrally, the postparietal overlaps with the supraoccipital. Laterally, it contacts the tabular, but their contact is unclear.

The occiput of BP/1/8740 is not well preserved and has a smooth external surface without ornamentation and is thus similar to the holotype of *Patranomodon* (Rubidge & Hopson, 1990). The foramen magnum is rounded and dorsally bordered by the supraoccipital and laterally by the exoccipital (Figs. 3 & 4). The state of preservation of the occiput suggests that the basioccipital is preserved, but its borders are not exposed. A post-temporal foramen is present on the occiput, similar to the condition described in the holotype of *Patranomodon*, where post-temporal openings are dorsally bordered by the tabular and squamosal laterally, supraoccipital medially, and opisthotic ventrally (Rubidge & Hopson, 1996; Duhamel et al. 2024).

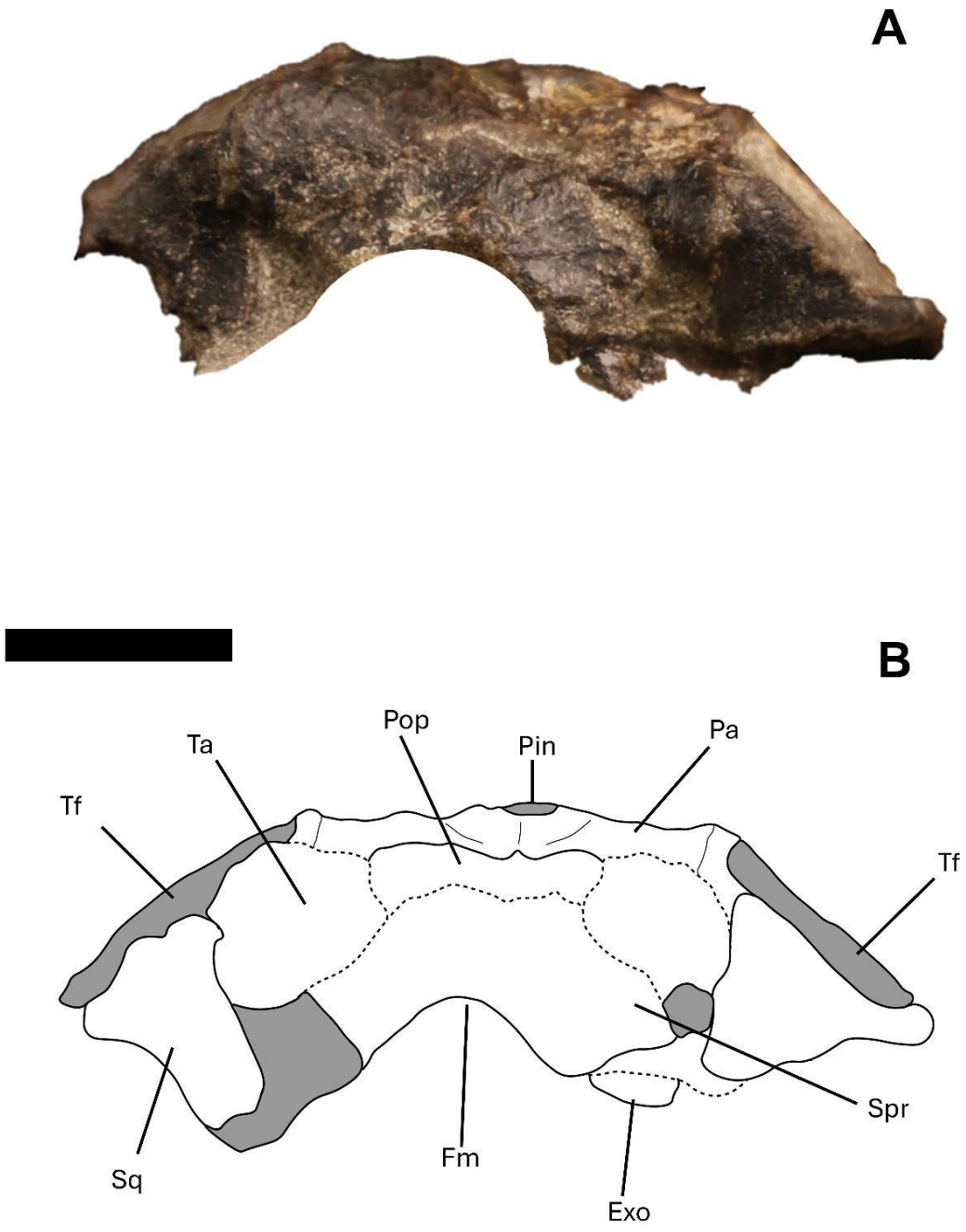


Figure 4: Occipital view of BP/1/8740. **A**. Photograph; **B**. line illustration with bone labels. *Abbreviations*: Pin, pineal foramen; Pob, postorbital bar; Pa, parietal; Pop, lpostparietal; Sq, squamosal; Ta, tabular; Spr, supraoccipital; Exo, exoccipital; Fm, foramen magnum; Tf, temporal fenestra. Scale bar is 3 cm.

The *tabular* is present on the dorsolateral side of the occiput (Fig. 4) and is well preserved on both sides of the specimen. This element overlaps the posterolateral part of the parietal along the posteromedial edge of the temporal opening, and laterally, it overlies the medial aspect of the squamosal. Ventrally, the tabular shares a short transverse suture with the supraoccipital and contributes to the dorsolateral border of the postemporal opening. This element differs from the tabular in *Suminia* (Rybczynski, 2000) and *Otsheria* (Tchudinov, 1983), where it is L-shaped. In the holotype of *Patranomodon* the tabular is roughly rectangular, and it is a large sheet-like bone which is similar to that of basal therapsids (Rubidge & Hopson, 1996).

The *supraoccipital* is an unpaired bone that forms the semicircular dorsal border of the foramen magnum (Fig. 4). This element is broad and is the largest occipital bone in anomodonts (Rubidge & Hopson, 1996; Fröbisch & Reisz, 2008; Duhamel et al. 2024). Dorsally, the supraoccipital is overlapped by the postparietal, and dorsolaterally, it forms a straight contact with the tabular (Fig. 4). In posterior view, the supraoccipital contacts the exoccipital and meets the opisthotic ventromedially, however, their suture is unclear. This condition is similar to that exhibited by the holotype of *Patranomodon* as the opisthotic meets the supraoccipital ventrally and prevents it from making contact with the squamosal (Rubidge & Hopson, 1996). However, in *Suminia* the supraoccipital directly forms a short contact with the squamosal (Rybczynski, 2000). Laterally, the supraoccipital forms a diagonal margin bordering the postemporal fenestra.

The *exoccipital* is a small oval element forming the ventrolateral border of the foramen magnum (Fig. 4). This element is not fused to any surrounding bones ventral to it, and it is difficult to tell its relationship with the basioccipital as it is masked by an attached vertebra. Dorsally, the exoccipital is in contact with the

supraoccipital, but the nature of this contact is unclear. The contact with the opisthotic is also unclear, but it probably has a C-shaped contact as in *Otsheria*, the holotype of *Patranomodon*, and *Suminia* (Rubidge & Hopson, 1996; Rybczynski, 2000; Modesto & Rybczynski, 2001).

The *quadrate* is a small bone contacting the anterior surface of the squamosal and is best preserved on the right side. It comprises a dorsal plate and a ventral trochlea. The dorsal plate is flat and broad and has a concave posterior surface where it contacts the anterior surface of the squamosal ascending process. As the trochlea of the quadrate is preserved in articulation with the articular bone of the lower jaw, it is difficult to determine the morphology of the articulatory surface. On the medial side, the quadrate is met by the quadrate ramus of the pterygoid. The quadratojugal bone in BP/1/8740 and *Galepus* (Broom, 1914) is lost due to weathering, while in the holotype of *Patranomodon* (Rubidge & Hopson, 1996), *Anomocephalus* (Modesto et al. 1999), *Tiarajudens* (Cisneros et al. 2011), *Biseridens* (Liu et al. 2010), and *Suminia* (Rybczynski, 2000) it is still present.

The palatal surface is very delicate, and both mechanical and acid preparation were used to expose palatal features of BP/1/8740. From the palatal elements exposed, the palate of BP/1/8740 looks like that of the holotype of *Patranomodon*. The CT scans of this newly discovered specimen were not workable as the material is filled with large amounts of ferruginous mineral goethite crystals and glue (Appendix 1). The following description is based on bones that are visible. A notable feature is the complete absence of palatal teeth.

The *vomers* are paired elongated structures in the palate with a prominent ventral midline trough, which runs from the anterior end of the premaxilla to where the

vomer ends (Fig. 5). The vomer forms the medial and posterior margins of the choana. A midline vomerine suture is present similar to all basal anomodonts, and even sometimes in juvenile dicynodonts this suture remains open (Brinkman, 1981; King, 1988; Rubidge & Hopson, 1990; Rybczynski, 2000). This feature is also present in adult *Eodicynodon*, and it is considered a primitive character (Rubidge, 1990). The ventral plate of the vomer is not visible as it is obscured by the mandible. However, in the holotype of *Patranomodon*, the vomer reaches the premaxillary palatal process anteriorly (Rubidge & Hopson, 1996; Duhamel et al. 2024). Posteriorly, the vomer borders the interpterygoid vacuity, and its contact with the palatine is not visible due to the lower jaw.

The *palatine* of BP/1/8740 is not exposed. It is masked by the lower jaw in ventral view and thus cannot be described here. Attempts at CT examination (using neutron and X-ray scanning) have failed. It may have been similar to that of the holotype of *Patranomodon* (Rubidge, 1990; Rubidge & Hopson, 1996; Duhamel et al. 2024).

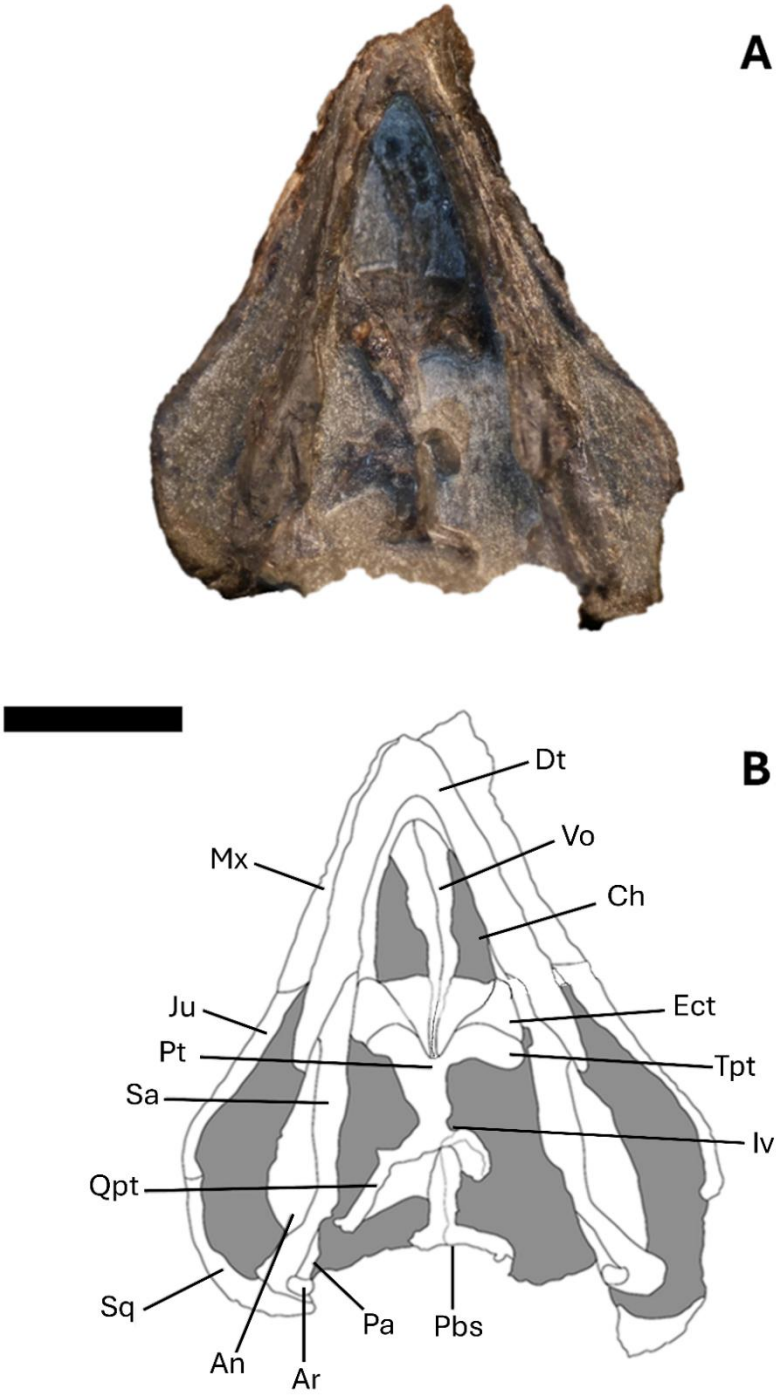


Figure 5: Ventral view of BP/1/8740. **A**. Photograph; **B**. line illustration with bone labels. *Abbreviations*: Mx, maxilla; Ju, jugal; Dt, dentary; Vo, vomer; Ch, choana; Pal, palatine, Pt, pterygoid; Ect, ectoperygoid; Tpt, transverse process of pterygoid; Sa, surangular; Qpt, quadrate process of pterygoid; Sq, squamosal; An, angular; Ar, articular; Pa, prearticular; Pbs, parabasisphenoid; Iv, interpterygoid vacuity. Scale bar is 3cm.

The *ectopterygoid* is a triangular element in the palate forming the anterolateral margin of the transverse process of the pterygoid (Fig. 5). Anteromedially, it is in contact with the vomer along an oblique suture. Posteriorly, it contacts the pterygoid along a curved suture. In specimen BP/1/8740, the ectopterygoid is edentulous, which differs from the condition in *Tiarajudens* which have teeth on the ectopterygoid (Cisneros et al. 2011). The contact between the ectopterygoid and the palatine is not visible as the lower jaw obscures the palatine.

The *pterygoids* are paired and form most of the posterior part of the palate. This element comprises three processes: the anterior process, transverse process, and quadrate ramus. The anterior process meets the posterior extension of the vomer medially (Fig. 5); this is similar to the condition in the holotype of *Patranomodon*, *Biseridens*, and *Suminia* (Rubidge & Hopson, 1996; Rybczynski, 2000; Liu et al. 2010). Anterolaterally, the pterygoid forms a transverse flange which has a flat triangular lateral surface near the inside of the mandible. This surface is preserved in the holotype of *Patranomodon* (Rubidge & Hopson, 1996), *Ulemica* (Tchudinov, 1983), and *Suminia* (Rybczynski, 2000), and its function may have been to brace the lower jaw in occlusion. The transverse process contacts the ectopterygoid anteriorly.

Posterior to the transverse flange, the pterygoid narrows just anterior to the quadrate rami, as in the holotype of *Patranomodon* (Rubidge & Hopson, 1996). Parts of the interpterygoid vacuity in specimen BP/1/8740 are present however their morphology and extent are not intact. The quadrate ramus originates in front of the anterior margin of the parabasisphenoid. In ventral view, the ramus appears as a thin, blade-like structure that is posterolaterally oriented. A narrow ridge is present on the lateral margin of the ramus , similar to that seen in the holotype of *Patranomodon*, and also *Ulemica*, and *Suminia* (Barghusen, 1976; Rubidge & Hopson, 1996; Rybczynski,

2000), and it could have served as an additional surface for the attachment of posterior pterygoid muscle (Rubidge & Hopson, 1996; Rybczynski, 2000). In ventral view, the pterygoid surface between the quadrate ramus and parabasisphenoid is deeply concave. This concavity is also present in the holotype of *Patranomodon* (Rubidge & Hopson, 1996; Duhamel et al. 2024), *Ulemica* (Tchudinov, 1983), and *Suminia* (Rybczynski, 2000).

The *parabasisphenoid* appears to be formed by the fusion of the parasphenoid and the basisphenoid into a single element. As a result of poor CT scans, it is difficult to investigate this element further. In the holotype of *Patranomodon*, the basisphenoid and parasphenoid are separate elements (Duhamel et al. 2024). In specimen BP/1/8740, this element is narrow and extends posteriorly, where it forms two projections that are obtusely directed posterolaterally (Fig. 5), similar to the condition in *Suminia* (Rybczynski, 2000)

The lower jaw is slender and consists of the dentary, angular, splenial, and surangular elements, but the coronoid is absent. The lower jaw of BP/1/8740 has a mandibular fenestra, as in all anomodonts.

The *dentary* forms the anterior half of the mandible (Fig. 2). Unlike in *Galechirus*, *Suminia*, *Biseridens*, and *Anomocephalus*, the dentaries are fused anteriorly, and this is a similar condition described in the holotype of *Patranomodon*, *Ulemica*, and *Galeops*. The dentary is not heavily pitted, unlike the condition in *Galechirus* and *Galeops* (Brinkman, 1981), suggesting that a keratinous beak was not present (Benoit et al. 2018). The dentary has a lateral dentary shelf which forms the dorsal border of the mandibular fenestra, similar to the condition in *Suminia*. A lateral

dentary shelf is also present in *Suminia*, *Ulemica*, the holotype of *Patranomodon*, and some dicynodonts (King, 1988; Rybczynski, 2000). This feature is absent in *Biseridens*, *Galeops*, and *Anomocephalus* and not preserved in *Tiarajudens*, *Galechirus*, and *Galepus.* The dentary extends posterodorsally behind the level of the mandibular fenestra as in the holotype of *Patranomodon* (Rubidge & Hopson, 1996) and forms the anterior and ventral sides of the mandibular fenestra. In lateral view, it is difficult to determine if it overlies the surangular. Because the jaws are tightly occluded, it is impossible to determine whether teeth are present in the dentary.

The *angular* is the bone forming the posterior end of the lower jaw. This bone forms a less prominent reflected lamina extending below the jaw. The angular is overlapped by the dentary anteriorly (Fig. 2). Ventromedially, the angular is overlapped by the splenial on the anterior side. Posteriorly and posteroventrally, it is overlapped by the prearticular. The angular forms the posterior border of the mandibular fenestra.

The *splenial* is a thin flat bone covering the ventromedial part of the lower jaw. This element continues posteriorly below the mandibular fenestra. It contacts the dentary anteroventrally along the ventral margin of the dentary with a short straight suture (Fig. 2). Anteriorly, the splenial becomes narrow, and it seems to contribute to the formation of the mandibular symphysis. The posterior border of the splenial contacts the angular; however, their suture is unclear.

Postcranium.

Several postcranial elements are preserved in articulation with the skull (Fig. 6), namely, cervical vertebrae, the right humerus, and the pectoral girdle.

The cervical series consists of five cervical vertebrae (Figs. 6 & 7). These vertebrae are regarded as cervicals because the intercentrum is preserved between the atlas and axis. In dorsal view, the cervicals are subrectangular in shape, with the cervical centra relatively longer compared to their width (Fig. 7). The transverse processes are short and posterolaterally oriented. The last cervical vertebrae differ from the other cervicals in that the centra is as long as it is wide, and the pre- and postzygapophysis are larger than in other cervicals. This last vertebra is considered a cervical because in *Galechirus* (Brinkman, 1981) and *Patranomodon* (Rubidge & Hopson, 1996) there are 5 cervical vertebrae.

The neural spines are oriented slightly forward, and their dorsal ends are slightly curved. The prezygapophysis elongates anteriorly over the posterior part of the preceding centrum. The postzygapophysis elongates slightly over the succeeding centrum. In BP/1/8740, the ventral surface of the vertebra is not sufficiently exposed, and it is difficult to identify if the cervicals had a longitudinal midventral ridge as has been reported for *Patranomodon* (Rubidge & Hopson, 1996) and *Galechirus* (Brinkman, 1981).

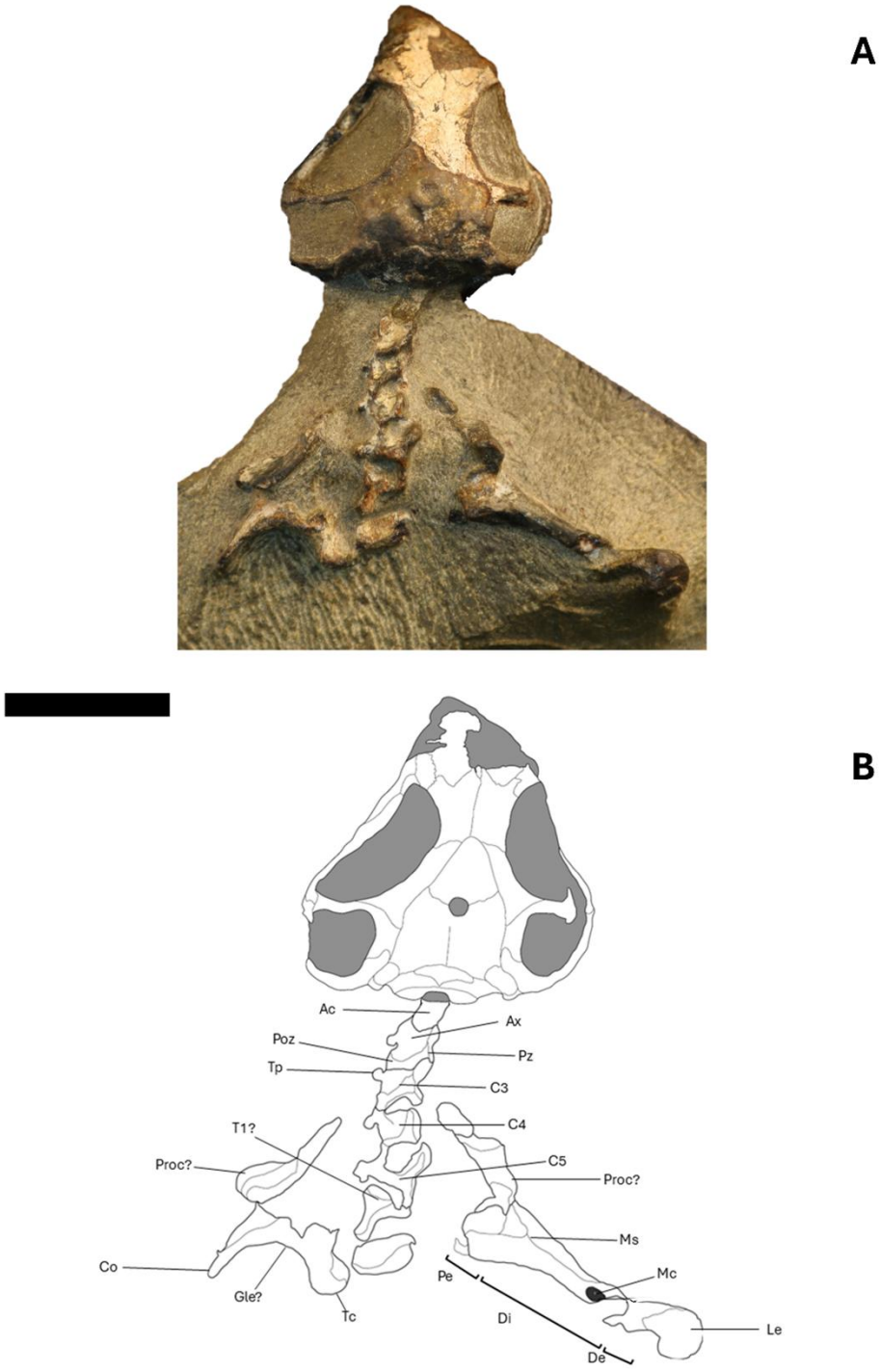


Figure 6: Skull and postcranial elements of BP/1/8740 in dorsal view. **A**. Photograph; **B**. line illustration with bone labels *Abbreviations*: Ac, atlas; Ax, axis; Pz, prezygapophysis; Poz, postzygapophysis; Tp, transverse process; C3, third cervical; C4, fourth cervical; C5, fifth cervical; T1, first thoracic; Proc, procoracoid; Co, coracoid; Gle, glenoid; Tc, tuber coracoidens; Pe, proximal epiphysis; Di, diaphysis;

De, distal epiphysis; Mc, medullary cavity; Ms, medial supracondylar; Le, lateral epicondyle. Scale bar is 3cm.

The humerus is generally well preserved (Figs. 6 & 8), but part of the distal shaft is weathered and only the lateral epicondyle and the capitulum of the distal portion are preserved. The total length of the humerus from the proximal head to the distal head is 30mm. The proximal epiphysis is slightly broader than the distal epiphysis. Proximally, the humerus is in articulation with the glenoid via the glenohumeral joint.

The pectoral girdle of BP/1/8740 only has the *scapula* preserved, consisting of the procoracoid, coracoid, glenoid, and tuber coracoidens (Figs. 6 & 9). This element has an overall slender morphology (Fig. 9) with a narrow dorsal blade, and the ventral plate is not visible as it is not yet prepared. The glenoid is rounded and is posterolaterally oriented, similar to that of *Suminia.* This differs from the screw-shaped morphology of the glenoid of basal synapsids (Fröbisch & Reisz, 2011). In BP/1/8740, an acromion process is not present, as is the condition in other basal anomodonts such as *Galeops*, *Galechirus*, and *Suminia.* However, its presence has been noted in *Eodicynodon* (Rubidge et al. 1994). The procoracoid and coracoid are not visible ventrally, but they may possibly be exposed by further preparation in the future.

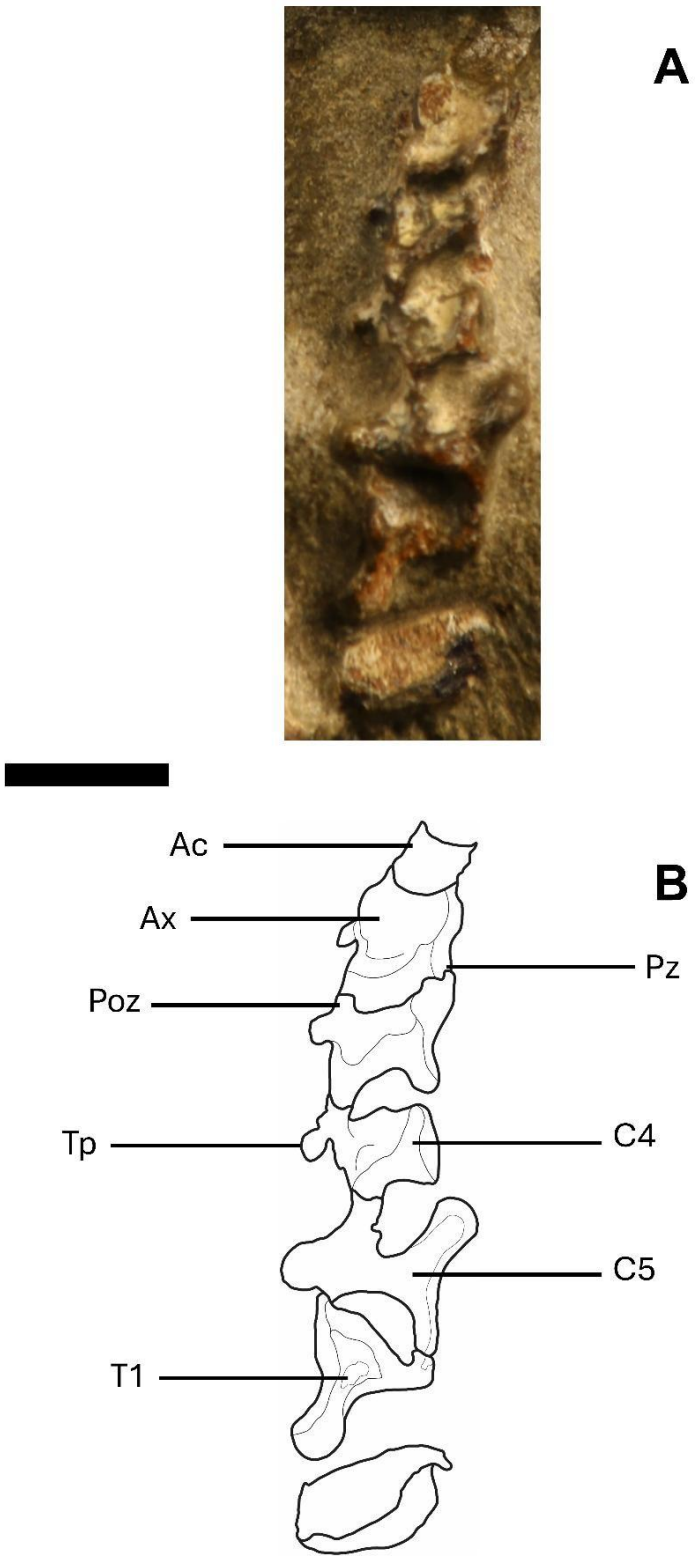


Figure 7: Vertebrae of BP/1/8740 in dorsal view. **A**, photograph; **B**, illustration. *Abbreviations*: Ac, atlas; Ax, axis; Pz, prezygapophysis; Poz, postzygapophysis; Tp, transverse process; C3, third cervical; C4, fourth cervical; C5, fifth cervical; T1, first thoracic. Scale bar is 3cm.

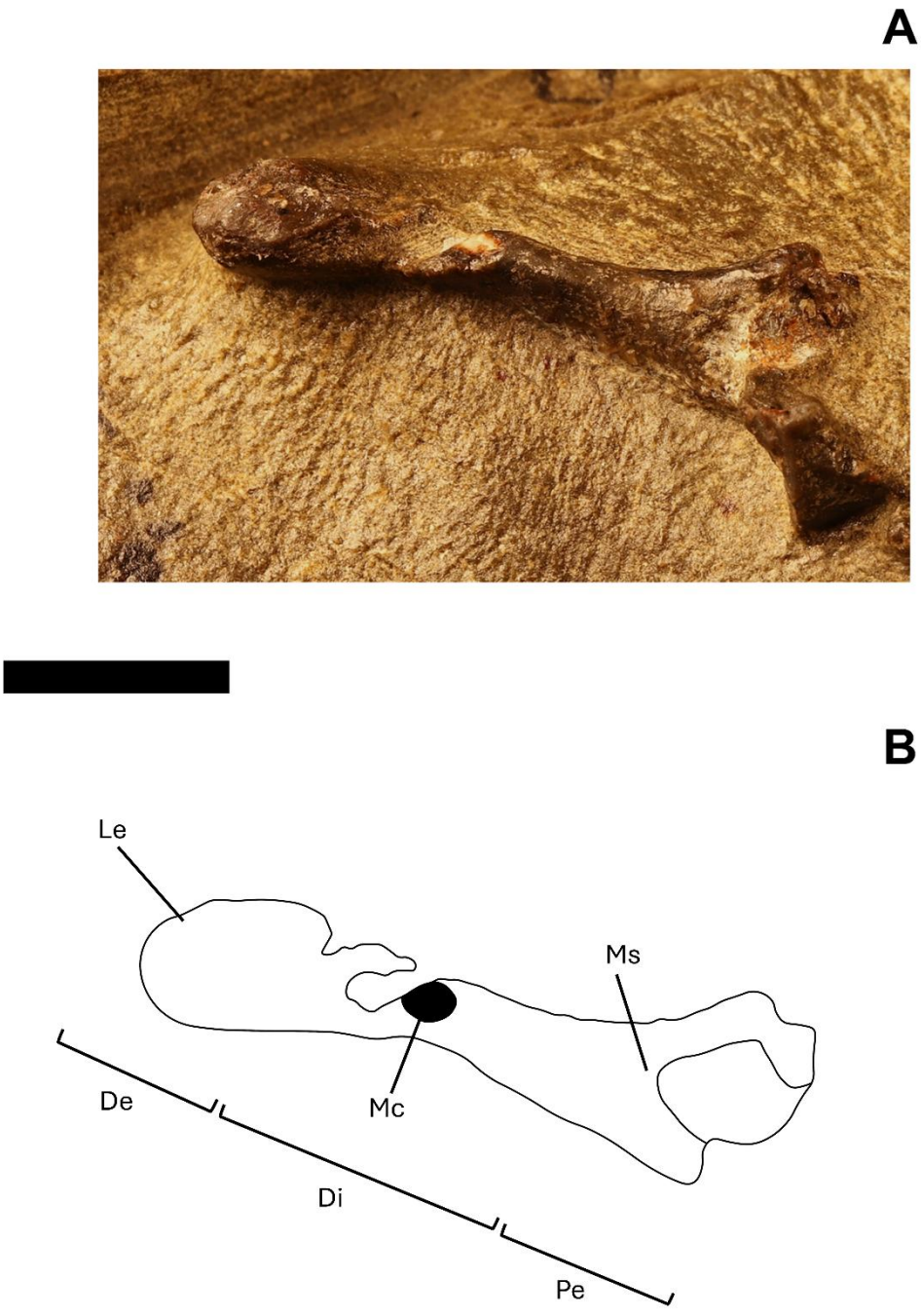


Figure 8: Humerus of BP/1/8740 in oblique view. **A**. Photograph; **B**. line illustration with bone labels *Abbreviations*: Pe, proximal epiphysis; Di, diaphysis; De, distal epiphysis; Mc, medullary cavity; Ms, medial supracondylar; Le, lateral epicondyle. Scale bar is 3cm.

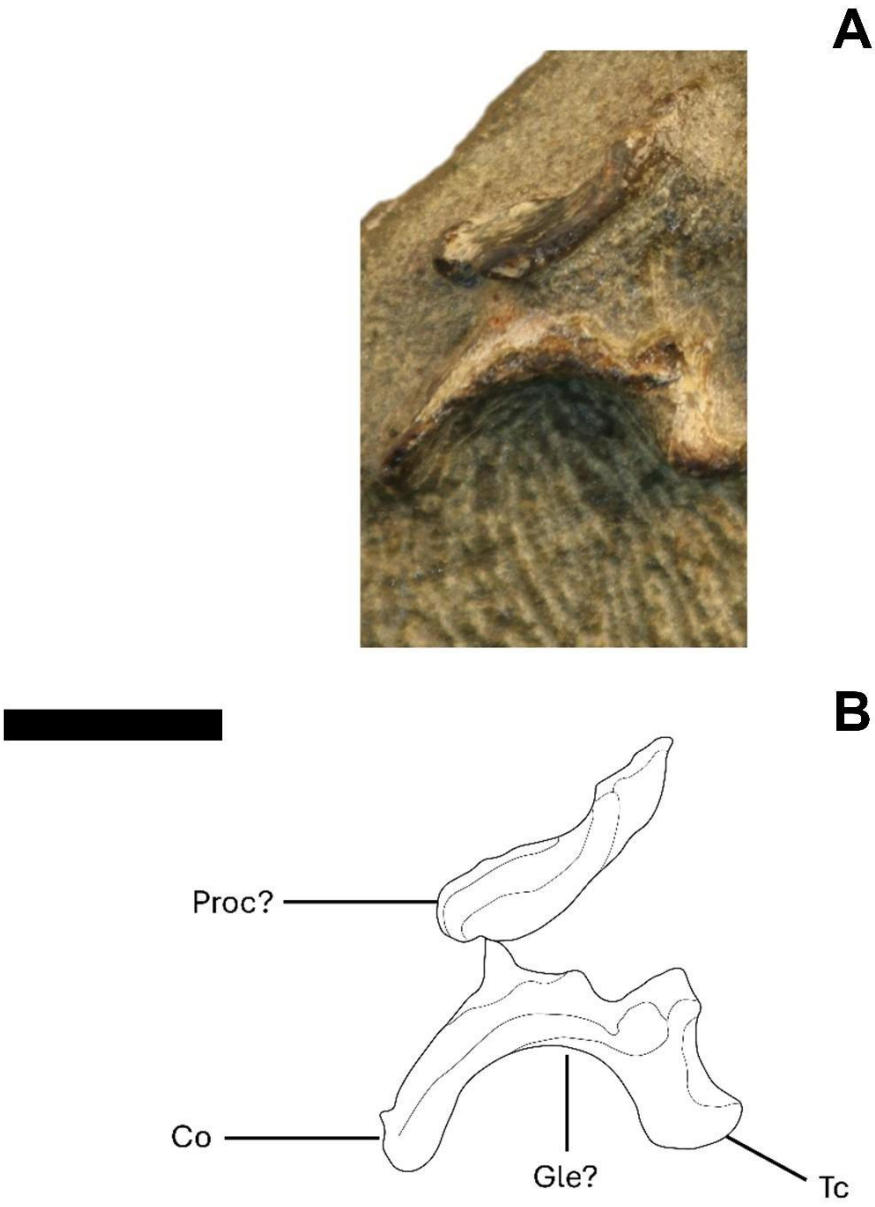


Figure 9: Scapula of BP/1/8740 in dorsal view. **A**. Photograph; **B**. line illustration with bone labels. *Abbreviations*: Proc, procoracoid; Co, coracoid; Gle, glenoid; Tc, Tuber coracoidens. Scale bar is 3cm.

4.1.2 Description of specimen BP/1/8500 (basal dicynodont)

SYSTEMATIC PALAEONTOLOGY

THERAPSIDA Broom (1905)

ANOMODONTIA Owen (1859)

DICYNODONTIA Owen (1859)

Genus and species *Ab* gen. et sp. nov.

Diagnosis – Large basal anomodont distinguished by the presence of the unique combination of the following characters: presence of an enlarged caniniform that is 20% longer than the antorbital height; presence of a beak like dicynodonts, but retains a single, long, and pointed postcanine on the maxilla; absence of secondary palate. It is also the only known dicynodont to have transversely expanded palatal teeth on the pterygoid.

Type locality – Combrinkskraal farm, Combrinkskraal Member of the Abrahamskraal Formation. *Eodicynodon* Assemblage Zone, Beaufort Group, Karoo Supergroup, South Africa.

Description – This description focuses on the skull of BP/1/8500, which was fully prepared for this study. Specimen BP/1/8500 is a complete but badly eroded and laterally compressed skull without a lower jaw. Most of the bone has been eroded away on the left side, leaving the impressions of their former shape. The right side is not as well preserved as a result of deformation of the specimen. Accordingly, the following description will be based mainly on the left side unless otherwise stated.

This skull belongs to a medium-sized dicynodont with a skull length of 19cm from the tip of the premaxilla to the posterior-most part of the squamosal. Before fossilisation

the skull would have been longer, but taphonomic processes caused the occiput to be pushed forward during the preservation. As preserved, the preorbital region is relatively long, forming more than half the length of the skull. The snout is dorsoventrally very deep, and its anterior margin is rounded. The orbits are laterally oriented, and the post-orbital bar is thin. The temporal fenestra is triangular and, uniquely among dicynodonts, appears smaller than the orbit. This may however be due to the lack of preservation of most of the posterodorsal part of the squamosal or deformation of the posterior region of the skull. The intertemporal region appears to be broad, as is the condition with all anomodont taxa from the Abrahamskraal Formation. The occiput is distorted, and preserved elements are beyond identification.

The *premaxilla* is a triangular edentulous bone forming the anteriormost part of the snout (Fig. 10). Its anterior surface is weathered, and only the impression of the bone is preserved, however, the general shape of this bone can be traced. It appears that the premaxillae were fused into a single element as in other dicynodonts from the *Tapinocephalus* Assemblage Zone, which include *Pristerodon*, *Eosimops*, *Robertia*, *Brachyprosopus*, *Diictodon*, *Proscictodon*, *Emydops*, *Colobodectes*, and *Lanthanostegus* (Day & Rubidge, 2020). This appears different from the condition in *E. oosthuizeni* and *Nyaphulia oelofseni*, the only other dicynodonts from the *Eodicynodon* Assemblage Zone where the premaxilla are unfused (Rubidge, 1990; Duhamel et al. 2024). The tip of the premaxilla forms a hook that extends ventrally to the level of the alveolar margin of the maxilla (Fig. 10). Posterodorsally, the premaxilla forms a wedged sutural contact with the nasal as in all other dicynodonts (Rubidge, 1990).

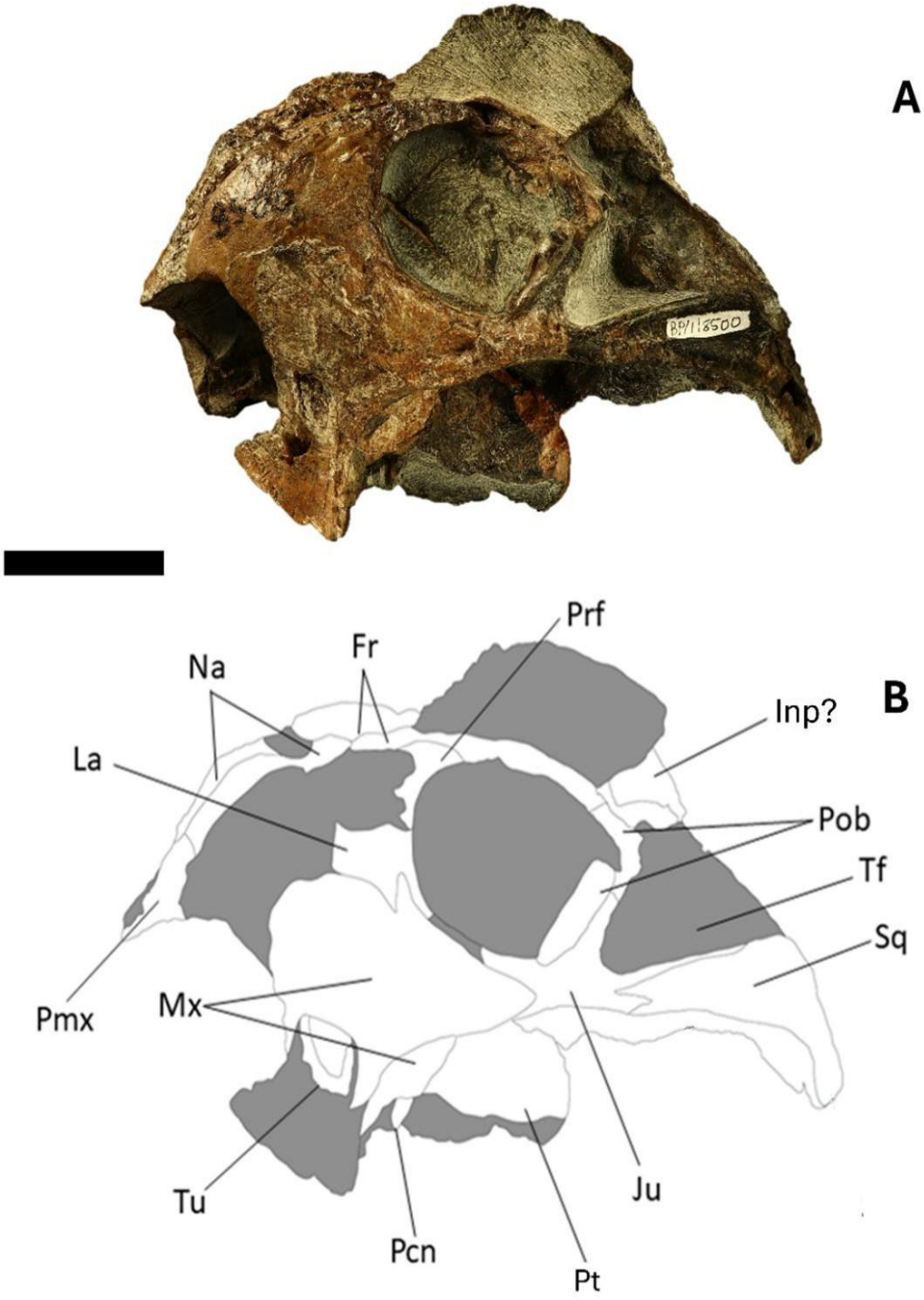


Figure 10: Left lateral view of BP/1/8500. **A**. Photograph; **B**. line illustration with bone labels*. Abbreviations*: Pmx, premaxilla; Na, nasal; Mx, maxilla; La, lacrimal; Ju, jugal; Fr, frontal; Prf, prefrontal; Tu, tusk; Pcn, postcanine; Pal, palatine; Inp, interparietal; Pob, postorbital; Sq, squamosal. Scale bar is 3cm.

On the ventral surface of the skull, there is no secondary palate, and only the dorsal

part of the premaxilla is visible (Figs. 13A & 13B). The absence of a secondary palate is not due to postmortem damage, it suggests that this specimen had no separation between the nasal cavity and oral cavity.

The *maxilla* forms most of the antorbital region of the snout and in lateral view is roughly rectangular (Fig. 10). On the left side, the maxilla is almost completely preserved, but the contact with the premaxilla is not clear, and sutural contacts between the maxilla, nasal, and septomaxilla are not preserved. Posterodorsally, the maxilla has a horizontal sutural contact with the lacrimal. Posteriorly, the maxilla overlies the jugal with a pointed contact ventral to the orbit.

In ventral view, no sutures are visible between the maxilla and premaxilla (Fig. 13B). The maxilla forms the alveolar margin, and the caniniform process (which houses a single tusk) is clearly visible in lateral view (Fig 10). Judging by the portion which is preserved, the caniniform process would have been quite large and prominent ventrally. The right tusk is completely missing, and only the root is preserved (Fig. 13D), while the left tusk is broken off at the level of the palatal rim. Because of the poor preservation of the tusks, it is difficult to tell how far they extended ventrally, but the preserved impression of the tusk in the matrix is 55mm long. A single postcanine tooth that is peg-like and has no expanded cusps is present on the right side (Fig. 10). It is situated postero-medial to the tusk, similar to the condition in *Eosimops* (Broom, 1921; Angielczyk & Rubidge, 2012), *Robertia* (Boonstra, 1948), and *Prosictodon* (Angielczyk & Rubidge, 2010). This differs from the condition in *E. oosthuizeni* (Rubidge, 1990), *Pristerodon* (Olson, 1944; Castanhinha et al. 2013), and *Compsodon* (Angielczyk & Kammerer, 2017) which have more laterally positioned postcanines than any other dicynodonts. The postcanine in BP/1/8500 is very long (17mm long) and the cross section is diamond-shaped , as in some non-

dicynodont anomodonts such as *Anomocephalus* (Modesto et al. 1999), *Tiarajudens* (Cisneros et al. 2015), and *Suminia* (Rybczynski, 2000).

The *nasals* form part of the anterodorsal surface of the snout. They have a rugose surface which is covered with foramina. This specimen appears to have non-terminal nostrils as suggested by the indentation of the nasal posterior to the nasal boss. Anteriorly, the nasal contacts the premaxilla along a V-shaped suture which points posteriorly as in *Eodicynodon* and other dicynodonts (Rubidge, 1990; Castanhinha et al. 2013; Angielczyk et al. 2021). Laterally, the contact between the nasal and maxilla is not preserved, and posteriorly, the contact between the nasal and frontal is also not preserved.

The *lacrimal* is a relatively small, elongated bone positioned horizontally above the maxilla and forms the anteroventral margin of the orbit. The left lacrimal is better preserved than the right; accordingly, this description is based on the left lacrimal. The narrow shape of the lacrimal is similar to the condition in *E. oosthuizeni* and differs from the condition in the holotype of *Patranomodon*, where it is dorsally expanded (Rubidge, 1990; Rubidge & Hopson, 1996). No lacrimal foramen is preserved, unlike the condition in *E. oosthuizeni* (Rubidge, 1990), *Eosimops* (Angielczyk & Rubidge, 2012), *Compsodon* (Angielczyk & Kammerer, 2017), *Cryptocynodon* (Angielczyk, 2007), *Diictodon* (Angielczyk & Sullivan, 2008), and *Emydops* (Fröbisch & Reisz, 2008). Anteroventrally, the lacrimal contacts the maxilla along an oblique suture which is 20mm long. Posteroventrally, the lacrimal meets the jugal but this sutural contact is unclear. Dorsally and anterodorsally, this element meets the prefrontal and nasal respectively, however, their sutural contacts are not clear.

The *prefrontal* is a roughly triangular element forming the anterior portion of the skull

roof and contributing to the anterodorsal rim of the orbit (Fig. 10). This element is not well preserved on either side of the specimen. It contacts the lacrimal ventrally, nasal medially, and frontal posteriorly, however, their sutural contacts remain unclear.

The *frontal* makes up most of the dorsal margin of the orbit (Fig. 10), but because this bone (on both sides of the skull) is deformed and poorly preserved, its extent and configuration are uncertain. If this element was completely preserved, it would most likely contact the nasal anteriorly and the prefrontal anterolaterally as in all dicynodonts (Modesto et al. 2002). The parietals in this specimen are not preserved.

The *jugal* forms a small portion of the ventral border of the orbit and contributes to the anteriormost portion of the zygomatic arch and the anteroventral border of the temporal fenestra (Fig. 10). It separates the maxilla, postorbital, and squamosal. In lateral view (Fig. 10), the jugal has a posteriorly oriented pointed contact with the maxilla. Anterodorsally, it is unclear whether the jugal meets the lacrimal. A dorsal process of the jugal extends dorsally along the posterior surface of the orbit and contacts the postorbital bar dorsally with a short horizontal suture. In ventral view, the contacts between the jugal and palatal bones are unclear.

As in all dicynodonts, the *postorbital* forms part of the skull roof dorsal to the temporal fenestra and forms the entire postorbital bar which separates the orbit from the temporal fenestra (Fig. 10). Dorsally, this element contacts part of the postfrontal anteromedially but this suture is not clearly visible. In lateral view, the postorbital bar thickens ventrally, and overall, it is thin, rod-like, and does not have ornamentation. It is not expanded anteroposteriorly as is the case in *Lanthanostegus* (Modesto et al. 2002), *Eosimops* (Angielczyk & Rubidge, 2012), *Compsodon* (Angielczyk &

Kammerer, 2017), *Kunpania* (Angielczyk et al. 2021), and *Brachyprosopus* (Angielczyk et al. 2016).

The *squamosal* is a prominent bone which, where it is preserved on BP/1/8500, forms the posterior and ventral margins of the temporal fenestra as is common in therapsids (Rubidge et al. 2021). In dicynodonts, the squamosal comprises three processes: the dorsal process making most of the posterior region of the temporal fenestra and part of the occipital plate; the zygomatic process that extends anteriorly, and a quadrate process that is ventrally expanded and reinforces the articulation with the lower jaw around the quadrate and quadratojugal (Angielczyk, 2007; Castanhinha et al. 2013, Angielczyk & Rubidge, 2013).

In specimen BP/1/8500 the dorsal process is missing, and only the zygomatic and a portion of the quadrate processes are preserved (Fig. 10). The preserved processes do not have ornamentation or pachyostosis, similar to the condition in *Eosimops* (Angielczyk & Rubidge, 2013), *Aulacephalodon* (Kammerer et al. 2015), *Pelanomodon* (Keyser, 1968; King, 1988; Kammerer et al. 2015), and *Geikia* (Kammerer & Angielczyk, 2009; Kammerer et al. 2011). The zygomatic process of the squamosal tapers anteriorly and forms a pointed contact with the jugal. It has a shallow triangular depression as in *Anomocephalus* and *Tiarajudens*.

The preserved portion of the zygomatic process does not exhibit the lateral flange for the attachment site of the lateral division of the external adductor musculature. This may be due to the erosion of this part of the squamosal, although the redescription of NMQR 2913 (*Nyaphulia oelofseni)* mentions that it has a squamosal that is slender and unfolded as in non-dicynodont anomodonts, such as *Anomocephalus* (Modesto et al. 1999), *Tiarajudens* (Cisneros et al. 2011) and *Ulemica* (Tchudinov, 1983)

(Duhamel et al. 2024). As such, the absence of a lateral squamosal flange could be a genuine feature of this dicynodont, although better-preserved material will have to be discovered to address this possibility.

On the zygomatic arch, the squamosal meets the jugal anteriorly and does not contact the maxilla, a condition that is similar to that in *Eodicynodon* (Rubidge, 1990; Duhamel et al. 2024), *Lanthanostegus* (Modesto et al. 2002; Rubidge et al. 2021), *Eosimops* (Angielczyk & Rubidge, 2013), and *Compsodon* (Angielczyk et al. 2023).

The squamosal probably contacts the supraoccipital and tabular as in all dicynodonts, but the deformation of the occiput makes it impossible to determine. The squamosal also bears the post temporal fenestra that is almost bilaterally symmetrical (Figs. 11 & 12).

The occiput of BP/1/8500 is poorly preserved and has been laterally compressed. The occipital bones are mostly unidentifiable (Figs. 11 & 12). As a consequence, it is difficult to provide a detailed description of the occipital surface, and the identifications of the bones hereby provided should be viewed as tentative. The preserved occiput of BP/1/8500 is triangular and has an uneven surface. There are no sutures visible on the occiput, which may be due to damage or could suggest the co-ossification of occipital bones. The foramen magnum is circular and has a diameter of 30mm. The palate of BP/1/8500 is strongly compressed laterally, sheared, and heavily damaged, such that it is difficult to provide a detailed description. The anterior half of the palate comprises the premaxilla and vomer, but the suture between them is not visible. Despite extensive preparation, it appears that the premaxilla does not form a secondary palate.

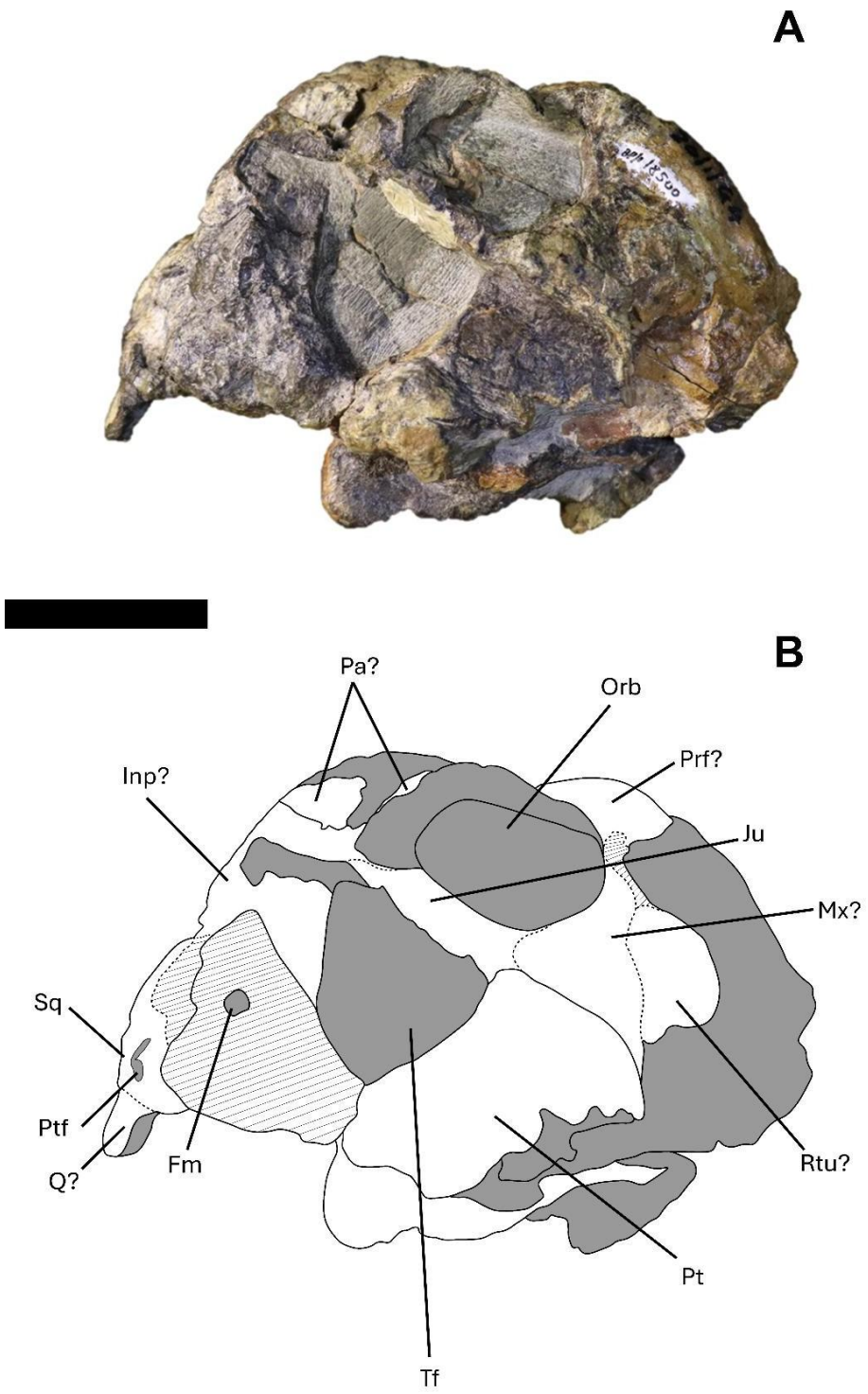


Figure 11: Right lateral view of BP/1/8500 with the occiput folded. **A**. Photograph; **B**. line illustration with bone labels. *Abbreviations*: Ju, jugal; Pa, parietal; Ptf, post temporal fenestra; Sq, squamosal; Q, quadrate; Inp, interparietal; Pt, pterygoid; Orb, orbit; Mx, maxilla; Rtu, right tusk; Prf, prefrontal; Tf, temporal fenestra. Oblique lines indicate unidentifiable bones. Scale bar is 3cm.

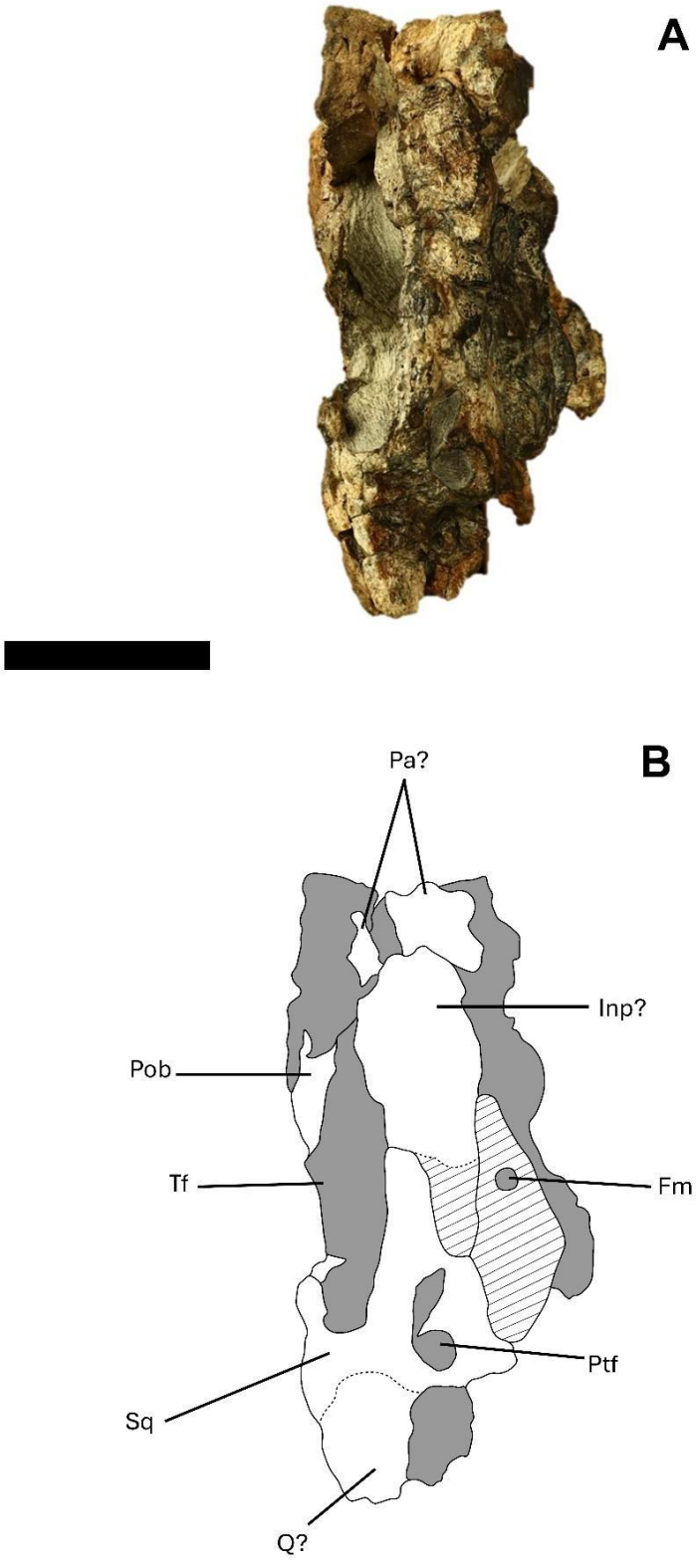


Figure 12: Occipital view of BP/1/8500. **A**. Photograph; **B**. line illustration with bone labels. *Abbreviations*: Pa, parietal; Inp, interparietal; Fm, foramen magnum; Ptf, post temporal fenetra; Sq, squamosal; Q, quadrate; Tf, temporal fenestra; Pob, post orbital bar. Oblique lines indicate unidentifiable bones. Scale bar is 3cm.

The ventral-most parts of the premaxilla and vomer could have been damaged before or during the fossilisation process, but the palate of the specimen was deeply embedded in matrix when it was discovered and no remnants of these structures were found during preparation, which makes it unlikely that such a large amount of the premaxilla is lost. A single postcanine maxillary tooth is also visible in ventral view.

The *vomer* is a bone situated at the anterior-most part of the palate (Fig. 13C). In BP/1/8500, this element is partially exposed ventrally but it is unclear how far this element extends anteriorly, dorsally, laterally, and posteriorly.

The *pterygoid* is a prominent bone of the palate, but only the anterior process is preserved. These pterygoid processes are anteroposteriorly elongated. They are most noticeable in lateral view, forming a prominent triangular process that projects ventrally to the skull. The ventral surface is smooth and there is no indication of teeth but the CT scan reveals the presence of thirteen large transversely expanded alveoli for teeth along the entire length of the pterygoid (Fig. 13D). This is similar to the condition in *Tiarajudens* and *Anomocephalus* (Modesto et al. 1999; Cisneros et al. 2011, 2015). The mesial and distal margins of the alveoli are almost parallel.

Palatal teeth on the pterygoid are absent in all anomodonts except the basal anomodonts *Tiarajudens* (Cisneros et al. 2011), *Anomocephalus* (Modesto et al. 1999), and *Biseridens* (Liu et al. 2010). In ventral view, the alveoli of BP/1/8500 suggest that the specimen had thecodont implantation of the teeth as in the above-cited taxa. The transverse axis of the alveoli is oriented perpendicularly to the sagittal plane, unlike in *Tiarajudens*, in which it is slightly oblique in ventral view.

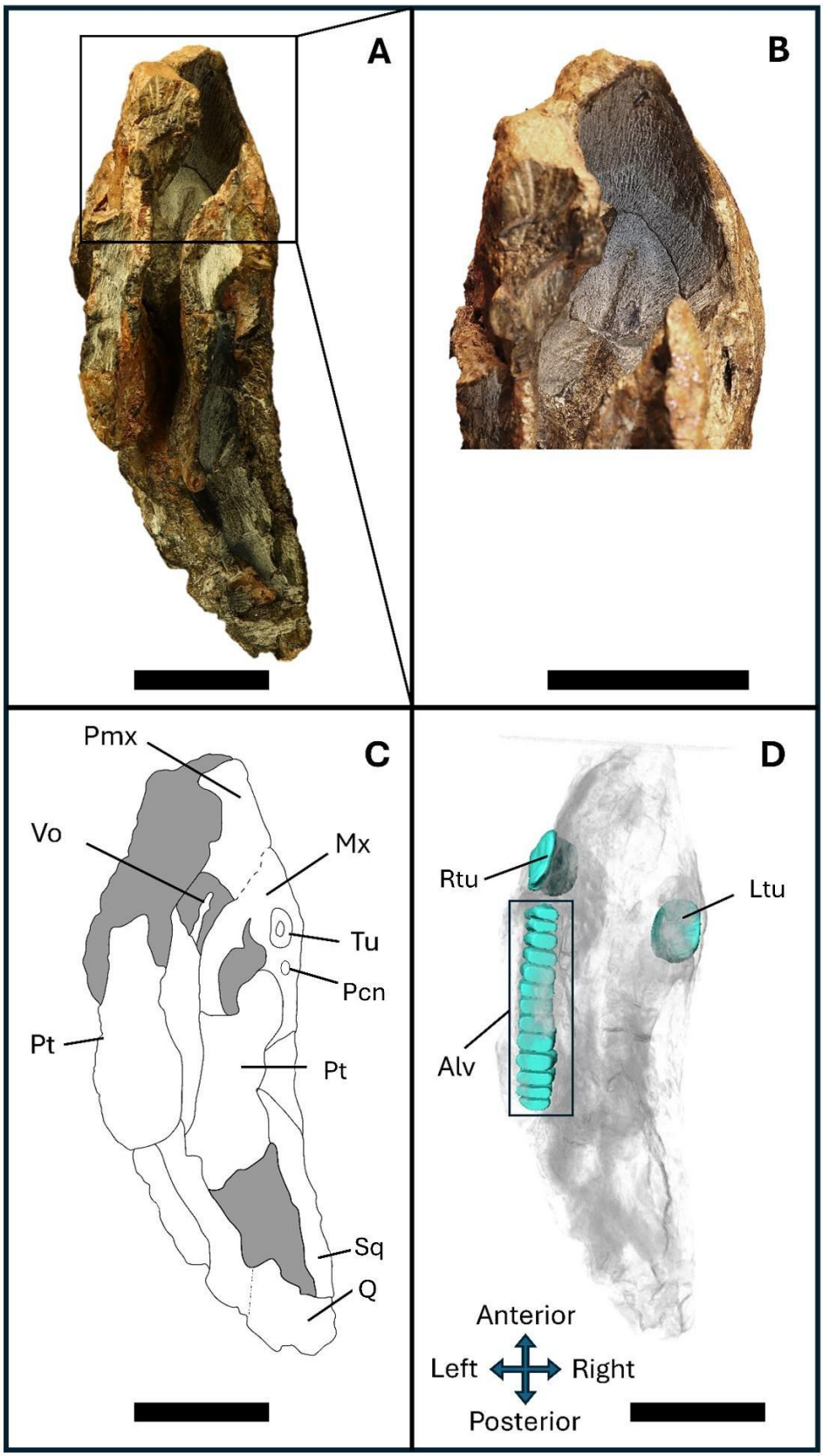

A
B
C
Pmx
Vo
Mx
Tu
Pcn
Pt
Pt
Sq
Q
D
Rtu
Ltu
Alv
Anterior
Left
Right
Posterior

Figure 13: Ventral view of BP/1/8500; **A**. photograph of specimen BP/1/8500 in ventral view; **B**. closeup view of the anterior portion of the palate; **C**. line illustration with bone labels; **D**. CT scan of BP/1/8500 with segmentation of the tusks and alveoli. The grey material on the CT scans represents the skull. *Abbreviations*: Pmx, premaxilla; Vo, vomer; Mx, maxilla; Pcn, postcanine; Tu, tusk; Pt, pterygoid; Sq, squamosal; Ltu, left tusk; Rtu, right tusk; Alv, alveoli. Scale bar for A, C, and D is 3cm, and the scale bar for B is 4cm.

4.2 Phylogenetic analysis

To assist with taxonomic determination and the phylogenetic position of the two newly described anomodont specimens, a cladistic analysis was run using TNT 1.1 (May 2014 version) (Goloboff et al. 2008). The Angielczyk et al. (2021) anomodont matrix was used to score characters of BP/1/8740 and BP/1/8500 as it includes all anomodonts and the Duhamel et al. (2024) matrix was used to update the Angielczyk et al. (2021) matrix as it encompasses the most recent taxonomic revision of *Patranomodon nyaphulii*, *Eodicynodon oosthuizeni*, and *Nyaphulia oelofseni* (previously *Eodicynodon oelofseni*). No characters were added or removed from the matrices, and the final dataset included 174 characters (See appendix 3).

The cladistic analysis retained 100 trees, and 526 648 513 rearrangements were examined for the Tree Bisection Reconnection algorithm. The minimum tree length obtained after updating the Angielczyk et al. (2021) matrix is 1003 steps. The strict consensus tree is presented in Figure 14 and is well resolved. The following statistical supports were obtained: consistency index (CI) = 0.24, retention index (RI) = 0.75, homoplasy index (HI) = 0.8.

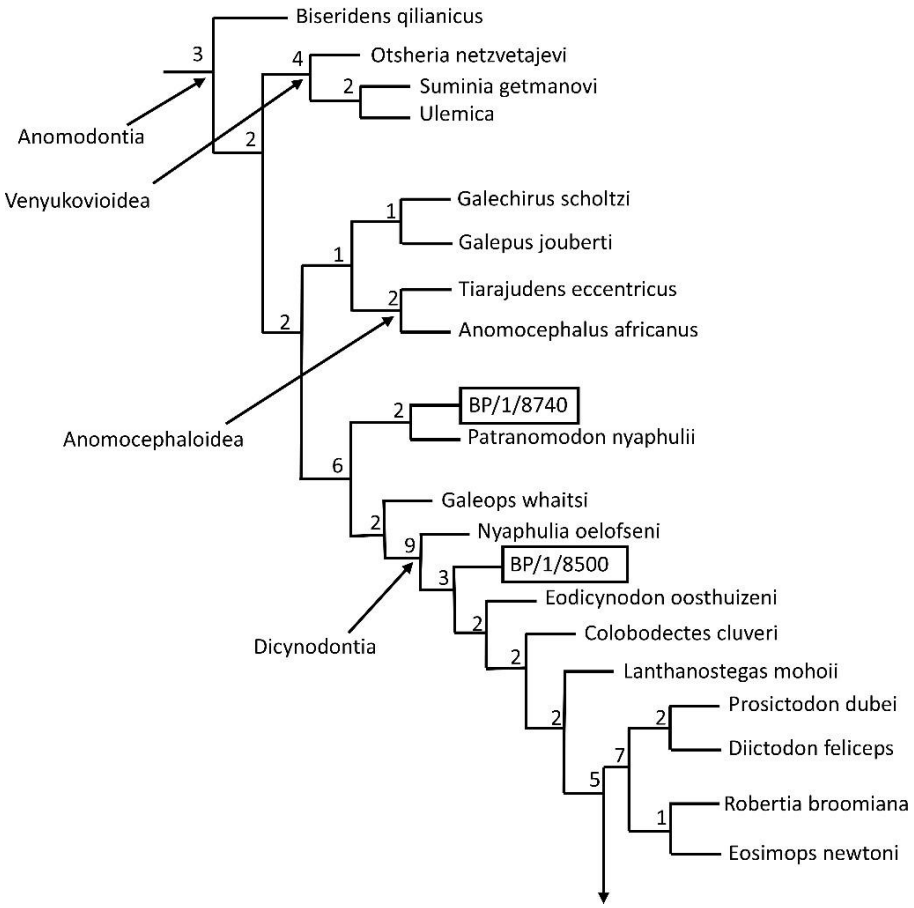


Figure 14: Strict consensus of 20 most parsimonious cladograms from the phylogenetic analysis. Numbers at the nodes are Bremer support values. Specimens described here are indicated by the black rectangles.

4.2.1 Description of phylogenetic results

The cladistic analysis resulted in a well-resolved strict consensus cladogram (Fig. 14). Specimen BP/1/8740 is recovered as sister taxon to the holotype of *Patranomodon*, and their clade is supported by three synapomorphies: the absence of lateral ridges bounding the preparietal (46 [0]); the postparietal not bulging outwards as swellings at the posterior end of the sagittal crest (50 [0]); the absence of oblique ridge on the lateral side of the zygomatic arch (64 [0]).

The autapomorphies found in BP/1/8740 are: palatal surface of premaxilla not exposed in lateral view (21 [0]); the ventral surface of the median pterygoid plate is depressed (92 [0]); the reflected lamina is round and unornamented (135 [0]); and the cleithrum is absent (144 [0]).

The autapomorphies present in the holotype of *Patranomodon* are: the naso-frontal suture is gently bowed (35 [0]), and the parasphenoid is excluded from the interpterygoid vacuity (97 [0]). These may be due to the size difference between the holotype and the referred specimen, the latter of which is much smaller and may be a juvenile.

In most previous phylogenetic analyses, the Anomocephaloidea are positioned stemwards to the clade bearing *Patranomodon* and more derived anomodonts (see Cisneros et al. (2011); Boos et al. (2016); Kammerer & Smith (2017); and Angielczyk et al. (2021)). In the current analysis, *Tiarajudens* and *Anomocephalus* form a clade (here referred to as the Anomocephaloidea clade) (Fig.14) that is supported by two synapomorphies: the squamosal does not expand dorsoventrally posterior to the postorbital bar (62 [0]), and the ectopterygoid expands further posteriorly than the palatine (24 [0]). This clade is itself the sister group to the former Galesauria which comprises *Galechirus* and *Galepus*, and they share the following synapomorphies: the palatal surface if the premaxilla exposed in lateral view (21 [0]); the absence of postnarial excavation (19 [0]); and the absence of angular with anterolateral trough for the posterior process of the dentary (134 [0]).

Galeops is recovered as the sister group to Dicynodontia. This is similar to previous phylogenetic analyses (see Boos et al. (2016); Cisneros et al. (2011); Kammerer et al. (2011); Angielczyk et al. (2021)), but it differs from the analysis of Fröbisch &

Reisz (2008), which recovers *Galeops* as a sister taxon to the venyukovids. In the current analysis, *Galeops* shares the following synapomorphies with dicynodonts: nasals with a short median suture and frontals and premaxilla in close proximity (33 [1]); the interparietal makes a large contribution to intertemporal skull roof (57 [2]); the dorsal surface of the dentary does not have dorsally-convex cutting blade (126 [0]); and the reflected lamina with reticulate ridges (135 [3]).

Specimen BP/1/8500 is recovered as the second most basal dicynodont after *Nyaphulia oelofseni*. It holds a more basal position than *Eodicynodon*, *Lanthanostegus*, *Colobodectes*, *Eosimops*, *Pristerodon*, *Brachyprosopus*, *Prosictodon*, and *Robertia*, which are the other Middle Permian basal dicynodonts.

Specimen BP/1/8500 and dicynodonts share the following synapomorphies: absence of premaxillary teeth (8 [2]); palatal surface of premaxilla not exposed in lateral view (21 [0]); the maxillary canine present as tusk (22 [2]); absence of serrations on the maxillary teeth (25 [1]); the postcaniniform crest is absent (31 [0]); the erupted portion of the tusk is anterior to the orbital margin (32 [0]); the temporal portion of the postorbital is close to vertical (51 [1]); the posteroventral process of the squamosal is long (60 [1]).

From this analysis, *Eodicynodon* shares the following characters with other dicynodonts, with the exception of BP/1/8500: squamosal with a lateral fossa for the origin of lateral branch of the adductor mandibulae externus (58 [2]) and the absence of the suborbital boss on the jugal (68 [0]). In addition, previous studies determined that *Eodicynodon* shares the following characters with other dicynodonts: presence of well-developed caniniform tusks (Rubidge & Sidor, 2001; Kammerer et al. 2011), squamosal that is robust and folded (Duhamel et al. 2024); septomaxilla not laterally

exposed (Angielczyk et al. 2017), presence of a secondary palate consisting of the premaxilla and the choana opening posterior to the tusk (Fröbisch & Reisz, 2008; Kammerer et al. 2011); and parasphenoid that is excluded from the interpterygoid vacuity (Duhamel et al. 2024).

4.3 Body size estimates

As the fossil record of anomodonts is represented mostly by skulls, basal skull length was used as a proxy for body size (Angielczyk & Walsh 2008) for 97 dicynodont species from the entire time spectrum that dicynodonts existed . The first and last stratigraphic occurrence of each dicynodont species was taken from the literature, and the methodology is explained in the method section (pages 25 and 26).

The resulting time-calibrated phylogeny incorporates 97 taxa that range in time from the Guadalupian (Middle Permian) to upper Triassic, but most of the taxa date from the Guadalupian to Lopingian (Late Permian). Taxa which are represented by only incomplete skulls or which do not have skull length recorded in the literature were excluded from the body size estimates. Skull measurement data is presented in Appendix 5.

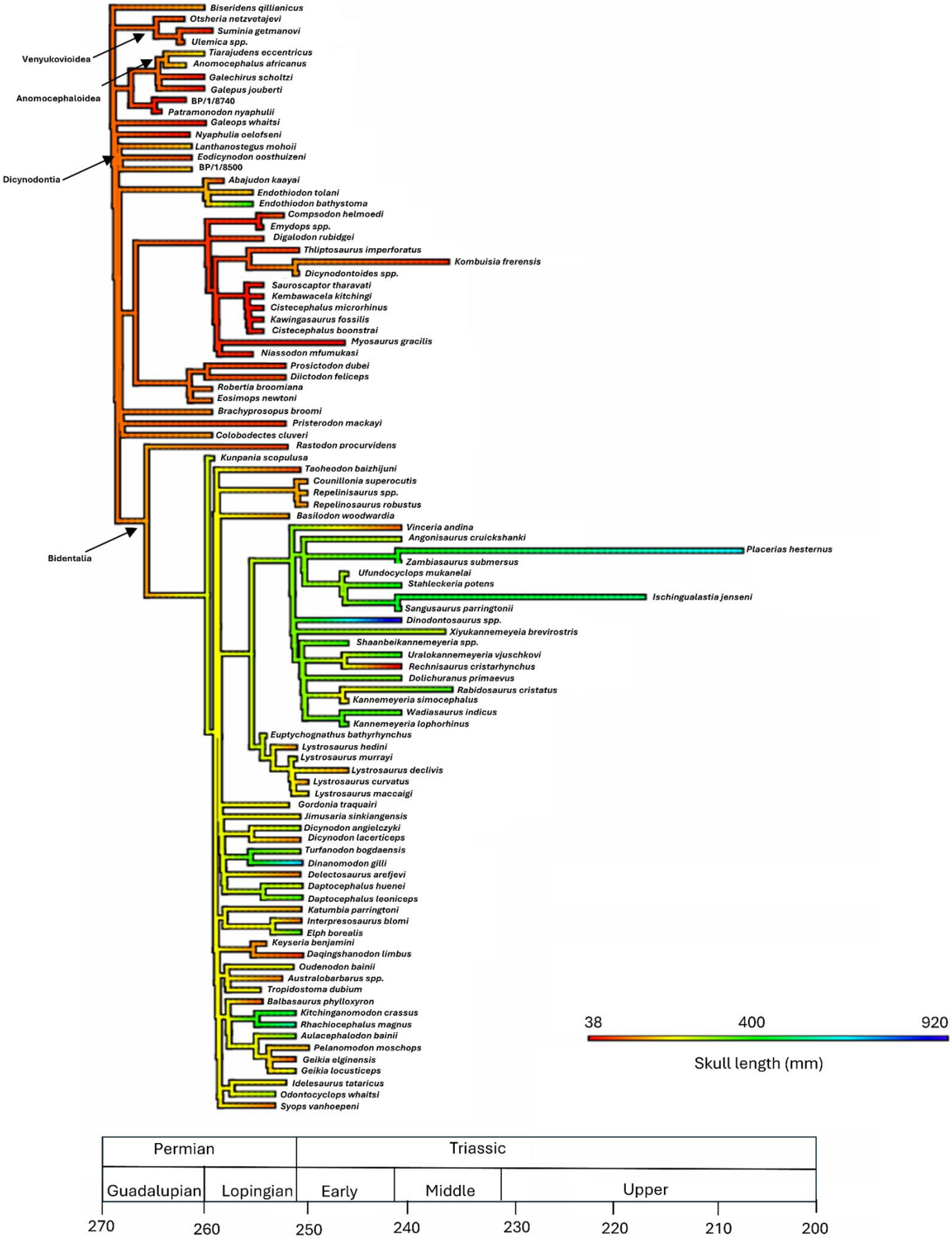

Biseridens qillianicus
Otsheria netzvetajevi
Suminia getmanovi
Ulemica spp.
Tiarajudens eccentricus
Anomocephalus africanus
Galechirus scholtzi
Galepus jouberti
BP/1/8740
Patramonodon nyaphulii
Galeops whaitsi
Nyaphulia oelofseni
Lanthanostegus mohoii
Eodicynodon oosthuizeni
BP/1/8500
Abajudon kaayai
Endothiodon tolani
Endothiodon bathystoma
Compsodon helmoedi
Emydops spp.
Digalodon rubidgei
Thliptosaurus imperforatus
Kombuisia frerensis
Dicynodontoides spp.
Sauroscaptor tharavati
Kembawacela kitchingi
Cistecephalus microrhinus
Kawingasaurus fossilis
Cistecephalus boonstrai
Myosaurus gracilis
Niassodon mfumukasi
Prosictodon dubei
Diictodon feliceps
Robertia broomiana
Eosimops newtoni
Brachyprosopus broomi
Pristerodon mackayi
Colobodectes cluveri
Rastodon procurvidens
Kunpania scopulusa
Taoheodon baizhijuni
Counillonia superocutis
Repelinisaurus spp.
Repelinosaurus robustus
Basilodon woodwardia
Vinceria andina
Angonisaurus cruickshanki
Placerias hesternus
Zambiasaurus submersus
Ufundocyclops mukanelai
Stahleckeria potens
Ischingualastia jenseni
Sangusaurus parringtonii
Dinodontosaurus spp.
Xiyukannemeyeia brevirostris
Shaanbeikannemeyeria spp.
Uralokannemeyeria vjuschkovi
Rechnisaurus cristarhynchus
Dolichuranus primaevus
Rabidosaurus cristatus
Kannemeyeria simocephalus
Wadiasaurus indicus
Kannemeyeria lophorhinus
Euptychognathus bathyrhynchus
Lystrosaurus hedini
Lystrosaurus murrayi
Lystrosaurus declivis
Lystrosaurus curvatus
Lystrosaurus maccaigi
Gordonia traquairi
Jimusaria sinkiangensis
Dicynodon angielczyki
Dicynodon lacerticeps
Turfanodon bogdaensis
Dinanomodon gilli
Delectosaurus arefjevi
Daptocephalus huenei
Daptocephalus leoniceps
Katumbia parringtoni
Interpresosaurus blomi
Elph borealis
Keyseria benjamini
Daqingshanodon limbus
Oudenodon bainii
Australobarbarus spp.
Tropidostoma dubium
Balbasaurus phylloxyron
Kitchinganomodon crassus
Rhachiocephalus magnus
Aulacephalodon bainii
Pelanomodon moschops
Geikia elginensis
Geikia locusticeps
Idelesaurus tataricus
Odontocyclops whaitsi
Syops vanhoepeni
Venyukovioidea
Anomocephaloidea
Dicynodontia
Bidentalia
38
400
920
Skull length (mm)
Permian
Triassic
Guadalupian
Lopingian
Early
Middle
Upper
270
260
250
240
230
220
210
200

Figure 15: Projection of basal skull length onto the anomodont phylogenetic tree. The colour gradient shows changes in skull length over time (millions of years). The red colour indicates smaller skulls (minimum skull length being 38mm), yellow colour indicates slightly larger skulls, green colour indicates moderately large skulls, and the blue colour indicates larger skulls (maximum skull length of 920mm).

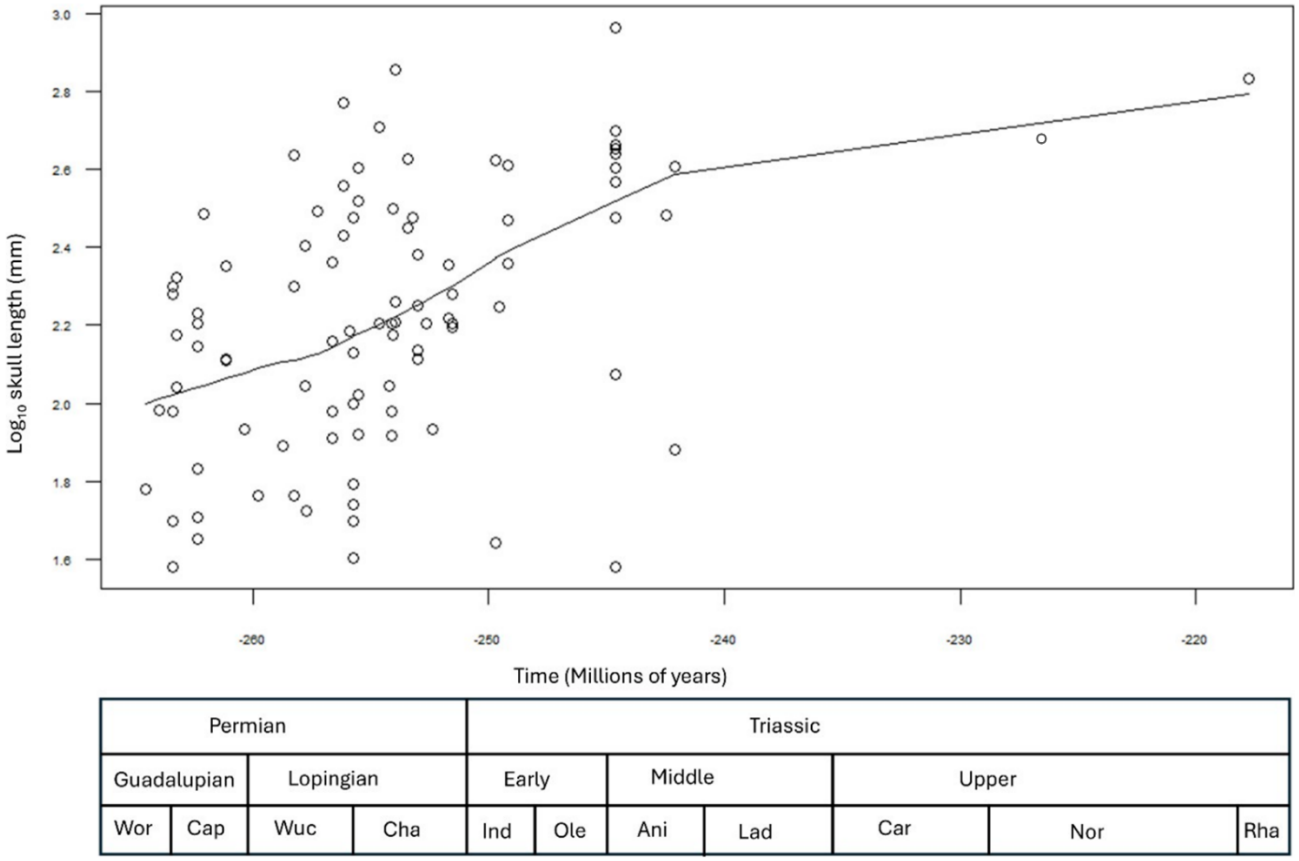


Figure 16: Log skull length (proxy for body size) of anomodont taxa from Middle Permian to Late Triassic plotted at the stratigraphic range midpoints for each taxon with the Lowess regression line fitted. The circles in the graph represent each taxon used in the body size analysis. This figure is a graphical representation of the phylogeny in Figure 15. *Abbreviations*: Wor, Wordian; Cap, Capitanian; Wuc, Wuchiapingian; Cha, Changsingian; Ind, Induan; Ole, Olenekian; Ani, Anisian; Lad, Ladinian; Car, Carnian; Nor, Norian; Rha, Rhaetian.

4.3.1 Description of body size estimation

The body-size data indicates a consistent increase in anomodont size over time (Figs. 15 & 16). Anomodonts attained larger sizes only during the Late Permian. Before the Capitanian extinction (260 Ma), the majority of anomodonts had smaller body sizes as indicated by the red colour on the tree (Fig. 15) with *Biseridens*, *Tiarajudens*, *Anomocephalus*, *Lanthanostegus*, and BP/1/850 being exceptions. The smallest recorded anomodont during the Middle Permian is the newly discovered *Patranomodon* (specimen BP/1/8740) with a skull length of 38mm.

Following the Capitanian crisis (260 Ma), there is a slight decrease in the average body size of anomodonts as indicated by the Lowess regression line in Figure 16. This slight decrease is a result of the more small-bodied anomodonts which include *Emydops* (skull size of 53mm), *Niassodon mfumukasi* (58mm), *Sauroscaptor theravati* (50mm), *Kembawacela kitchingi* (55mm), *Pristerodon mackayi* (78mm), *Rastodon procurvidens* (86mm), and *Diictodon feliceps* (95mm) which dominated during the early Lopingian (Wuchiapingian) as seen by the red colour on the phylogeny in Figure 15. However, some taxa living during this time were larger, such as *Endothiodon bathystoma* (skull length of 434mm), *Endothiodon tolani* (skull length of 200mm), and *Dicynodontoides* (skull length of 161mm).

Following the Capitanian extinction event, during the Lopingian, anomodonts reached their peak taxonomic diversity and also experienced an average increase in body size, with the maximum skull size of 718mm for *Dinanomodon gilli* and the smallest, being 40mm for *Kawingasaurus fossilis*. Other large-sized anomodonts during this period are *Aulacephalodon* (skull size of 361mm), *Oudenodon* (270mm), *Rhachiocephalus* (590mm), *Odontolocyclops* (311mm), *Kitchinganomodon* (509mm), and *Pelanomodon* (182mm).

At the end of the Permian, the diversity of anomodonts decreased, showing the impact of the end-Permian extinction event on the terrestrial ecosystems. Although the global anomodont diversity rapidly collapsed, the overall body size of anomodonts remained larger than during the Middle Permian as indicated by the yellow, green and blue colours in the phylogeny (Fig. 15). During the mid-Triassic, anomodont size increased fairly consistently, with the maximum skull size recorded as 920mm for *Dinodontosaurus*, larger than any other anomodont in the fossil record. It is thus evident that large-bodied anomodonts were more common in the Triassic than during the Middle Permian period. Also, during the Triassic, their taxonomic diversity remained low until the extinction of the clade during the Late Triassic (Rhaetian).

CHAPTER 5: DISCUSSION

5.1 Identification and comparison

5.1.1 Identification of BP/1/8740 as *Patranomodon*

Specimen BP/1/8740 is a basal anomodont because it possesses the following cranial characters: shortening of the preorbital region of the skull, presence of incisors, peg-like teeth on maxilla, squamosal descending to level of the tooth row, lower jaw lacking coronoid process, orbits larger than temporal fenestra, a parietal region that is broad, a thin postorbital bar, absence of palatal teeth, zygomatic arch that is dorsally bowed, and reduced lateral process of the pterygoid.

It is not a venyukovid because it has the following characters: a gracile skull, the snout slopes gently anteriorly, it has a homodont dentition, the lower jaw is slender and has a concave ventral margin, and it does not possess the following characters: leaf-shaped teeth with talon-and-heel morphology, first two premaxillary teeth larger than the rest of the teeth, robust and straight ventral margin of the lower jaw. A symplesiomorphic character that is shared by *Venyukovia* (Tchudinov, 1960), *Eodicynodon*, the holotype of *Patranomodon* (Duhamel et al. 2024), and the new *Patranomodon* specimen is the presence of a paired vomer, and this character is not present in later dicynodonts. The parabasisphenoid of the new *Patranomodon* specimen (BP/1/8740) appears to have been formed by the fusion of the basisphenoid and the parasphenoid; however, due to the absence of workable CT data, it is difficult to tell if they were fused or separated as in the holotype of *Patranomodon* (Duhamel et al. 2024).

Comparison of BP/1/8740 with chainosaurians has limitations because all described non-dicynodont chainosaurians are preserved as natural moulds and not in 3-

dimensions, with the exception of *Patranomodon*. Specimen BP/1/8740 is not referrable to *Galechirus* because it has very few small teeth, the dentaries are unfused, and it does not possess heavily pitted dentaries. It is not referrable to *Galepus* because its premaxillary teeth are not vertical but procumbent, and its lower jaw is not robust (Rubidge, 1990). It is also not referrable to *Galeops* as it does not have an edentulous premaxilla, a squamosal that is flared, and fused dentaries that are heavily pitted suggesting a keratinous beak was present (Broom, 1912; Rubidge, 1990; Benoit et al. 2018).

Patranomodon (as based on direct observations of the holotype) has the following characters: short snout, anterolaterally oriented orbits which are larger than the temporal fenestra, absence of tusks, homodont dentition, nasal process of the premaxilla which intrudes into the nasal bones, a skull with a broad intertemporal region, a squamosal that is not flared, presence of preparietal, absence of an expanded premaxillary secondary palate, narrow interpterygoid vacuity, occiput sloping ventrally immediately posterior to the pineal foramen, slender postorbital bar, vomer that is paired, choana that is large and extends the entire length of the vomer, a broad lateral flange of the pterygoid, absence of the quadratojugal bone, a slender lower jaw with prominent reflected lamina of the angular, mandibular fenestra and no coronoid bone or process (Rubidge & Hopson, 1996; Duhamel et al. 2024).

Specimen BP/1/8740 has all the above-mentioned characters but differs from the holotype of *Patranomodon* in that its pineal foramen is comparatively smaller than in the holotype of *Patranomodon*. The squamosal of the *Patranomodon* holotype descends far below the level of the tooth row to reach the jaw articulation (Rubidge & Hopson, 1996; Duhamel et al. 2024), while in the newly discovered specimen, the squamosal descends to the level of the tooth row. Six homodont teeth are present on

the maxilla of *Patranomodon*, while only three are visible on the maxilla of BP/1/8740. It is evident that the similarities outnumber the differences between BP/1/8740 and the holotype of *Patranomodon* (NMQR 3000). The identification of BP/1/8740 as *Patranomodon* is further supported by the phylogenetic analysis, as specimen BP/1/8740 is recovered as a sister taxon to the holotype of *Patranomodon* (Fig. 14).

Specimen BP/1/8740 is smaller than the *Patranomodon* holotype and is thus likely a juvenile. Although the number of *Patranomodon* specimens is too small to undertake a quantitative study of intraspecific morphological variation, several distinct qualitative variations between the two specimens could be related to intraspecific ontogenetic variation. There are no studies that have considered the ontogeny of non-dicynodont anomodonts because they are rare in the fossil record, and most of them are only known from single occurrences. A few studies have considered dicynodont ontogeny in greater detail, such as Tollman et al. (1980), Sullivan et al. (2003), Sullivan and Reisz (2005), Grine and Cluver (2006), Angielczyk and Rubidge (2009), and Kammerer et al. (2015); and their observations can be applied to non-dicynodont anomodonts.

The most obvious ontogenic difference between BP/1/8740 and the holotype of *Patranomodon* is skull size: the small specimen (BP/1/8740) has a skull length of 38mm, whereas the holotype of *Patranomodon* (NMQR 3000) has a skull length of 60mm, thus BP/1/8740 is 37% smaller than the holotype of *Patranomodon*. Smaller skull size and larger orbits are commonly observed in juvenile therapsids compared to adults, and they are known to change over the course of ontogeny (Ivakhnenko, 1999; Sidor & Rubidge, 2006).

The other noteworthy difference is the number of teeth. Specimen BP/1/8740 has fewer maxillary teeth than the holotype of *Patranomodon*. An increase in the number of teeth through ontogeny is also observed in some cynodonts, such as *Cynosaurus suppostus* (Norton et al. 2021) and *Galesaurus planiceps* (Norton et al. 2020).

The size of the pineal foramen is also a character that may vary across ontogeny (Angielczyk & Rubidge, 2009). The pineal foramen of BP/1/8740 is smaller than that of the holotype of *Patranomodon*, suggesting that it may display positive allometry as in some dinocephalians and dicynodonts (Roth et al. 1986; Benoit et al. 2015, 2016).

As a consequence, BP/1/8740 differs from the holotype of *Patranomodon nyaphulii* in the following respects: small skull length, fewer maxillary teeth, and a smaller pineal foramen, but assignation to a new species would be premature because they are not at the same growth stage. The differences listed above between the holotype and the new specimen are accountable by ontogenetic variability, and as such, BP/1/8740 is, for now, considered a juvenile individual of the species *Patranomodon nyaphulii.*

5.1.3 Identification of BP/1/8500 and comparison

The skull of specimen BP/1/8500 is a dicynodont because it possesses the following diagnostic dicynodont synapomorphies: the absence of lateral anterior palatal ridge, palatal surface of premaxilla not exposed in lateral view, the absence of premaxillary teeth (i.e. presence of a beak), the maxillary canine is present as a tusk, the erupted portion of the tusk is anterior to the orbital margin, maxillary non-caniniform teeth are located medially, absence of serrations on the maxillary teeth, and a maxillary caniniform process is present.

Even though specimen BP/1/8500 is a dicynodont, it does have characteristics which are present in some non-dicynodont anomodonts such as *Anomocephalus* and *Tiarajudens*. BP/1/8500 shares the following characters with the latter non-dicynodont taxa: an overall deep skull with the lateral surface dominated by the dorsoventral expansion of the maxilla, large orbits, the pterygoid bone that is large, the presence of transversely expanded palatal teeth on the pterygoid, squamosal that appears to not being flared, a narrow postorbital bar, a temporal fenestra that is triangular and smaller than the orbit, and the maximum skull height being anterior to the orbit (Fig. 17).

The phylogenetic analysis recovers specimen BP/1/8500 as a basal dicynodont rather than a non-dicynodont anomodont (Fig. 14). It is more closely related to *Eodicynodon* and other dicynodonts than it is to *Nyaphulia oelofseni.* It differs from *Nyaphulia* in that it has tusks, the maxillary teeth point ventrally while in *Nyaphulia* they point in an anterior direction, and it has teeth on the pterygoid while *Nyaphulia* does not have teeth on the pterygoid.

Specimen BP/1/8500 thus displays a unique combination of non-dicynodont characters (e.g. enlarged pterygoid teeth) and the classical dicynodont cranial morphology (e.g. presence of a beak, tusks, and medial maxillary postcanines). Accordingly, it can be safely stated that BP/1/8500 belongs to a new dicynodont genus and species. Formal description of the new taxon will not be done here, as a dissertation is not the correct forum for the description of a new taxon.

This specimen is a sister taxon to the clade bearing *Eodicynodon oosthuizeni* and other dicynodonts, and this relationship has a branch support of 2. It differs from *Eodicynodon* by the presence of the following characters: a triangular temporal

fenestra that is smaller than the orbit, absence of the premaxillary secondary palate separating the oral cavity from the nasal cavity, the postorbital contacts the jugal more dorsally while in *Eodicynodon* they contact each other more ventrally, medially located postcanine, enlarged pterygoid, squamosal that appears to not being flared, the zygomatic process of the squamosal not extending anteriorly to reach the orbit, long straight root of the tusk reaching the orbit, and the presence of teeth on the pterygoid.

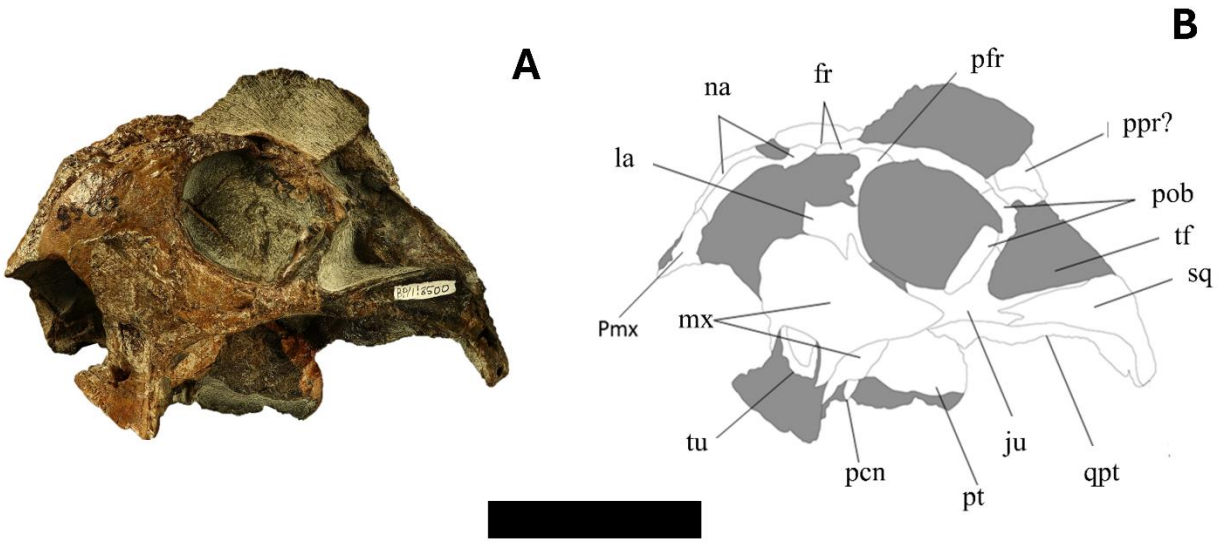
Specimen BP/1/8500 differs from other dicynodonts in that the preserved portion of the zygomatic process of the squamosal appears to not be transversely expanded, the maxillary postcanine is long, the jugal has a dorsal process which extends along the postorbital, and it has an enlarged ventrally projecting and dentigerous triangular process of the pterygoid.

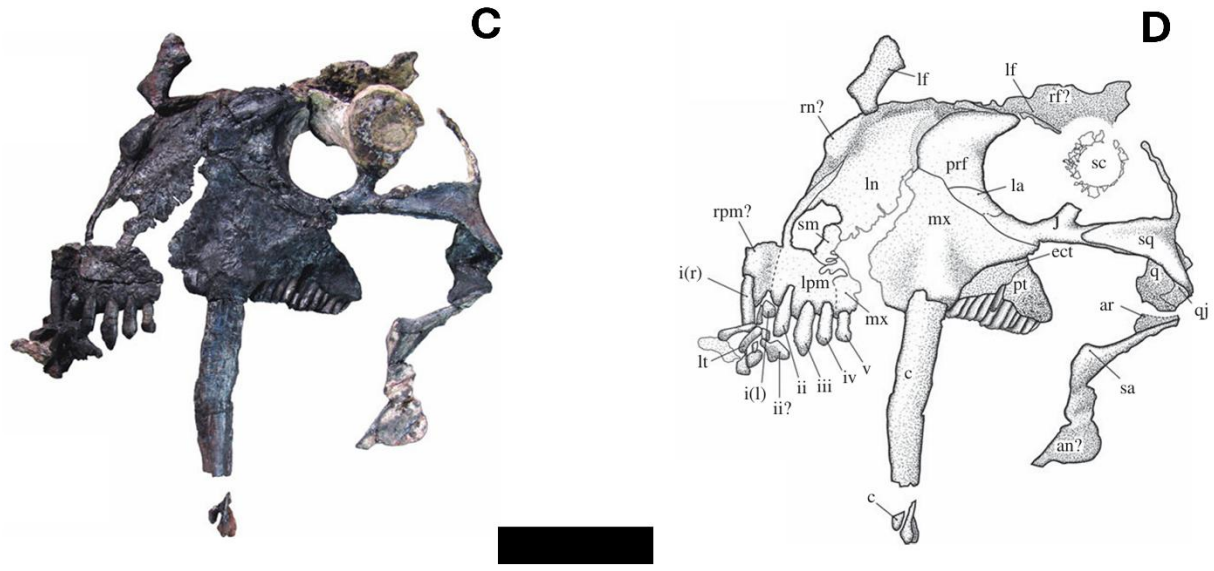
On the basis of these characters, as well as the phylogenetic position of BP/1/8500 in the phylogenetic tree presented above (Fig. 14), it seems justified to regard this specimen as a separate genus and species of dicynodont. This species adds up to the diversity of anomodonts in the *Eodicynodon* Assemblage Zone, which was limited to *Nyaphulia oelofseni*, *Eodicynodon oosthuizeni* and *Patranomodon nyaphulii* so far.

In addition, this specimen is important in that it is a dicynodont that has anomocephaloid synapomorphies (the large pterygoid teeth being the most important of them) (Fig. 17). The presence of pterygoid dentition is suggestive of a highly herbivorous diet (Modesto et al. 1999; Cisneros et al. 2015). Previous phylogenetic analyses (Cisneros et al. 2011; Boos et al. 2016; Kammerer & Smith, 2017; Angielczyk & Kammerer, 2017; Angielczyk et al. 2021; Duhamel et al. 2024)

recover anomocephaloids to be less derived than the dicynodonts as such pterygoid teeth can be seen as a primitive feature that is convergent in BP/1/8500 and lost in more derived dicynodonts.

Among anomodonts, transversely expanded pterygoid teeth are present only in Anomocephaloidea (*Tiarajudens* and *Anomocephalus*) and BP/1/8500, which are Gondwanan anomodonts. This observation supports the observations of Modesto and Rybczynski (1999) that anomodonts were characterised by endemism early in their evolutionary history.


A
B
na
fr
pfr
ppr?
la
pob
tf
sq
Pmx
mx
tu
pcn
pt
ju
qpt


C
D
lf
lf
rn?
rf?
sc
prf
ln
la
rpm?
sm
mx
sq
ect
i(r)
lpm
pt
q
ar
qj
mx
lt
iv
v
c
i(l)
ii
iii
ii?
sa
an?
c

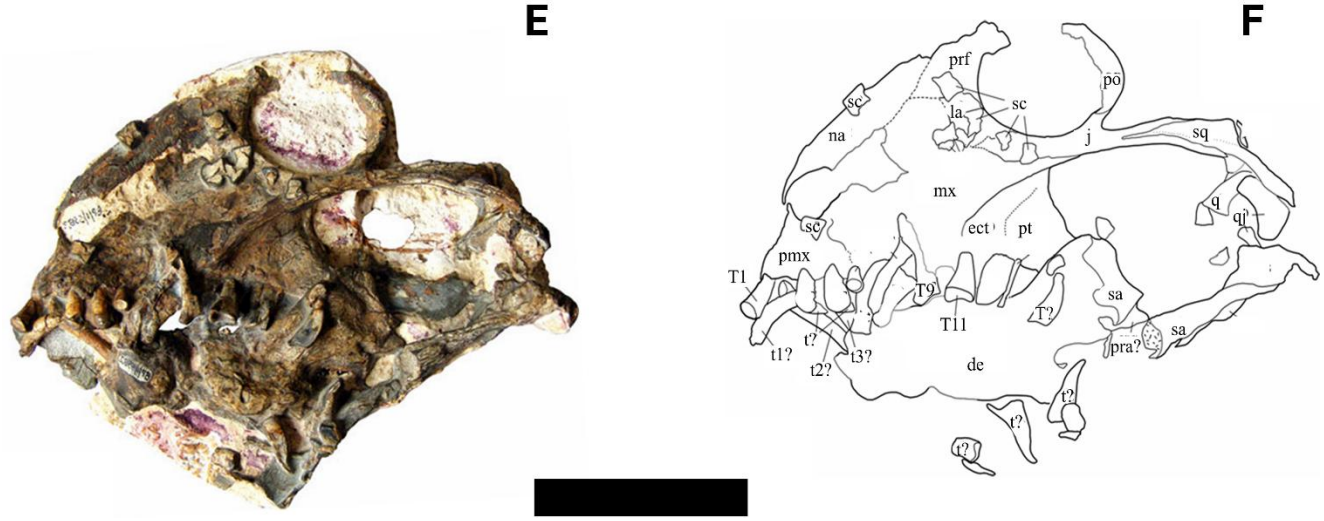

E
F
prf
pō
sc
sc
la
na
j
sq
mx
q
qj
sc
ect
pt
pmx
T1
T9
T11
T?
sa
t?
t1?
t2?
t3?
de
pra?
sa
t?
t?
t?

Figure 17: Comparison of three basal anomodonts taxa from Gondwana. **A**) left lateral view of BP/1/8500 from Middle Permian of South Africa, **B**) illustration of BP/1/8500, **C**) left lateral view of *Tiarajudens eccentricus* (UFRGS PV393P) from Middle Permian of Brazil, **D**) illustration of *Tiarajudens eccentricus* obtained from Cisneros et al. 2011, **E**) right lateral view of *Anomocephalus africanus* (BP/1/5582) from Middle Permian of South Africa, **F**) illustration of *Anomocephalus africanus* obtained from Cisneros et al. 2015. The scale bar for A, B, E and F is 3cm and the scale bar for C and D is 2cm.

5.2 Implication for body size evolution

Body size is a fundamental determinant of organisms' biology and ecology (Brown et al. 2004; White et al. 2007; Hantak et al. 2021; Stockdale & Benton, 2021). The results of the body size estimate undertaken in this project show an overall increase in anomodont body size during phylogenetic development (Figs. 15 & 16).

During the Middle Permian, most dicynodonts exhibited relatively small body sizes, with the exception of the medium-sized *Lanthanostegus*, *Colobodectes*, and *Brachyprosopus*. The discovery of BP/1/8500 contributes to the list of medium-sized dicynodonts (Fig. 15). The Capitanian crisis imposed a tetrapod faunal shift from one which is dinocephalian-dominated to being dicynodont-dominated, and there was a reduction in the diversity across tetrapod clades (Day & Rubidge, 2021). The taxa that became extinct as a result of the Capitanian crisis are the dinocephalians and bradysaurian pareiasaurs (Romano & Rubidge, 2019). The loss of these large-bodied taxa created an ecological gap that favoured the appearance of large dicynodonts during the Lopingian (Smith et al. 2012; Day et al. 2015).

The radiation of large-sized dicynodonts began with the appearance of *Endothiodon bathystoma* (Araújo et al. 2017; Maharaj et al. 2019), *Rachiocephalus magnus*

(Kammerer et al. 2011), *Oudenodon bainii* (Owen, 1960), *Aulacephalodon bainii* (Seeley, 1898), and *Dicynodontoides* during the Wuchianpingian age. However, the majority of dicynodonts at this time were medium-sized.

During the Changsingian, just before the PTB, there is an overall increase in dicynodont body size, although it is crucial to note that species diversity was lower than in the Wuchianpingian, Capitanian, and Wordian (Viglietti, 2020; Day & Rubidge, 2021). This suggests that the increase in body size may be due to the selective loss of small-bodied taxa (e.g. emydopoids, *Pristerodon*, and *Diictodon*).

After the end Permian extinction event, medium-sized dicynodonts dominated and included the *Lystrosaurus* species: *L. murrayi* and *L. declivis* (Botha & Smith, 2020; Day & Rubidge, 2021). *Myosaurus*, which is relatively small, was also part of the early Triassic dicynodont fauna but was a minor component. Subsequently, anomodont size increased consistently during the Triassic, but taxonomic diversity was extremely low.

CHAPTER 6: CONCLUSION

Taxa comprising the relatively diverse fossil therapsid fauna from the *Eodicynodon* Assemblage Zone of the Beaufort Group are considered to be phylogenetically and morphologically more primitive than those from the overlying biozones of the Beaufort Group (Rubidge, 1990). This research focuses on the cranial description and phylogenetic analysis of two newly discovered anomodont specimens (BP/1/8740 and BP/1/8500) from the *Eodicynodon* Assemblage Zone. Based on the recent data matrices of Angielczyk et al. (2021) and Duhamel et al. (2024), a detailed phylogenetic analysis was undertaken using TNT and Mesquite.

The results of this analysis indicate that specimen BP/1/8740 is an additional specimen of the basal anomodont *Patranomodon*. The differences between the two *Patranomodon* specimens can be attributed to growth status, as is indicated by the smaller size, fewer maxillary teeth, and smaller pineal foramen of the referred specimen.

By contrast, specimen BP/1/8500 is a new basal dicynodont genus which is phylogenetically positioned between non-dicynodont anomodonts and dicynodonts. Phylogenetically, this specimen is recovered as the second most basal dicynodont, following *Nyaphulia oelofseni*, and holds a more basal position than *Eodicynodon*. Predictably, although it is a dicynodont, it does possess characters of non-dicynodont anomodonts such as the presence of teeth on the pterygoid, a squamosal that appears to not be flared, a narrow postorbital bar, and a temporal fenestra that is triangular.

The phylogenetic analysis indicates that the most primitive dicynodonts are from southern Africa, especially from the South Africa’s Karoo Basin. Many of the earliest

and most primitive dicynodonts from the Middle Permian and Late Permian such as *Nyaphulia oelofseni* (Duhamel et al. 2024), *Eodicynodon oosthuizeni* (Rubidge, 1990), *Colobodectes cluveri* (Modesto et al. 2003; Angielczyk & Rubidge, 2009), *Lanthanostegus mohoii* (Modesto et al. 2002; Rubidge et al. 2021), *Eosimops newtoni* (Angielczyk & Rubidge, 2013), *Robertia broomiana* (Boonstra, 1948), *Prosictodon dubei* (Rubidge, 2010), *Pristerodon mackayi* (Laaß, 2015), and *Brachyprosopus broomi* (Angielczyk et al. 2016) are from the South African Karoo Basin. The presence of these early dicynodonts from the Karoo Basin supports that southern Africa is the place of origin of Dicynodontia, and from here they expanded across Pangea to become the dominant land vertebrates during the Permian and Triassic periods.

The body size analysis (using cranial length as a proxy for body size) of a large sample of different dicynodont taxa which were present around the globe from the Permian to the Late Triassic, suggests that the body size of anomodonts has gradually increased over time, but at the same time, diversity has decreased. Before the Capitanian extinction event, most of the anomodonts were small. Interestingly, these small-bodied taxa are from the *Eodicynodon* and *Tapinocephalus* Assemblage Zones of the Karoo Basin, the lowermost biozones of the Beaufort Group. The Capitanian extinction event imposed a tetrapod faunal shift from one that was dinocephalian dominated to being dicynodont dominated. Following this extinction, although there were still small-bodied dicynodonts, the radiation of large-sized dicynodonts began with the appearance of *Endothiodon bathystoma*, *Rachiocephalus magnus*, *Oudenodon bainii*, *Aulacephalodon bainii*, and *Dicynodontoides* during the Wuchianpingian age.

Just before the end-Permian mass extinction (the most devastating mass extinction in Earth's history), there was an overall increase in anomodont body size, and species richness was lower than that of the Middle and early Late Permian. During the Triassic, anomodont body size increased consistently, but taxonomic diversity was at its lowest.

REFERENCES

Angielczyk, K.D. 2004. Phylogenetic evidence for and implications of a dual origin of propaliny in anomodont therapsids (Synapsida). *Paleobiology*, **2**, 268-296.

Angielczyk, K.D. 2007. New specimens of the Tanzanian dicynodont "*Cryptocynodon parringtoni*" von Huene, 1942 (Therapsida, Anomodontia), with an expanded analysis of Permian dicynodont phylogeny. *Journal of Vertebrate Paleontology*, **1**, 116-131.

Angielczyk, K.D., Sullivan, C. 2008. *Diictodon feliceps* (Owen, 1876), a dicynodont (Therapsida, Anomodontia) species with a Pangaean distribution. *Journal of Vertebrate Paleontology*, **3**, 788-802.

Angielczyk, K.D., Walsh, M.L. 2008. Patterns in the evolution of nares size and secondary palate length in anomodont therapsids (Synapsida): implications for hypoxia as a cause of end-Permian tetrapod extinctions. *Journal of Paleontology*, **3**, 528-542.

Angielczyk, K.D., Rubidge, B.S. 2010. A new pylaecephalid dicynodont (Therapsida, Anomodontia) from the *Tapinocephalus* assemblage zone, Karoo basin, Middle Permian of South Africa. *Journal of Vertebrate Paleontology*, **5**, 1396-1409.

Angielczyk, K.D., Rubidge, B.S. 2013. Skeletal morphology, phylogenetic relationships and stratigraphic range of *Eosimops newtoni.* Broom, 1921, a

pylaecephalid dicynodont (Therapsida, Anomodontia) from the Middle Permian of South Africa. *Journal of Systematic Palaeontology*, **11**, 191–231.

Angielczyk, K.D., Rubidge, B.S., Day, M.O., Lin, F. 2016. A reevaluation of *Brachyprosopus broomi* and *Chelydontops altidentalis*, dicynodonts (Therapsida, Anomodontia) from the Middle Permian *Tapinocephalus* Assemblage Zone of the Karoo Basin, South Africa. *Journal of Vertebrate Paleontology*, **2**, e1078342.

Angielczyk, K.D., Kammerer, C.F. 2017. The cranial morphology, phylogenetic position and biogeography of the upper Permian dicynodont *Compsodon helmoedi* van Hoepen (Therapsida, Anomodontia). *Papers in Palaeontology*, **3**, 513–545.

Angielczyk, K.D., Hancox, P., Nabavizadeh, A. 2017. A redescription of the Triassic kannemeyeriiform dicynodont *Sangusaurus* (Therapsida, Anomodontia), with an analysis of its feeding system. *Journal of Vertebrate Paleontology*, **37**, 189–227.

Araújo, R., Fernandez, V., Polcyn, M.J., Fröbisch, J., Martins, R.M. 2017. Aspects of gorgonopsian paleobiology and evolution: insights from the basicranium, occiput, osseous labyrinth, vasculature, and neuroanatomy. *PeerJ*, **5**, e3119.

Angielczyk, K.D., Kammerer, C. 2018. Non-Mammalian synapsids: the deep roots of the mammalian family tree. In: Zachos, F. and Asher, R. ed. *Mammalian Evolution, Diversity and Systematics*. Berlin, Boston: De Gruyter, **5**,117-198.

Angielczyk, K.D., Liu, J., Yang, W. 2021. A Redescription of *Kunpania scopulusa*, a Bidentalian Dicynodont (Therapsida, Anomodontia) from the Guadalupian of Northwestern China. *Journal of Vertebrate Paleontology*, e1922428.

Bapst, D.W. 2013. A stochastic rate-calibrated method for time-scaling phylogenies of fossil taxa. *Methods in Ecology and Evolution*, **8**, 724-733.

Bapst, D.W. 2014. Assessing the effect of time-scaling methods on phylogeny-based analyses in the fossil record. *Paleobiology*, **3**, 331-351.

Barghusen, H.R. 1976. Notes on the adductor jaw musculature of Venjukovia, a primitive anomodont therapsid from the Permian of the U.S.S.R. *Annals of the South African Museum*, **69**, 249-260.

Barry, T. 1974. A new dicynodont ancestor from the Upper Ecca (lower Middle Permian) of South Africa. *Annals of the South African Museum*, **64**, 117–136.

Battail, B. 2000. A comparison of Late Permian Gondwanan and Laurasian amniote faunas. *Journal of African Earth Sciences*, **31**, 165–174.

Benoit, J., Abdala, F., Van den Brandt, M.J., Manger, P., Rubidge, B.S. 2015. Physiological implications of the abnormal absence of the parietal foramen in a Late Permian cynodont (Therapsida). *The Science of Nature*, **102**, 69.

Benoit, J., Abdala, F., Manger, P., Rubidge, B.S. 2016. The sixth sense in mammalians forerunners: Variability of the parietal foramen and the evolution of the pineal eye in South African Permo-Triassic eutheriodont therapsids. *Acta Palaeontologica Polonica*, **61**, 777–789.

Benoit, J., Angielczyk, K.D., Miyamae, J.A., Manger, P., Fernandez, V., Rubidge, B.S. 2018. Evolution of facial innervation in anomodont therapsids (Synapsida): Insights from X-ray computerized microtomography. *Journal of Morphology*, **279**, 673–701.

Blob, R.W. 2001. Evolution of hindlimb posture in nonmammalian therapsids: biomechanical tests of paleontological hypotheses. *Paleobiology*, **1**,14-38.

Boonstra, L.D. 1948. On the anomodont reptiles from the *Tapinocephalus*-zone of the Karroo System. In: Du Toit, A. L (ed). *Robert Broom Commemorative Volume*. Special Publication of the Royal Society of South Africa*. Royal Society of South Africa*, *Cape Town*, 57-64.

Boos, A.D.S., Kammerer, C.F., Schultz, C.L., Paes Neto, V.D. 2015. A tapinocephalid dinocephalian (Synapsida, Therapsida) from the Rio do Rasto Formation (Parana Basin, Brazil): Taxonomic, ontogenetic and biostratigraphic considerations. *Journal of South American Earth Science*, **63**, 375–384.

Botha, J., Smith, R.M. 2020. Biostratigraphy of the Lystrosaurus declivis Assemblage Zone (Beaufort Group, Karoo Supergroup), South Africa. *South African Journal of Geology*, **123**, 207-216.

Brinkman, D. 1981. The structure and relationships of the dromasaurs (Reptilia: Therapsida). *Breviora*, **465**, 1-34.

Brocklehurst, N. 2019. Morphological evolution in therocephalians breaks the hypercarnivore ratchet. *Proceedings of the Royal Society B*, **286**, p.20190590.

Broom, R. 1905. On the use of the term Anomodontia. *Records of the Albany Museum*, **1**, 266–269.

Broom, R. 1907. On some new fossil reptiles from the Karroo beds of Victoria West, South Africa. *Transactions of the South African Philosophical Society*, **18**, 31–42.

Broom, R. 1910. A comparison of the Permian reptiles of North America with those of South Africa. *Bulletin of the American Museum of National History*, **28**, 197–234.

Broom, R. 1912. On some new fossil reptiles from the Permian and Triassic beds of South Africa. *Proceedings of the Zoological Society of London*, **82**, 859–876.

Broom, R. 1921. On some new genera and species of anomodont reptiles from the Karroo beds of South Africa. *Proceedings of the Zoological Society of London,* **91**, 647–674.

Campione, N.E., Evans, D.C., Brown, C.M., Carrano, M.T. 2014. Body mass estimation in non-avian bipeds using a theoretical conversion to quadruped stylopodial proportions. *Methods in Ecology and Evolution*, **9**, 913-923.

Castanhinha, R., Araújo, R., Júnior, L.C., Angielczyk, K.D., Martins, G.G., Martins, R.M.S., Chaouiya, C., Beckmann, F., Wilde, F. 2013. Bringing dicynodonts back to life: paleobiology and anatomy of a new emydopoid genus from the Upper Permian of Mozambique. *PLoS ONE*, **8**, e80974.

Cisneros, J.C., Abdala, F., Rubidge, B.S., Dentzien-Dias, P.C., de Oliveira Bueno, A. 2011. Dental occlusion in a 260-million-year-old therapsid with saber canines from the Permian of Brazil. *Science*, **331**, 1603–1605.

Cisneros, J.C., Abdala, F., Jashashvili, T., de Oliveira Bueno, A., Dentzien-Dias, P. 2015. *Tiarajudens eccentricus* and *Anomocephalus africanus*, two bizarre anomodonts (Synapsida, Therapsida) with dental occlusion from the Permian of Gondwana. *Open Science*, **2**, 150090.

Cluver, M.A. 1971. The cranial morphology of the dicynodont genus *Lystrosaurus*. Unpublished PhD thesis, University of Stellenbosch, 1-214.

Cluver, M.A. 1975. A new dicynodont reptile from the *Tapinocephalus* zone (Karoo System, Beaufort Series) of South Mica, with evidence of the jaw adductor musculature. *Annals of the South African Museum*, **67**, 7-23.

Cluver, M.A., King, G.M. 1983. A reassessment of the relationships of Permian Dicynodontia (Reptilia, Therapsida) and a new classification of dicynodonts. *Annals of the South African Museum*, **91**, 195-273.

Cole, D.I., Wipplinger, P.E. 2001. Sedimentology and molybdenum potential of the Beaufort Group in the main Karoo Basin, South Africa. *Memoirs of the Council for Geoscience*, **80**, 225.

Crompton, A.W., Hotton III, N. 1967. Functional morphology of the masticatory apparatus of two dicynodonts (Reptilia, Therapsida). *Postilla Yale Peabody Museum*, **109**, 1-52.

Day, M.O., Rubidge, B.S. 2014. A brief lithostratigraphic review of the Abrahamskraal and Koonap Formations of the Beaufort Group, South Africa: towards a basin-wide stratigraphic scheme for the Middle Permian Karoo. *Journal of African Earth Sciences*, **100**, 227–242.

Day, M.O., Ramezani, J., Bowring, S.A., Sadler, P.M., Erwin, D.H., Abdala, F., Rubidge, B.S. 2015. When and how did the terrestrial mid-Permian mass extinction occur? Evidence from the tetrapod record of the Karoo Basin, South Africa. *Proceedings of the Royal Society B: Biological Sciences*, **282**, 20150834.

Day, M.O., Güven, S., Abdala, F., Jirah, S., Rubidge, B., Almond, J. 2015. Youngest dinocephalian fossils extend the Tapinocephalus zone, Karoo Basin, South Africa. *South African Journal of Science*, **111**, 1–5.

Dias-da-Silva, S. 2012. Middle–Late Permian tetrapods from the Rio do Rasto Formation, Southern Brazil: a biostratigraphic reassessment. *Lethaia*, **45**, 109–120.

Duhamel, A., Benoit, J., Wynd, B., Wright, A.M., Rubidge, B.S. 2024. Redescription of three basal anomodonts: a phylogenetic reassessment of the holotype of *Eodicynodon oelofseni* (NMQR 2913). *Frontiers in Earth Science*, **11**, 1220341.

Foote, M. 2001a. Evolutionary rates and the age distributions of living and extinct taxa. **In**: Jackson, J. B. C.; McKinney, F. K.; and Lidgard, S., eds. Evolutionary patterns: growth, form, and tempo in the fossil record. Chicago, University of Chicago Press, 245–294.

Foote, M. 2000b. Origination and extinction components of taxonomic diversity: general problems. *Paleobiology*, **4**, 74-102.

Friedman, M., Brazeau, M.D. 2011. Sequences, stratigraphy and scenarios: what can we say about the fossil record of the earliest tetrapods? *Proceedings of the Royal Society B: Biological Sciences*, **1704**, 432-439.

Fröbisch, J., Reisz, R.R. 2008. A new species of *Emydops* (Synapsida, Anomodontia) and a discussion of dental variability and pathology in dicynodonts. *Journal of Vertebrate Paleontology*, **28**, 770–787.

Fröbisch, J. 2009. Composition and similarity of global anomodont-bearing tetrapod faunas. *Earth Science Reviews*, **95**, 119–157.

Garbe, U., Randall, T., Hughes, C., Davidson, G., Pangelis, S., Kennedy, S.J. 2015. A new neutron radiography/tomography/imaging station DINGO at OPAL. *Physics Procedia,* **69**, 27-32.

Goloboff, P.A., Mattoni, C.I., Quinteros, A.S. 2006. Continuous characters analyzed as such. *Cladistics*, **6**, 589-601.

Goloboff, P.A., Farris, J.S., Nixon, K.C. 2008. TNT, a free program for phylogenetic analysis. *Cladistics*, **5**, 774-786.

Hancox, P.J., Rubidge, B.S. 2001. Breakthroughs in the biodiversity, biogeography, biostratigraphy, and basin analysis of the Beaufort Group. *Journal of African Earth Science*, **33**, 563–577.

Hantak, M.M., McLean, B.S., Li, D. Guralnick, R. 2021. Mammalian body size is determined by interactions between climate, urbanization, and ecological traits. *Communications Biology*, **4**, 972.

Hopson, J., Barghusen, H. 1986. An analysis of therapsid relationships. In N. Hotton III, P. D. MacLean, J. J. Roth, & E. C. Roth (Eds.). *In The Ecology and Biology of Mammal-Like Reptiles*. Smithsonian Institution Press, 83–106.

Hurlburt, G. 1999. Comparison of body mass estimation techniques, using Recent reptiles and the pelycosaur *Edaphosaurus Boanerges*. *Journal of Vertebrate Paleontology*, **19**, 338–350.

Hutchinson, J.R., Bates, K.T., Molnar, J., Allen, V., Makovicky, P.J. 2011. A computational analysis of limb and body dimensions in *Tyrannosaurus rex* with implications for locomotion, ontogeny, and growth. *PloS one*, **10**, e26037.

Huxley, T.H. 1868. On *Saurosternon bainii*, and *Pristerodon mckayi*, Two New Fossil Lacertilian Reptiles from South Africa. *Geological Magazine*, **5**, 201–205.

Ivakhnenko, M.F. 1996. Primitive anomodonts, venyukoviids, from the Late Permian of Eastern Europe. Paleontological Journal, **30**, 77-84.

Ivakhnenko, M.F. 2003. Eotherapsids from the east European placket (Late Permian). *Paleontological Journal*, **37**, 339–465.

Jinnah, Z.A., Rubidge, B.S. 2007. A double-tusked dicynodont and its biostratigraphic significance. *South African Journal of Science*, **103**, 51–53.

Jirah, S., Rubidge, B.S. 2014. Refined stratigraphy of the Middle Permian Abrahamskraal Formation (Beaufort Group) in the southern Karoo Basin. *Journal of African Earth Sciences*, **100**, 121-135.

Kammerer, C.F., Angielczyk, K.D., Fröbisch, J. 2011. A comprehensive taxonomic revision of *Dicynodon* (Therapsida, Anomodontia) and its implications for dicynodont phylogeny, biogeography, and biostratigraphy. *Journal of Vertebrate Paleontology*, **31**, 1–158.

Kammerer, C.F., Angielczyk, K.D., Fröbisch, J. 2015. Redescription of the geikiid Pelanomodon (Therapsida, Dicynodontia), with a reconsideration of 'Propelanomodon'. *Journal of Vertebrate Paleontology*, **36**, e1030408.

Kammerer, C.F., Smith, R.M.H. 2017. An early geikiid dicynodont from the *Tropidostoma* Assemblage Zone (Late Permian) of South Africa. *PeerJ*, **5**, e2913.

Kemp, T.S. 2005. *The origin and evolution of mammals* (Oxford University).

King, G.M., Rubidge, B.S. 1993. A taxonomic revision of small dicynodonts with postcanine teeth. *Zoological Journal of the Linnean Society*, **2**, 131-154.

King, G.M. 1988. Anomodontia. *Handbuch der Paliioherpetologie*, **17**, 1-174.

King, G.M., Cluver, M.A. 1990. The aquatic *Lystrosaurus:* An alternative lifestyle. *Historical Biology*, **4**, 323–341.

Laaß, M. 2015. Virtual reconstruction and description of the cranial endocast of *Pristerodon mackayi* (Therapsida, Anomodontia). *Journal of Morphology*, **276**, 1089–1099.

Laaß, M., Schillinger, B., Kaestner, A. 2017. What did the "Unossified zone" of the non-mammalian therapsid braincase house? *Journal of Morphology*, **278**, 1020–1032.

Langer, M.C. 2000. The first record of dinocephalians in South America Late Permian (Rio do Rasto Formation) of the Parana´Basin. *Neues Jahrbuch fur Geologie und Palaontologie Abhandlugen*, **215**, 69–95.

Le Roux, J.P. 1985. Palaeochannels and uranium mineralization in the main Karoo Basin of South Africa. Unpublished Ph.D. Thesis, University of Port Elizabeth, 250.

Li, J., Cheng, Z. 1997. First discovery of eotitanosuchian (Therapsida, Synapsida) of China. *Vertebrata Palasiatica*, **35**, 268–282.

Liu, J., Rubidge, B.S., Li, J. 2010. A new specimen of *Biseridens qilianicus* indicates its phylogenetic position as the most basal anomodont. *Proceedings of the Royal Society of London B: Biological Sciences*, **277**, 285–292.

Loock, J.C., Brynard, H.G., Heard, R.G., Kitching, J.W., Rubidge, B.S. 1994. The stratigraphy of the lower Beaufort Group in an area north of Laingsburg, South Africa. *Journal of African Earth Sciences*, **18**, 185–195.

Maddison, W.P., Maddison, D.R. 2015. Mesquite: a modular system for evolutionary analysis. Version 3.04. http://mesquiteproject.org.

Mays, C., Bevitt, J., Stilwell, J. 2017. Pushing the limits of neutron tomography in palaeontology: Three-dimensional modelling of in situ resin within fossil plants, *Palaeontologia Electronica*, **20**, 1-12.

Modesto, S., Rubidge, B.S., Welman, J. 1999. The most basal anomodont therapsid and the primacy of Gondwana in the evolution of the anomodonts.

Proceedings of the Royal Society of London B: Biological Sciences, **266**, 331–337.

Modesto, S., Rybczynski, N. 1999 The amniote faunas of the Russian Permian: implications for Late Permian terrestrial vertebrate biogeography. In The age of dinosaurs in Russia and Mongolia: fossil vertebrates from the Permian and Mesozoic of the former Soviet Union and Mongolia (ed. M. J. Benton, E. N. Kurochkin, M. A. Shishkin & D. M. Unwin). Cambridge University Press.

Modesto, S., Rubidge, B.S., Welman, J. 2002. A new dicynodont therapsid from the lowermost Beaufort Group, Upper Permian of South Africa. *Canadian Journal of Earth Sciences,* **39**, 1755–1765.

Modesto, S., Rubidge, B.S., Visser, I., Welman, J. 2003. A new basal dicynodont from the Upper Permian of South Africa. Palaeontology, **46**, 211–223.

Norton, L. A., Abdala, F., Rubidge, B.S., Botha, J. 2020. Tooth replacement patterns in the Early Triassic epicynodont *Galesaurus planiceps* (Therapsida, Cynodontia). *PLoS ONE*, **15**, e0243985.

Norton, L.A., Abdala, F., Rubidge, B.S., Botha, J. 2021. Tooth replacement in the non-mammalian cynodont *Cynosaurus suppostus* (Therapsida) from the Late Permian of South Africa. *Journal of Vertebrate Paleontology*, **41**, e2001650.

Olroyd, S.L., Sidor, C.A., Angielczyk, K.D. 2018. New materials of the enigmatic dicynodont *Abajudon kaayai* (Therapsida, Anomodontia) from the lower Madumabisa Mudstone Formation, Middle Permian of Zambia. *Journal of Vertebrate Paleontology*, **37**, e1403442.

Olson, E.C. 1944. Origin of mammals based upon cranial morphology of the therapsid suborders. *Geological Society of America*, **55**, 136.

Owen, R. 1859. On the orders of fossil and recent Reptilia and their distribution in time. *Report of the British Association for the Advancement of Science*, **29**, 153–166.

Owen, R. 1876. *Descriptive and illustrative catalogue of the fossil Reptilia of South Africa in the collection of the British Museum (Natural History)*. London: Taylor and Fransis, 88.

Ray, S., Chinsamy, A. 2004. *Diictodon feliceps* (Therapsida, Dicynodontia): bone histology, growth, and biomechanics. *Journal of Vertebrate Paleontology*, **1**,180-194.

Reisz, R.R., Sues, H.D. 2000. Herbivory in Late paleozoic and triassic terrestrial vertebrates. In: Sues H-D, editor. *Evolution of herbivory in terrestrial vertebrates*. Cambridge: Cambridge University Press, 9-41.

Reisz, R.R. 2006. Origin of dental occlusion in tetrapods: signal for terrestrial vertebrate evolution? *Journal of Experimental Zoology Part B: Molecular and Developmental Evolution*, **306**, 261–277.

Romano, M., Rubidge, B.S. 2019. Long bone scaling in Captorhinidae: do limb bones scale according to elastic similarity in sprawling basal amniotes? *Lethaia*, **52**, 389–402.

Romano, M., Manucci, F. 2021. Resizing *Lisowicia bojani*: volumetric body mass estimate and 3D reconstruction of the giant Late Triassic dicynodont. *Historical Biology*, **33**, 474 – 479.

Romer, A.S., Price, L.W. 1940. Review of the Pelycosauria. *Geological Society of America Special Papers*, **28**, 1–534.

Rubidge, B.S. 1990. The cranial morphology of a new species of the genus *Eodicynodon* (Therapsida, Dicynodontia). *Navorsinge van die Nasionale Museum*, **7**, 38–39.

Rubidge, B.S., Hopson, J.A. 1996. A primitive anomodont therapsid from the base of the Beaufort Group (Upper Permian) of South Africa. *Zoological Journal of the Linnean Society*, **117**, 115–139.

Rubidge, B.S., Sidor, C.A. 2001. Evolutionary patterns among Permo-Triassic therapsids. *Annual Review of Ecology and Systematics*, **32**, 449–480.

Rubidge B.S. 2005. 27th Du Toit Memorial Lecture: Re-uniting lost continents – Fossil reptiles from the ancient Karoo and their wanderlust. *South African Journal of Geology*, **1**, 135–172.

Rubidge, B.S., Day, M.O., Barbolini, N., Hancox, P.J., Choiniere, J.N., Bamford, M.K., Viglietti, P.A., McPhee, B.W., Jirah, S. 2016. Advances in nonmarine Karoo biostratigraphy: significance for understanding basin development. *Origin and evolution of the Cape Mountains and Karoo Basin*, Springer International Publishing, 141-149.

Rubidge, B.S., Day, M.O. 2020. Biostratigraphy of the *Eodicynodon* Assemblage Zone (Beaufort Group, Karoo Supergroup), South Africa. *South African Journal of Geology*, **123**, 141–148.

Rubidge, B.S., Day, M.O., Benoit, J. 2021. New Specimen of the Enigmatic Dicynodont *Lanthanostegus mohoii* (Therapsida, Anomodontia) from the Southwestern Karoo Basin of South Africa, and its Implications for Middle Permian Biostratigraphy. *Frontiers in Earth Science*, **9**, 668143.

Ruta, M., Angielczyk, K.D., Fröbisch, J. & Benton, M.J. 2013. Decoupling of morphological disparity and taxic diversity during the adaptive radiation of

anomodont therapsids. *Proceedings of the Royal Society B: Biological Sciences*, **280**, 20131071.

Rybczynski, N. 2000. Cranial anatomy and phylogenetic position of *Suminia getmanovi*, a basal anomodont (Amniota: Therapsida) from the Late Permian of Eastern Europe. *Zoological Journal of the Linnean Society*, **130**, 329–373.

Rybczynski, N., Reisz, R.R. 2001. Earliest evidence for efficient oral processing in a terrestrial herbivore. *Nature*, **411**, 684–687.

Sennikov, A.G., Golubev, V.K. 2017. Sequence of Permian tetrapod faunas of Eastern Europe and the Permian–Triassic ecological crisis. *Paleontological Journal*, **51**, 600–611.

Seeley H.G. 1898. On Oudenodon (Aulacocephalus) pithecops from the Dicynodon Beds of East London, Cape Colony. *Geological Magazine*, **5**, 107-110.

Sidor, C. A. 2001. Evolutionary trends and relationships within the Synapsida. Ph.D. thesis. The University of Chicago.

Sidor, C.A., Smith, R.M.H. 2007. A second burnetiamorph therapsid from the Permian Teekloof Formation of South Africa and its associated fauna. *Journal of Vertebrate Paleontology*, **27**, 420–430.

Sidor, C.A., Welman, J. 2003. A second specimen of *Lemurosaurus pricei* (Therapsida: Burnetiamorpha). *Journal of Vertebrate Paleontology*, **23**, 631–642.

Sidor, C.A., Rubidge, B.S. 2006. Herbivorous adaptations in the synapsid dentition. In Carrano, M. T., Gaudin, T. J., Blob, R. W., & Wible, J. R. (Eds.), in *Amniote paleobiology: Perspectives on the evolution of Mammals, Birds, and Reptiles,* University of Chicago Press, 76–113.

Smith, R.M.H., Rubidge, B.S., Van der Walt, M. 2012. Therapsid biodiversity patterns and paleoenvironments of the Karoo Basin, South Africa. In: A. Chinsamy (Editor), *The forerunners of mammals: radiation, histology and biology*. Indiana University Press, Bloomington, 31-62.

Smith, R.M.H., Rubidge, B.S., Day, M.O., Botha, J. 2020. Introduction to the tetrapod biozonation of the Karoo Supergroup. *South African Journal of Geology*, **123**, 131–140.

Sookias, R.B., Benson, R.B., Butler, R.J. 2012. Biology, not environment, drives major patterns in maximum tetrapod body size through time. *Biology Letters*, **4**, 674-677.

Stanley, S.M. 1985. Rates of evolution. *Paleobiology*, **1**, 13-26.

Strong, E.E., Lipscomb, D. 2000. Character coding and inapplicable data. *Cladistics*, **15**, 363–371.

Sulej, T., Bronowicz, R., Tałanda, M., Niedzwiedzki, G. 2010. A new dicynodont–archosaur assemblage from the Late Triassic (Carnian) of Poland. *Earth and Environmental Science Transactions of the Royal Society of Edinburgh*, **101**, 261–269.

Sullivan, C., Reisz, R.R. 2005. Cranial anatomy and taxonomy of the Late Permian dicynodont *Diictodon*. *Annals of the Carnegie Museum*, **74**, 45–75.

Sullivan, C., Reisz, R.R., Smith, R.M.H. 2003.The Permian mammal-like herbivore Diictodon, the oldest known example of sexually dimorphic armament. *Proceedings of the Royal Society of London*, **270**, 173–178.

Tchudinov, P.K. 1960. Upper Permian therapsids from the Ezhovo locality. *Paleontologičeskij žurnal*, **4**, 81–94.

Tockdale, M.T., Benton, M.J. 2021. Environmental drivers of body size evolution in crocodile-line archosaurs. *Communications Biology*, **4**, 38.

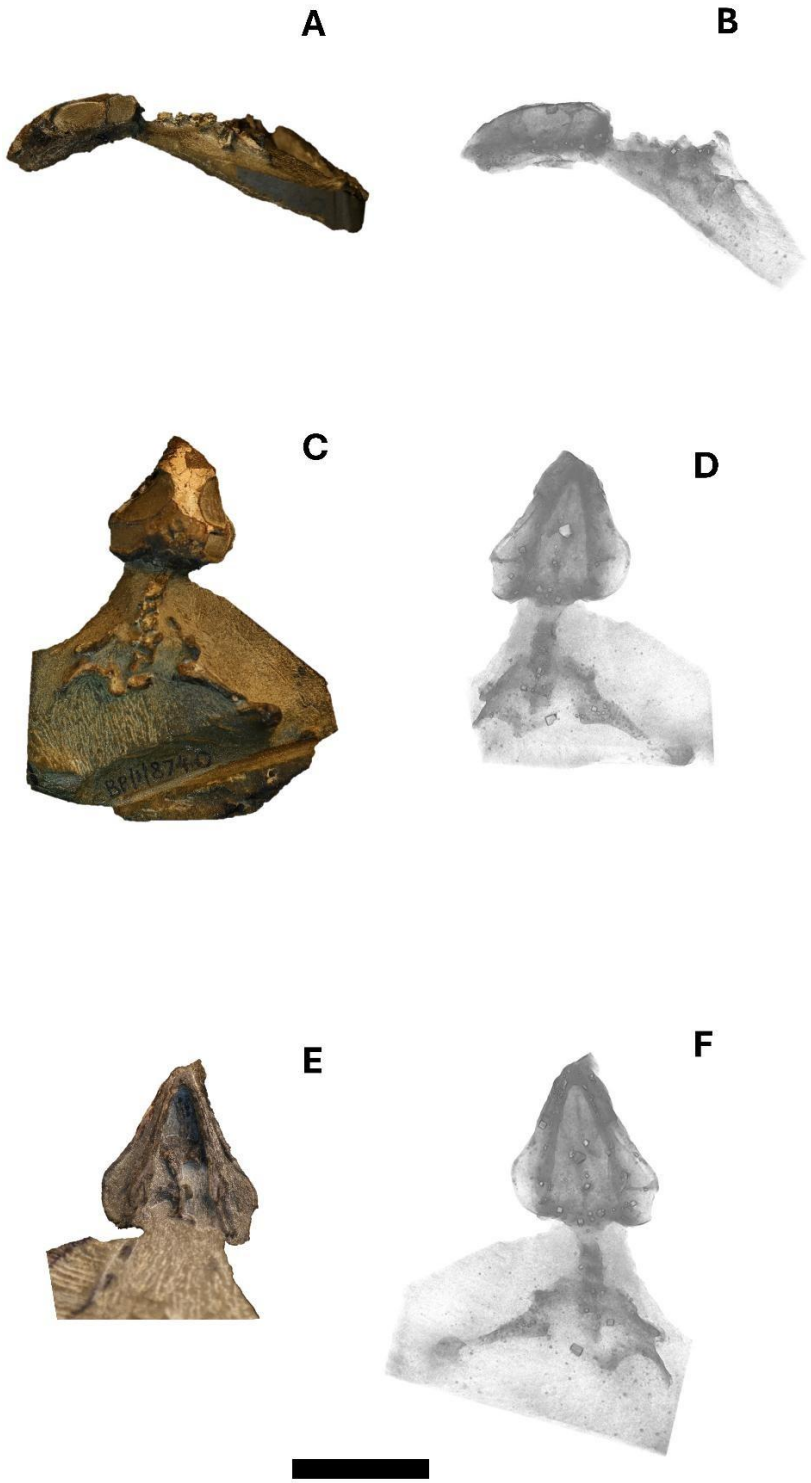
Tollman, S.M., Grine, F.E., Hahn B.D. 1980. Ontogeny and sexual dimorphism in Aulacephalodon (Reptilia, Anomodontia). *Annals of the South African Museum*, **81**, 159–186.

Viglietti, P. 2020. Biostratigraphy of the *Daptocephalus* Assemblage Zone (Beaufort Group, Karoo Supergroup), South Africa. *South African Journal of Geology*, **123**, 191–206.

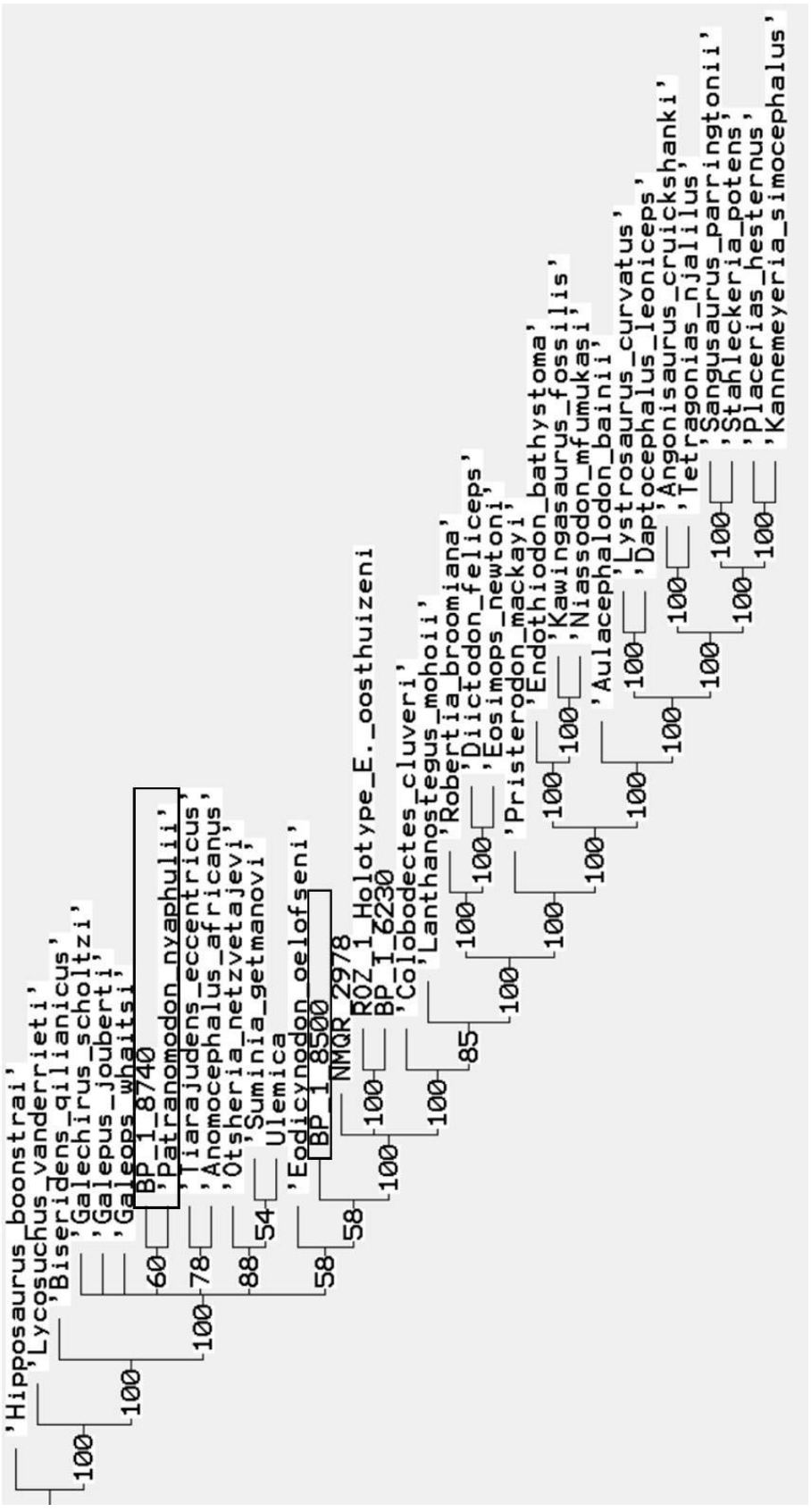
White, E.P., Ernest, S.K.M., Kerkhoff, A.J., Enquist, B.J. 2007. Relationship between body size and abundance in ecology. *Trends in Ecology and Evolution*, **22**, 323–330.

APPENDICES

Appendix 1: Photographs and scans of BP/1/8740. **A**. left lateral view, **B**. left lateral view scan, **C**. dorsal view, **D**. dorsal view scan, **E**. ventral view, **F.** ventral view scan. The scale bar is 3cm.



Appendix 2: Strict consensus tree of Duhamel et al. 2024 showing the phylogenetic position of BP/1/8740 and BP/1/8500 using black rectangles.



Appendix 3: Character list for the phylogenetic analysis.

1. Premaxillae unfused (0) or fused (1).
2. Paired anterior ridges on palatal surface of premaxilla absent (0), present and converge posteriorly (1), or present and do not converge (2).
3. Lateral anterior palatal ridges absent (0) or present (1).
4. Rounded depression on anterior palatal surface of premaxilla: absent (0); present (1).
5. Posterior median ridge on palatal surface of premaxilla absent (0), present with a flattened, expanded anterior area (1), or present without a flattened, expanded anterior area (2).
6. Palatal surface of premaxilla with well-defined depressions with curved sides lateral to median ridge (if present) (0), with distinct accessory ridges lateral to medial ridge (1), or relatively flat with poorly defined or no depressions present (2).
7. Palatal surface of premaxilla with antero-posterior vascular groove lateral to median ridge (if present) absent (0); present (1).
8. Location of premaxillary teeth lateral (0), medial (1) or absent (2).
9. Posterior exposure of the premaxilla on the palate: absent (0), present (1).
10. Posterior process of the premaxilla with a non-bifurcated posterior tip (0) or with a bifurcated posterior tip (1).
11. Palatine shelf ventral to internal naris: absent (0), present (1).
12. Anterior tip of snout rounded (0), squared off (1), or with a deep central invagination, giving the snout a ‘hare-lip’ appearance in anterior view (2).
13. Marked anterior expansion of preorbital region absent (0) or present (1).
14. Snout roughly parallel to long axis of skull (0) or strongly angled ventrally (1).

15. Height of canine-bearing portion of maxilla: relatively short (0); extremely deep, with long caniniform process, but with equally long premaxilla resulting in an overall tall snout (1); extremely long caniniform process offset from rest of snout (2).
16. Snout open to back of the skull (0) or anterior margin of orbit extended posteromedially to partly close off the snout from the rest of the skull (1).
17. Septomaxilla posterodorsal spur present and widely separates nasal and maxilla (0), spur present but does not separate maxilla and nasal (i.e., nasal-maxilla suture present and well defined in this region) (1), septomaxilla spur absent (2).
18. Notch on dorsal edge of narial opening absent (0) or present (1).
19. Postnarial excavation absent (0), present, relatively small, and rounded posteriorly (1), or present, very large, and elongate (2).
20. Maxillary alveolar region short, occupying less than 53% of the ventral length of the bone (0) or tooth bearing region long, occupying 72% or more of the ventral length of the bone (1).
21. Palatal surface of premaxilla exposed in lateral view (1) or not exposed in lateral view (0).
22. Maxillary canine present as large member of tooth series (0), absent (1), or present as tusk (2).
23. Maxillary non-caniniform teeth located near lateral margin of maxilla (0), located more medially, (1), or absent (2).
24. Shelf-like area lateral to the maxillary non-caniniform teeth absent (0) or present (1).
25. Fine serrations on maxillary teeth present (0), serrations absent (1), or coarse serrations present (2).

26. Sutural contact of maxilla and prefrontal present (0) or absent (1).
27. Caniniform process absent (0) or present (1).
28. Caniniform depression: has the form of an embayment bounded by a ridge medially of palatal rim anterior to caniniform process or tusk (1), has the form of a notch in palatal rim anterior to caninfiorm process (2), or absent (0).
29. Distinct lateral caniniform buttress absent (0), present (1), or present with posteroventral furrow (2).
30. Keel-like extension of the palatal rim posterior to the caniniform process absent (0) or present (1).
31. Postcaniniform crest absent (0) or present (1).
32. Ventral edge of the caniniform process or dorsal edge of the erupted portion of the canine tusk anterior (0) to, or at the same level to slightly posterior to (1) the anterior orbital margin.
33. Nasals with a long median suture that separates the premaxilla from the frontals (0) or with a short median suture and frontals and premaxilla in close proximity (1)
34. Nasal bosses absent (0), present as a median swelling with a continuous posterior margin (1), present as paired swellings near the dorsal or posterodorsal margin of external nares (2), present as paired swellings that meet in the midline to form a swollen anterodorsal surface on the snout (3).
35. Naso-frontal suture relatively straight, interdigitated, or gently bowed (0), with a distinct anterior process (1), or with a distinct posterior process (2).
36. Transverse crest approximately at level of naso-frontal suture absent (0); present and straightly transverse to curved with posterior convexity (1); present and strongly curved with posterior concavity (2).

37. Lacrimal does not contact septomaxilla (0) or does contact septomaxilla (1).
38. Prefrontal bosses absent (0), present but separate from nasals (1), or present and confluent with nasal bosses (2).
39. Raised, sometimes rugose, circumorbital rim absent (0) or present (1).
40. Frontal contribution to the dorsal rim of the orbit: broad, frontal forms a major part of the orbital rim (0); thin or absent, if present a thin frontal process extends laterally between the prefrontal and postorbital to reach the orbital margin (1).
41. Postfrontal bone present on dorsal surface of skull (0) or absent (1).
42. Postorbital bar without (0) or with thickenings and rugosities (1).
43. Mediolateral flattening and anteroposterior expansion of postorbital bar for most or all of its length absent (0) or present (1).
44. Temporal portion of skull roof relatively straight, without a strong break in slope (0), or temporal portion of skull roof angled dorsally with a strong break in slope near its anterior end (1).
45. Preparietal bone absent (0), present and flush with skull roof (1), present and depressed (2).
46. Lateral ridges bounding preparietal absent (0) or present (1).
47. Parietals' contribution to skull table transversely as broad as long (0), longer anteroposteriorly than broad (1), or shorter anteroposteriorly than broad (2).
48. Parietal posterolateral process slender and elongate (0), or short (1).
49. Parietals well exposed on the skull roof and relatively flat (0), parietals exposed in midline groove or channel (1), dorsal parietal exposure narrow and crest-like (2).
50. Postparietal bulges outwards as ovoid swellings at posterior end of sagittal crest: no (0); yes (1).

51. Orientation of the temporal portion of the postorbital: relatively flat, so that most of the exterior surface of the bone faces dorsally (0), close to vertical, so that most of the exterior surface of the bone faces laterally (1), or bi-planar, with approximately equally-sized dorsal and lateral surfaces that are close to perpendicular (2).
52. Postorbitals extend the entire length of intertemporal bar (0) or do not extend the entire length of intertemporal bar, such that the posterior portion of the bar is formed only by the parietals (1).
53. Fossa on the ventral surface of the intertemporal bar formed by the postorbital and parietal large (0), reduced (1), or absent (2).
54. Pineal foramen present (0); absent (1).
55. Circumpineal ornamentation: chimney-like boss (0); no boss, foramen flush with skull surface (1); dome- or collar-like boss, rugosity present (2); boss present with incomplete border, more strongly developed on lateral edges of pineal foramen (3).
56. Orientation of pineal foramen: exits perpendicular to long axis of intertemporal bar (0); angled anterior to perpendicular relative to long axis of intertemporal bar (1).
57. Interparietal does not contribute to intertemporal skull roof (0), makes a small contribution to intertemporal skull roof (1), or makes a large contribution to intertemporal skull roof (2).
58. Squamosal without (0) or with (1) a small or (2) large lateral fossa for the origin of the lateral branch of the M. adductor mandibulae externus. ORDERED
59. Distinct dorsolateral notch in squamosal below zygomatic arch in posterior view absent (0) or present (1).

60. Squamosal posteroventral process short such that there is relatively extensive exposure of quadrate and quadratojugal in posterior view and the quadrate foramen (if present) is visible in posterior view) (0) or long such that nearly all of the quadrate and quadratojugal are covered by the squamosal in posterior view and the quadrate foramen (if present) is not visible in posterior view (1).
61. Zygomatic portion of the squamosal without folded edge (0), out-turned to downturned (1) (*Oudenodon*, *Odontocylops*, etc.), or folded-over (2) (*Pelanomodon*, *Geikia*). ORDERED.
62. Dorsoventral expansion of squamosal posterior to postorbital bar: (0) absent (1) present.
63. Zygomatic process of squamosal parasagittally deep (0), narrow and rod-like (1), or transversely expanded (2).
64. Oblique ridge on lateral side of zygomatic arch giving triangular cross-section and overhanging a weak groove present (1) or absent (0).
65. Squamosal zygomatic process narrowly based and in line with occipital condyle (0) or widely based and flares posteriorly beyond occipital condyle (1).
66. Sutural contact of squamosal and maxilla absent (0) or present (1).
67. Squamosal separated by tabular bone from supraoccipital (0) or contacts supraoccipital (1).
68. Suborbital boss on jugal absent (0) or present (1).
69. Quadratojugal narrow and rod-like (0) or plate-like distally (1).
70. Quadrate with a dorsal lobe that has a convex, rounded anterior edge that rests against quadrate ramus of pterygoid (0) or with a dorsal lobe that is developed into a distinct process that extends anteriorly along the quadrate ramus of the pterygoid and is triangular to sub-triangular in shape (1).

71. Vomers unfused (0) or fused (1).
72. Mid-ventral plate of vomers with an expanded, oval-shaped area posterior to junction with premaxilla (0) or without a notable expanded area posterior to junction with premaxilla (1).
73. Mid-ventral plate of vomers relatively wide in ventral view (0), more narrow and blade-like in ventral view (1).
74. Trough on mid-ventral plate of vomers (i.e., ventral surface concave ventrally with raised edges): present (0) or absent (1).
75. Palatine dentition present (0) or absent (1).
76. Bone texture of the palatine: primarily smooth, without evidence of keratinized covering (0); relatively smooth but with fine pitting and texturing suggestive of a keratinized covering (1); rugose and textured (2).
77. Position of palatine: raised, central palatine boss present (0); entire palatine flush with surrounding palatal elements (1); raised posterior section with anterior section that is flush with the secondary palate (2).
78. Paired fossae on palatine surface absent (0); present (1).
79. Palatine widest at its approximate midpoint of length (0), widens posteriorly (1), width relatively constant for entire length (2), widens anteriorly forming a palatine pad (3). ORDERED
80. Foramen on the palatal surface of the palatine absent (0) or present (1).
81. Lateral palatal foramen absent (0), present at level of the anterior, expanded palatal exposure of the palatines (1), present posterior and dorsal to the level of the anterior, expanded palatal exposure of the palatines (2).
82. Sutural contact of palatine and premaxilla absent (0) or present (1).
83. Labial fossa surrounded by maxilla, jugal, and palatine absent (0) or present (1).

84. Ectopterygoid extends further posteriorly than palatine in palatal aspect (0), or does not extend further posteriorly than palatine in palatal aspect (1), or absent (2).
85. Ectopterygoid dentition absent (0) or present (1).
86. Pterygoids contact anteriorly (0) or separated by vomers (1).
87. Transverse flange of pterygoid projects laterally, free of posterior ramus (0), projects laterally, bound by posterior ramus (1) does not project laterally (2).
88. Anterior pterygoid keel: absent (0); present (1).
89. Anterior pterygoid keel extending for most of the length of anterior ramus of pterygoid (0); anterior pterygoid keel restricted to the anterior tip of the anteritor ramus of the pterygoid (1).
90. Contact of pterygoid and maxilla absent (0) or present (1).
91. Converging ventral ridges on posterior portion of anterior pterygoid rami absent (0) or present (1).
92. Ventral surface of the median pterygoid plate depressed (0), smooth and flat (1), with a thin median ridge (2), with a wide, boss-like median ridge (3), or with a low rugose median swelling (4), or with a conical ventral projection (5), or with thin paried ridges that are contiguous with the edges of the interpterygoid vacuity (6).
93. Pterygoid dentition present, conical (0); absent (1); present, bucco-lingually expanded.
94. Posterior edges of the interpterygoid vacuity located dorsal to the median pterygoid plate (0) or extended ventrally such that they are flush with the median pterygoid plate (1).
95. Development of the pila antotica as a rod-like process on the anterior edge of the periotic with a corresponding notch for the trigeminal never posterior to it (0), or

pronounced pila antotica absent and trigeminal notch is a horizontal hollow in the anterior edge of the periotic (1).

96. Contact between periotic and parietal absent (0) or present (1).

97. Parasphenoid excluded from (0) or reaches (1) interpterygoid vacuity.

98. Basisphenoid contribution to the basisphenoid-basioccpital tubera slopes anterodorsally at a shallow angle, forming elongate ridges on the basicranium that are close to the same height as the tubera for most of their length (0), slopes anterodorsally at a steeper angle such that the parabasisphenoid conribution is still somewhat ridge-like but the portion of the ridge on the anterior surface of the tuber is more vertically-oriented (1), or is nearly vertical, forming very weak ridges if any (2).

99. Stapedial facet of basisphenoid-basioccipital tuber exposed laterally (0), exposed ventrolaterally (1), or exposed ventrolaterally and open distally (2).

100. Exposure of internal cartoid between mid-pterygoid plate and parasphenoid: directed laterally (0); directed medially (1).

101. Shape of basal tubera: bifurcating and posteriorly-directed(0); laterally directed anteroposteriorly elongate with relatively narrow edges (1); strongly rounded, such that anterior and posterior tips of tuber curve towards each other, nearly enclosing the stapedial facet; tuber inflated (2); elongate, nearly quadrangular, with tubera extremely close together (3).

102. Margin of fenestra ovalis formed predominantly by parabasisphenoid, with little or no contribution from basioccipital (0), formed by approximately equal portions of parabasisphenoid and basioccipital (1), or formed predominantly by basioccipital, with little or no contribution by parabasisphenoid (2).

103. Intertuberal ridge absent (0) or present (1).

104. Dorsal process on anterior end of epipterygoid footplate absent (0) or present (1).

105. Stapedial foramen present (0) or absent (1).

106. Dorsal process of the stapes present (0) or absent (1).

107. Tabular contacts opisthotic (0) or separated from opisthotic by squamosal (1).

108. Prootic bearing rectangular alar process that forms a plate raised above surface of temporal fenestra wall, in front of fossa: absent (0) present (1).

109. Exoccipital and basioccipital contributions to the occipital condyle distinct (0) or co-ossified into a single unit (1).

110. Occipital condyle round to subspherical in posterior view (0) or distinctly tri-radiate (1) in posterior view.

111. Circular central depression or fossa on the occipital condyle between the exoccipitals and basioccipital present (0) or absent (1).

112. Lateral edge of paroccipital process drawn into sharp posteriorly-directed process that is distinctly offset from the surface of the occipital plate: absent (0) present (1).

113. Floccular fossa present (0) or absent (1).

114. Mandibular fenestra absent (0), present (1), or present but occluded by a thin sheet of the dentary (2).

115. Jaw ramus straight in dorsal view, without strong lateral bends (0), or bends strongly laterally (1) posterior to symphysis.

116. Dentaries sutured (0) or fused (1) at symphysis.

117. Teeth present on dorsal surface of dentaries (0), medially displaced, sometimes on a swelling or shelf (1), or absent (2).

118. Fine serrations on dentary teeth present (0), serrations absent (1), or coarse serrations present (2).

119. Denticulated cingulum on dentary teeth absent (0) or present (1).

120. Anteriormost dentary tooth: not distinct from rest of tooth row (0); massively enlarged and incisiform (1).

121. Jaw symphysis terminates in dorsal platform bearing the incisors and canine elevated above level of posterior dentary ramus (0); Symphyseal region of lower jaw smoothly rounded and at same level as rest of dentary ramus in lateral view (1), with an upturned beak that is raised above the level of the dorsal surface of the jaw rami and has a scooped-out depression on its posterior surface (2), drawn into a sharp, spiky beak (3), or shovel-shaped beak with a rounded or squared-off edge and a weak depression on its posterior surface (4).

122. Curved ridge that follows the profile of the symphysis present on the edge between the anterior and lateral surfaces of the dentary absent (0) or present (1).

123. Boss present on ventral surface of anterior dentary ramus. absent (0) present (1).

124. Dentary table absent (0) or present (1).

125. Posterior dentary sulcus absent (0), present but does not extend past dentary teeth (if present) (1), present and extends past dentary teeth (if present), but is relatively wide and shallow (2), or present, extends past dentary teeth (if present) and is narrower and deeper (3).

126. Tall, dorsally-convex cutting blade on medial edge of dorsal surface of dentary absent (0) or present (1).

127. Lateral dentary shelf absent (0), present but relatively small (1), present and well developed (2).

128. Anterodorsal edge of lateral dentary shelf relatively flat (0), with a groove (1), or developed into a rounded swelling (2).

129. Lateral dentary shelf relatively thick, with distinct dorsal and ventral surfaces above the mandibular fenestra (0) or a thin ventrolaterally-directed sheet that forms the dorsal margin of the mandibular fenestra (1).

130. Splenial symphysis unfused (0) or fused (1).

131. Spenial contribution to dentary symphysis: anterior process on splenial present in ventral view (0) or absent (1).

132. Exposed contribution of the angular to the symphysis: absent (0) present (1).

133. Coronoid bone present (0), or absent (1).

134. Angular with anterolateral trough for the posterior process of the dentary absent (0) or present (1).

135. Reflected lamina: (0) reflected lamina large, rounded, unornamented; (1) with perpendicular ridges; (2) with reticulate ridges; (3) triradiate, with distinct groove-ridge-groove morphology dorsoventrally arrayed along lamina; (4) small, tab-like (more elongate than rounded), unornamented (5); large, rounded, but with only a central groove bisecting the lamina.

136. Reflected lamina of angular closely approaches or touches articular (0) or widely separated from articular (1).

137. Prearticular with (0) or without (1) lateral exposure posteriorly.

138. Articular distinct (0) or at least partially fused to prearticular (1).

139. Surangular vertical lamina present and lateral to articular (0) or absent (1).

140. Jaw joint allows strictly orthal closure (0); allows parasagittal movement with joint surfaces of quadrate and articular approximately equal (1); allows

parasagittal movement with joint surfaces on articular large than that of quadrate (2). ORDERED

141. Enlarged dentary caniniform present (0) or absent (1).

142. Number of sacral vertebrae three (0), four (1), five (2), or six or more (3).

143. Number of sternal bosses: 2 (0), 4(1).

144. Cleithrum absent (0) or present (1).

145. Anterior edge of scapula extended laterally to form a strong crest (1) or not (0).

146. Origin of triceps on posterior surface of scapula relatively low (0) or developed into a prominent posterior projection (1).

147. Acromion process: absent or very small (0) or present and well defined (1).

148. Procoracoid foramen or notch entirely contained within the procoracoid (0) or formed by contributions of the procoracoid and scapula in lateral view (1).

149. Procoracoid does not participate in formation of glenoid (0) or participates in formation of glenoid (1).

150. Proximal articular surface of humerus formed by a slightly convex area on proximal surface of the bone without much expansion onto the dorsal surface (0), somewhat expanded with some encroachment onto the dorsal surface (1), or strongly developed and set off from rest of humerus by a weak neck (2). ORDERED

151. Insertion of M. subcoracoscapularis on humerus a rounded, rugose area on proximal end of humerus (0), short, pinna-like process (1); large elongate process (2). ORDERED

152. Insertion of M. latissimus dorsi at rugose tuberosity on the posteroventral surface of humerus (0) or extended into a dorsoventrally flattened pinna-like process (1).

153. Anterior and distal edges of deltopectoral crest close to perpendicular (0) or very obtuse (1)

154. Ectepicondylar foramen on humerus present (0) or absent (1).

155. Radial and ulnar condyle continuous (0) or well ossified and separate (1) on ventral surface of humerus.

156. Ulna with small olecranon process that does not extend far past the articular surface for the humerus (0), or with a large olecranon process that extends well past the articular surface for the humerus (1).

157. Distal carpal 5: present as a distinct element (0), not present as a distinct element (1).

158. Manual digit III, shape of second phalanx: short (disc-like) (0), absent (1).

159. Manual digit IV, phalangeal number: 5 (0), or 3 (1).

160. Dorsal edge of ilium: unnotched (0) or notched (1).

161. Pubic plate is significantly expanded anteroposteriorly, such that its length is comparable to that of ischium (0) or anteroposteriorly short, so that it is much shorter than ischium (1).

162. Pubic plate is significantly expanded ventrally such that it is nearly the same height as ischium (0) or reduced ventrally such that it is shorter than ischium (1).

163. Distinct cranial process on anterior end of pubis absent (0) or present (1).

164. Femoral head continuous with the dorsal margin of femur (0) or offset dorsally from dorsal margin (1).

165. Proximal articular surface of the femur present as a weak swelling that is mostly limited to the proximal surface of the bone (0) or present as a more rounded, hemispherical swelling that has some encroachment on the anterior surface of the femur (1).

166. Insertion of M. iliofemoralis present as a low rugosity on the dorsolateral portion of the femur (0), developed into a distinct crest that extends down part of the lateral surface of the femur (1) or a lateral crest that is split into a distinct first trochanter and third trochanter (2). ORDERED

167. Pedal digit III, shape of second phalanx: short (disc-like) (0), absent (1).

168. Pedal digit IV, phalangeal number: 5 (0), 4 (1), or 3 (2).

169. Pedal digit IV, shape of second and third phalanges: long (0), short (1).

170. Pedal digit V, shape of second phalanx: short (0), absent (1).

171. Greatly enlarged vascular channels present (1) or absent (0).

172. Anterior face of dentary symphysis: unornamented (0), with median ridge (1).

173. Supinator process above ectepicondyle of humerus absent (0), present (1).

174. Morphology of supinator process: low, broadly separated from the shaft (0), tall and subvertical, with dorsal margin close to base of shaft (1), discrete, tab-like process occupying restricted portion of anterior face of distal humerus (2).

Appendix 4: Updates to character state codings for *Patranomodon nyaphulii*, *Eodicynodon oosthuizeni, Nyaphulia oelofseni*, BP/1/8740 and BP/1/8500 on the Angielczyk et al. (2021) matrix.

Taxon	Characters (1-174)
Patranomodon nyaphulii	000?0?10101?00002000?100100?????0000000000010010000001 0000000100000000000100010?0110000?01011??0001100?101001 00?10?01001000000????0003100001 0????????????????0110???00 0?????0??
Nyaphulia oelofseni	???????01?1000002000010 01?0????????0?00000010??00100010 02010?200??0??0000111030????012???1310??000???0????0?10? 0101110020000 1001?01??1??121???????????????????????????? ???0??
Eodicynodon oosthuizeni	000010121010000020000200101000000110000000001001001000 1 002110020101010000011103010010121001310010000100001101 10 001010100200100200100113111121 0?000100000011 0?1101000001 ???100?
BP/1/8740	00000?1010100000?000?000100????? 0010000000001001000 0?010 0000001000000000001000100011001 0?01011??1001?00?1?100100 ?10101001000000????0003010001???100?0???00???????????? ??????
BP/1/8500	1000???2?0?01110??1002100110 0?0002??0??001?0?????110?0?0 ?10120200000 10????????????010???0??2????????0????0?1??1 ??? ??????

Appendix 5: Skull lengths and dates (first appearance and last appearance dates) of anomodonts in the phylogeny.

Taxa ID	Skull (mm) length	FAD (Ma)	LAD (Ma)
Biseridens qilianicus	170	264.4	260.23
Otsheria netzvetajevi	110	264.4	262.03
Ulemica spp.	150	264.4	262.03
Suminia getmanovi	58	260.259	259.262
Patranomodon nyaphulii	60	264.72	264.4
BP/1/8740	38	264.72	262,03
Anomocephalus africanus	210	264.4	262.03
Tiarajudens eccentricus	225	262.03	260.23
Galepus jouberti	51	264.4	260.23
Galechirus scholtzi	68	264.4	260.23
Galeops whaitsi	45	264.4	260.23
Nyaphulia oelofseni	50	264.72	262.03
BP/1/8500	190	264.72	262.03
Eodicynodon oosthuizeni	95	264.72	262.03
Colobodectes cluveri	160	264.4	260.23
Lanthanostegus mohoii	200	264.72	262.03
Eosimops newtoni	129	262.03	260.23
Robertia broomiana	130	262.03	260.23
Diictodon feliceps	95	260.23	253.02

Prosictodon dubei	81.6	260.23	253.02
Pristerodon mackayi	78	264.4	253.02
Brachyprosopus broomi	140	264.4	260.23
Abajudon kaayai	96	268.8	259.1
Endothiodon bathystoma	434	260.259	259.247
Endothiodon tolani	200	260.259	259.247
Emydops spp.	53	260.23	255.2
Compsodon helmoedi	111	255.2	253.2
Digalodon rubidgei	100	256.247	255.2
Niassodon mfumukasi	58	260.259	259.247
Myosaurus gracilis	44	252.24	247.2
Thliptosaurus imperforatus	86	253.02	251.7
Dicynodontoides spp.	161	256.247	251.7
Kombuisia frerensis	76	247.2	237
Sauroscaptor tharavati	50	256.247	255.2
Kembawacela kitchingi	55	256.247	255.2
Cistecephalus microrhinus	50	256.247	255.2
Cistecephaloides boonstrai	62	256.247	255.2
Kawingasaurus fossilis	40	256.247	255.2

Rastodon procurvidens	86	268.8	251.9
Kunpania scopulusa	307	265.1	259.1
Katumbia parringtoni	178	254.14	251.1
Elph borealis	400	259.1	251.9
Interpresosaurus blomi	130	254.14	251.9
Daqingshanodon limbus	83	259.1	251.9
Keyseria benjamini	153	256.247	255.5
Oudenodon bainii	270	259.262	253.02
Tropidostoma dubium	253	259.262	256.247
Autralobarbarus spp.	144	259.1	254.14
Odontocyclops whaitsi	311	259.262	255.12
Idelesaurus tataricus	230	259.1	254.14
Rhachiocephalus magnus	590	259.262	253.02
Kitchinganomodon crassus	509	256.247	253.02
Syops vanhoepeni	135	256.247	255.2
Bulbasaurus phylloxyron	111	259.262	256.247
Aulacephalodon bainii	361	259.262	253.02
Pelanomodon moschops	182	256.247	251.7
Geikia locusticeps	82.4	255.2	253.02

Geikia elginensis	95.15	255.2	253.02
Taoheodon baizhijuni	105	259.1	251.9
Counillonia superoculis	160	259.1	251.2
Repelinosaurus robustus	157	259.1	251.2
Repelinosaurus spp.	190	259.1	251.2
Basilodon woodwardi	160	256.247	253.02
Gordonia traquairi	160	255.2	253.02
Jimusaria sinkiangensis	240	254.14	251.9
Dicynodon lacerticeps	150	256.247	251.9
Dicynodon angielczyki	315	256.247	251.9
Delectosaurus arefjevi	137	254.14	251.9
Daptocephalus leoniceps	423	255.2	251.7
Daptocephalus huenei	282	255.2	251.7
Dinanomodon gilli	718	256.247	251.7
Turfanodon bogdaensis	330	259.1	251.9
Euptychognathus bathyrhunchus	300	256.247	255.2
Lystrosaurus hedini	160	253.02	252.24
Lystrosaurus murrayi	300	254.14	252.24
Lystrosaurus declivis	177	251.9	247.2

Lystrosaurus maccaigi	226	252.24	251.12
Lystrosaurus curvatus	165	252.24	251.12
Vinceria andina	119	247.2	242
Angiosaurus cruickshanki	300	247.2	242
Zambiasaurus submersus	450	247.2	242
Placerias hesternus	680	227	208.5
Ufundocyclops mukanelai	295	251.2	247.2
Stahleckeria potens	460	247.2	242
Sangusaurus parringtonii	500	247.2	242
Ischigualastia jenseni	550	227	208.5
Dinodontosaurus spp.	920	247.2	242
Xiyukannemeyeria brevirostris	303	247.2	237.7
Shaanbeikannemeyeria spp.	420	252.17	247.2
Rechnisaurus cristarhynchus	38	247.2	242
Uralokannemeyeria vjuschkovi	436	247.2	242
Dolichuranus primaevus	370	247.2	242
Kannemeyeria simocephalus	229	251.2	247.2
Rabidosaurus cristatus	404	247.2	237
Kannemeyeria lophorhinus	409	251.2	247.2
Wadiasaurus indicus	400	247.2	242

Appendix 6: R script used to construct changes is body size over time and Lowess line plot.

```
## Set working directory for the anomodonts
Setwd("C:/Users/fonda/Desktop/Fonda_files")
getwd

## Load the main packages
require(ape)
require(phytools)
require(paleotree)
require(geiger)

## Load and check trees and files
tree<-read.nexus("Contree.nex")
tree
plotTree(tree, fsize=0.2)

## Load the anomodont ages
anomodont.ages<-read.csv("Anomodont ages.csv",header = TRUE,row.names = 1)

## Check the first few rows
head(anomodont.ages)

## Load the skull length data
skull.length<-read.csv("Skull length.csv",header = TRUE,row.names = 1)

## Check the first few rows
head(skull.length)
```

```
## Check if the anomodont ages match the tree using Geiger
treedata(tree,anomodont.ages)
anomodont.ages
treedata(tree,anomodont.ages)

## Calibrating
likFun<-make_durationFreqCont(anomodont.ages)
parameters<-optim(parInit(likFun),
                  likFun,
                  lower = parLower(likFun),
                  upper = parUpper(likFun),
                  method = "L-BFGS-B",
                  control = list(maxit=1000000))

## Get brRate, exRate and sampRates
parameters[[1]][1]
parameters[[1]][2]
extRate<-parameters[[1]][1]
brRate<- extRate
sampRate<-parameters[[1]][2]

## The cal3 dating method
trees<-cal3TimePaleoPhy(tree,anomodont.ages,
                        brRate,
                        extRate,
                        sampRate,
                        ntrees = 100,
                        FAD.only = FALSE,
```

```
                dateTreatment = "firstLast",
                randres = TRUE,
                root.max = 0.5,
                step.size = 0.1,
                plot = FALSE)

## Least squares consensus
con.tree<-ls.consensus(trees,start = NULL,tol=1e-12)
con.tree<-minBranchLength(con.tree, mbl=0.1,modifyRootAge=TRUE)
plotTree(con.tree, fsize=0.2)

## Rooting a phylogenetic tree
con.tree<-root(con.tree,outgroup = "Biseridens_qilianicus",
          resolve.root = TRUE)
is.rooted(con.tree)

## Match tree and data, and data and tree
con.tree<-treedata(con.tree,skull.length,sort=T,warnings=T)$phy
con.tree
skull.length<-as.data.frame(treedata(con.tree,skull.length,sort=T,warnings=T)$data)
skull.length

## Use the tree to analyse the skull length
skulls <- as.matrix(skull.length)[,1]
map <-contMap(con.tree,skulls, plot = FALSE)
map

## Set the parameter margins
par(mar=c(3.1,3.1,1.1,1.1),las=1,cex.axis=0.5)
```

```
## Plot contmap
plot(map,legend=0.6*max(nodeHeights(con.tree)),fsize=0.8,lwd = 2)

## Adding the periods
plot(map,mar=c(1.8,0.2,0.2,0.2),legend=40,fsize=0.25,
    lwd = 0.7, type="phylogram", direction="rightwards", ftype="i")
axisPhylo(side = 1, root.time = 268.9, backward = TRUE, lwd=1,
        cex.axis=0.5)

## Adding the Lowess line plot
anomodont_data <- read.csv("Anomodont_ages_and_length.csv")
plot(anomodont_data$Ages, anomodont_data$Skull.length)
lines(lowess(anomodont_data$Ages, anomodont_data$Skull.length))
model<- lm(anomodont_data$Ages~anomodont_data$Skull.length)
abline(model, col="red")
plot(anomodont_data$Ages, log10(anomodont_data$Skull.length))
model2<- lm(anomodont_data$Ages~log10(anomodont_data$Skull.length))
lines(lowess(anomodont_data$Ages, log10(anomodont_data$Skull.length)))
summary(model2)
```